Detection and Mitigation of Impairments for Real-Time Multimedia Applications

Soshant Bali

Submitted to the Department of Electrical Engineering & Computer Science and the Faculty of the Graduate School of the University of Kansas in partial fulfillment of the requirements for the degree of Doctor of Philosophy

Committee:

Dr. Victor S. Frost: Chairperson

Dr. Joseph B. Evans

Dr. David W. Petr

Dr. James P. G. Sterbenz

Dr. Tyrone Duncan

Date Defended

2007/12/13

The dissertation Committee for Soshant Bali certifies
that this is the approved version of the following thesis:

Detection and Mitigation of Impairments for Real-Time Multimedia Applications

Committee:

_____

Chairperson

_____

_____

_____

_____

_____

Date Approved

Abstract

Measures of Quality of Service (QoS) for multimedia services should focus on phenomena that are observable to the end-user. Metrics such as delay and loss may have little direct meaning to the end-user because knowledge of specific coding and/or adaptive techniques is required to translate delay and loss to the user-perceived performance. Impairment events, as defined in this dissertation, are observable by the end-users independent of coding, adaptive playout or packet loss concealment techniques employed by their multimedia applications. Methods for detecting real-time multimedia (RTM) impairment events from end-to-end measurements are developed here and evaluated using 26 days of PlanetLab measurements collected over nine different Internet paths. Furthermore, methods for detecting impairment-causing network events like route changes and congestion are also developed. The advanced detection techniques developed in this work can be used by applications to detect and match response to network events. The heuristics-based techniques for detecting congestion and route changes were evaluated using PlanetLab measurements. It was found that Congestion events occurred for 6-8 hours during the days on weekdays on two paths. The heuristics-based route change detection algorithm detected 71% of the visible layer 2 route changes and did not detect the events that occurred too close together in time or the events for which the minimum RTT change was small. A practical model-based route change detector named the parameter unaware detector (PUD) is also developed in this deissertation because it was expected that model-based detectors would perform better than the heuristics-based detector. Also, the optimal detector named the parameter aware detector (PAD) is developed and is useful because it provides the upper bound on the performance of any detector. The analysis for predicting the performance of PAD is another important contribution of this work. Simulation results prove that the model-based PUD algorithm

has acceptable performance over a larger region of the parameter space than the heuristics-based algorithm and this difference in performance increases with an increase in the window size. Also, it is shown that both practical algorithms have a smaller acceptable performance region compared to the optimal algorithm. The model-based algorithms proposed in this dissertation are based on the assumption that RTTs have a Gamma density function. This Gamma distribution assumption may not hold when there are wireless links in the path. A study of CDMA 1xEVDO networks was initiated to understand the delay characteristics of these networks. During this study, it was found that the widely deployed proportional-fair (PF) scheduler can be corrupted accidentally or deliberately to cause RTM impairments. This is demonstrated using measurements conducted over both in-lab and deployed CDMA 1xEVDO networks. A new variant to PF that solves the impairment vulnerability of the PF algorithm is proposed and evaluated using ns-2 simulations. It is shown that this new scheduler solution together with a new adaptive-alpha initialization stratergy reduces the starvation problem of the PF algorithm.

Acknowledgments

It is my good fortune to have had Dr. Victor Frost as my advisor over the last few years. His knowledge, experience, unending enthusiasm, constant encouragement and support helped immensely in the completion of this research. I thank Dr. Frost for all this and I look forward to continue benefiting from interactions with him in future. I would also like to thank Dr. Joseph Evans, Dr. Tyrone Duncan, Dr. David Petr and Dr. James Sterbenz for helping me develop skills in computer networking and mathematics and for the feedback on this work.

The work on the proportional fair scheduler was completed at the Sprint Advanced Technology Laboratories in Burlingame, California and I am thankful to my colleagues Dr. Hui Zang, Dr. Sridhar Machiraju, Kosol Jintaseranee and Dr. Jean Bolot for the discussions and technical expertise that helped shape the wireless scheduler work.

I offer my heartfelt thanks to my parents who although far away were always close to me in my thoughts, for their everlasting encouragement, faith, support and love.

Contents

List of Figures

List of Tables

Chapter 1

Introduction and related work

1.1 Real Time Multimedia Impairments

Effective quality of service (QoS) metrics must relate to end-user experience. For real-time multimedia (RTM) services these metrics should focus on phenomena that are observable by the end-user. In this dissertation methods are developed to predict network events that are observable by end-users independent of coding, adaptive playout or packet loss concealment (PLC) techniques that are often employed in RTM application. Long bursts of packet losses, high delays and a high random packet loss rate are all observable impairments. Metrics such as long term average delay, loss and jitter may have little direct meaning to end-users of rapidly changing multimedia applications because knowledge of the specific coding, adaptive playout and PLC techniques is required to translate delay and loss into the user-perceived performance. A user-perceived impairment event as defined here will impact the customer's QoS independent of the specific coding mechanism or of attempts to mask and/or adaptively compensate for its effects. The QoS metric, that is a rate of user-perceived impairment events, is easily understood by

end-users and captures the network performance that is observable by network customers. Impairments arise from a variety of phenomena including long bursts of packet losses, random packet losses and high delays.

Long bursts of packet losses are known to be present in the Internet [BSUB98] [MT00] [JS00]. While loss concealment and channel coding techniques can improve overall performance in some cases, long sequences of packet losses causes a significant impairment. For example, when using the G.723.1 recommendation for compressed voice over IP networks (VoIP), only slight static and clipping result from one-to-four consecutive packet losses. However longer bursts of packet losses will significantly degrade the QoS delivered to the user. PLC and channel coding techniques attempt to hide the impact of a small number of losses. However, these techniques do not work when a large number of consecutive VoIP packets are lost. Thus, an impairment event occurs when a large number of consecutive packets are lost.

While long bursts of losses definitely cause user-perceived impairments, perceived quality also drops as random loss rate increases [JBG04]. The minimum loss rate at which perceived quality becomes unacceptable for a majority of the users depends on the coding and loss concealment technique in use. For VoIP, mean opinion score (MOS) is a widely used metric to rate the quality of voice calls. MOS ranges from 0 to 5, with 5 being the best possible and 0 being the worst. A MOS smaller than 3.6 is considered unacceptable. Independent of the coding technique in use, MOS drops below 3.6 when random loss rate exceeds about 10% [MTK03]. For RTM applications, channel coding is typically used in terms of block codes [WHZ00]. Specifically, for video streams a block code (e.g., Tornado code) is applied to a segment of k packets to generate a n packet block,

where $n > k$. The channel encoder places k packets in a group and creates additional packets from them so that the total number of packets is n. This group of packets is transmitted to the receiver, which receives K packets ($n - K$ packets are lost). To perfectly recover a segment, a user must receive at least k packets (i.e., $K \geq k$) in the n packet block. If more than $n - k$ packets are lost then channel coding cannot recover any portion of the original segment. Some video coders adaptively increase $n-k$ when the packet loss rate is high. However, $n-k$ cannot be made arbitrarily large because coding delay and required capacity also increase with an increase in n. Moreover, many transport protocols decrease the rate when packet loss rate increases (to avoid congestion collapse) [FHPW00]. In our work, if the random packet loss rate is greater than some fixed threshold, then an impairment event is determined to have occurred.

High delays can also cause user-perceived impairments. A mouth-to-ear delay less than 150 ms is considered acceptable for most VoIP [G.103] applications. However, if the mouth-to-ear delay is greater than 400 ms, then most end-users are dissatisfied with the service. For multiplayer interactive network games, end-to-end delays greater than 200 ms are "noticeable" and "annoying" to end-users [BCL$^+$04] [NC04] [PW02]. While end-users of sports and real-time strategy games are more tolerant to latency, even modest delays of 75-100 ms are noticeable in first person shooter and car racing games [BCL$^+$04] [NC04]. RTM applications employ playout delay buffers at the receiver to compensate for network jitter. When the jitter is very high, a large playout buffer is needed to avoid excessive packet losses due to late arrivals. Playout buffer delay however is added to the total delay (e.g., mouth-to-ear delay for VoIP). Thus, when the network jitter is high, playout delay buffer size is increased at the cost of increased total delay. In addition to

the playout delay, source/channel coding/decoding delays also contribute to the total delay. In this work, when the sum of mean estimated one-way delay and playout buffer delay are greater than some threshold delay (such that interactivity is impacted), then an impairment event is inferred.

Can end-to-end measurements be used to detect RTM impairments is one of the questions addressed by this dissertation. New methods are developed and evaluated using Internet measurements collected over the Planet-Lab infrastructure. In addition to the impairment events, methods for detecting network events that cause these impairments are also developed as a part of this dissertation.

1.2 Network events that cause RTM impairments

Impairment events may be caused by congestion or route changes or they may even be induced by packet schedulers used in wireless networks. Congestion is a state of sustained network overload, where demand for resources exceeds the supply for an extended period of time. A congestion event may cause a number of consecutive packet losses. Congestion may also cause the random packet loss rate, mean delay and variation of delay to increase significantly, thus resulting in impairment events. However, congestion may not be sufficiently severe to cause an impairment. Congestion detection is needed to investigate the characteristics of impairment events that occur during congestion. Two methods for detecting congestion events from end-to-end measurements are proposed in this dissertation.

Route changes can also cause impairments (long bursts of lost packets). Route changes can be caused by router or link failures or when a failed component recovers from a failure. Failures are often followed by a service disruption that lasts from a few seconds to a few minutes while routing protocols converge to the new

route [LABJ00] [LAJ98] [ICM+02]. Restoration at Layer 2 is usually faster than restoration at Layer 3 [ICBD04]. Layer 3 route changes can be detected at the end-node from IP time to live (TTL) and traceroute changes (if intermediate network elements allow) whereas Layer 2 route changes are more difficult to detect. Thus in some cases Layer 3 route changes can be explicitly detected while Layer 2 route changes must be indirectly inferred. A new heuristics based algorithm is proposed here to detect route changes. Note that even though route changes do not always cause an impairment, route change detection is needed to investigate the correlation between route changes and impairments and to segregate appropriately the observations, e.g. round trip times (RTTs) into statistically homogenous regions (see [ZDPS01]). A model based approach is also used in this dissertation to detect route changes. The parameter aware detector (PAD) or the ideal detector is proposed in this dissertation. The analysis needed to predict the performance of PAD as a function of the parameters of the RTT process is also developed here to upperbound the performance of route change detectors. The practical implementation directly based on the PAD, the parameter unaware detector (PUD) is also proposed in this dissertation. The performance of heuristics based and parameter unaware detectors is compared to the performance of the optimum algorithm.

RTM impairments may also be induced by the proportional fair (PF) downlink scheduler that is commonly used in infrastructure-based wireless networks. The PF scheduler is widely deployed because of its desirable property of optimizing sector throughput while maintaining fairness at the same time. One contribution of this dissertation is that it is shown that the PF scheduler can be easily corrupted, accidentally or deliberately to starve other users causing RTM impair-

ments. A new scheduling mechanism that mitigates this starvation vulnerability without compromising the fairness and throughput optimality properties of PF scheduler is proposed and analysed in this dissertation.

The methods to detect route changes and congestion that are proposed in this dissertation can have a significant impact on several network functions. Specifically, overlay network services can use congestion detection, and route change detection procedures to make better routing decisions. Internet service providers (ISPs) can use congestion detection techniques to collect and report impairment statistics to customers as part of SLAs. Customers can verify these impairment statistics reported in SLAs using the same end-to-end impairment detection techniques. ISPs, as discussed in [CMR03], can also use the route change and congestion detection algorithms to detect both layer 2 and layer 3 faults. Improved network tomography [DP04] techniques may result from the proposed research. Current methods assume the routing matrix to be constant throughout the measurement period [CHNY02]. The proposed techniques can be used to decide when and for which paths the topology needs to be recalculated. The Internet engineering task force (IETF) Next Steps in Signaling also requires knowledge of route changes [SSLB05]. Applications like distributed games and peer-to-peer services that require estimates of minimum round trip time (RTT) of the path can benefit from knowledge of route change induced changes in delay. Finally, transport protocols can also be improved by differentiating congestive losses from non-congestive losses. While the dynamic nature of networks has been considered by others, e.g., [WWTK03] and [CHNY02], most current approaches do not recognize the underlying cause of network dynamics, thus limiting the system's ability to appropriately respond. The result of this research is the knowledge of the un-

derlying cause of network dynamics, enabling network functions to match their response to the applicable conditions. The premise of this work is that matching the response to the applicable conditions will significantly improve network functions. The next section provides additional details about the relavance of this research.

1.3 Relevance of this research

The research in this dissertation has the following applications

1. Impairments QoS metric for (SLAs). Presently ISPs use delay and loss rate averaged over a long period of time as QoS metrics in SLAs. For example, ISWest offers an average packet loss rate less than 1 percent and average round trip latency less than 140 ms [Isw]. Average latency and loss are often calculated over a one-month period [Isw]. Such long-term average delay and loss metrics may not be relevant to end-users of real time multimedia (RTM) applications. New QoS metrics that directly relate to the duration of and time between impairments [Fro03] and [BJFD05] have been proposed. These metrics are easy to understand by end-users and are directly relevant to RTM applications. Statistics of observed impairments can then be used to formulate a SLA. Customers can use these same end-to-end techniques to verify the statistics reported by ISPs in SLAs.

2. Routing for overlay networks/content delivery networks CDNs. Overlay and content delivery networks (CDN) use measurements to decide paths on which to route packets. Packets are routed over paths that minimize latency or loss. None of the reported methods use measurements to infer the type

of event occurring in the path. Better routing decisions can be taken if end-to-end measurements are used to infer the type of event causing observed degradations. If congestion is detected in the path between two overlay nodes, that path should be avoided. Without a way to discriminate a route change may "appear" as congestion. However if a route change is detected in a path, then a change in the routing for the overlay network may not be not needed. In this way the routing in the underlay may be decoupled from the routing in the overlay network using knowledge derived from end-to-end measurements.

3. Improving Internet tomography. The goal of Internet tomography is the estimation of link parameters like loss rate and delay from end-to-end measurements [CHNY02]. The sender node sends either multiple back-to-back unicast probe packets or multicast probe packets to a group of destination nodes. End-to-end delay and loss measurements collected using these probe packets are then used to estimate delay distributions and loss rates of the individual links in the end-to-end paths. Link parameters can be estimated from end-to-end measurements only when the network topology is known. Network topology is however not always readily available. Most topology mapping tools require cooperation from individual routers in the end-to-end path in the form of traceroute. "These co-operative conditions are often not met in practice and may become increasingly uncommon as the network grows and privacy and proprietary concerns increase" [CHNY02]. For a situation like this in which topology mapping tools do not work, network topology can be inferred from end-to-end measurements using topology inference tools [MCN02], [DP00], [NGDD02]. Topology inference tools use the degree

of correlation of measurements between different receivers to infer the logical topology. The degree of correlation of delays, losses or delay differences between any two receivers is governed by number of links that are shared by the paths to these receivers. A large number of samples are needed before the logical topology can be statistically inferred from the data. Moreover, maximum likelihood estimation of the topology is very computationally intensive [MCN02]. Often topology inference tools [MCN02], [DP00], [NGDD02], assume that the topology does not change. This, however, may not be valid because of frequency of route changes. Delay-based route change detection algorithms proposed here can be used to detect topology changes. When a route change is detected, topology inference tools can be restarted and a new topology map can be inferred. Moreover, since topology inference tools are computationally intensive and consume network bandwidth, these tools can be programmed to remap the topology only for receivers that detected a route change. Hence, delay based route change detection tools can be used to decide when and for which paths topology should be remapped. Also, congestion and route-change detection algorithms proposed in this work can be used to locate the links that are experiencing congestion or route changes. If congestion or route changes are detected by a group of receivers, then it can be inferred that the anomalous event occurred in one of the links that is shared by the paths to those receivers.

4. Next Steps in Signaling. The Next-steps in signaling (NSIS) working group of the IETF is developing a generic signaling protocol that can manipulate control information along the flow path and can meet the needs of several applications, e.g., QoS, mobile applications, and NAT [RHdB05]. Once

the control state information is established in the network elements in the flow's path, data packets can start receiving the treatment requested using the signaling protocol. Route changes may cause the addition of several network elements in the path that have not been configured with the control information. The portion of the network path that is not configured with the control information may severely affect the application performance. The signaling application should detect route changes and should reconfigure the network elements in the new path with the control state information as soon as possible to minimize the performance degradation experienced by the application [RHdB05], [SSLB05]. Delay-based route change detection algorithms proposed in this work can be used to detect these route changes with predictable performance. Also, since it is important to detect a route change as soon as possible, the work on minimum number of samples needed to form a minimum RTT estimate can be used to minimize the time to detect a route change.

5. Fault and state detection for ISPs. In an operational setting, active measurement systems complement traditional passive measurement systems by monitoring network paths within the service provider's network. While high queuing delays and congestion events can be detected using passive measurements, routing loops [UHD02], route changes, packet reordering and customer affecting impairment events can be detected using active measurements. AT&T's active measurement system for detecting faults is discussed in detail in [CMR03]. This system uses traceroute to detect route changes and the impact of route changes on end-user can be estimated from duration of time for which probe packets are lost. The route change detection algo-

rithm proposed here can be used to enhance layer 3 route change detection process and to detect layer 2 route changes not visible with layer 3 tools like traceroute.

6. Estimating minimum RTT of path with confidence. Applications like distributed games [BCL+04] [NC04] [PW02], service mirroring, and peer-to-peer applications require measuring the minimum RTT between nodes. The accuracy or confidence in the measured minimum RTT is critical to the performance of these applications [AZJ03]. To achieve a certain level of confidence in the measurement, these applications usually send a large number of probes. A heuristic technique for determining the confidence in measured minimum RTT was proposed in [AZJ03]. Knowledge of route changes will improve estimates of minimum RTT of path with predictable confidence.

7. Increasing transport protocol throughput. On detecting lost packets, transport protocols, e.g., TCP, infer that there is congestion in the network and reduce their transmission rate to avoid congestion collapse. However, packet losses can be caused by events other than congestion (like route changes or wireless losses). Differentiating congestive losses from non-congestive losses can increase transport layer throughput. While there has been research in this area none of the proposed end-to-end methods are widely used either because they are based on unrealistic models or because they work only for a few selected cases. Here the source of the impairment will be identified so the transport protocol can respond appropriately.

1.4 Related Work

The characteristics of Internet paths as reported in several measurement studies are presented first. The impact of these events on user-perceived performance of several RTM applications is then discussed.

1.4.1 Characteristics of Internet Paths

Long bursts of packet losses are known to be present in the Internet [BSUB98] [JCBG95] [MYT99] [JS02]. For example in [BSUB98] end-to-end measurements were used to study the characteristics of packet loss bursts in the Internet. A packet was transmitted once every 30 ms to model the traffic generated by the ITU G.723.1 compressed voice coder. Losses were found to be bursty in nature with an average of 6.9 losses/burst. On one path less than 1% of all bursts accounted for nearly 50% of all individual losses. It was found in [JCBG95] that average length of bursts was more at 4 PM than it was at 8 AM suggesting that there is some correlation between burst length and network load.

In addition to congestion, network component failures may also cause burst packet losses. Failures happen due to events like fiber cut, failure of optical equipment, hardware failure, router processor overload, software error, protocol implementation and misconfiguration errors. Scheduled maintenance events like software upgrades may also cause failures. On the Sprint IP network about 20% of all failures are cause by planned maintenance activities [AMD04]. Of the unplanned failures, almost 30% are shared by multiple links and 70% affect a single link at a time. Multiple logical links may fail at the same time when they share a common optical fiber and either the fiber is cut or optical equipment fails. Multiple links may also fail at the same time when there are problems in the router that is

shared by these links. Routing protocols are designed to detect and route around failures. The time taken to converge to a new route is protocol and topology dependent [DPZ03]. During convergence, the service is disrupted and burst losses are observed. For IS-IS (an intra-domain routing protocol) a service disruption of 6.6 seconds can follow a failure [GID02]. The convergence time for IS-IS can be reduced from more than six seconds to less than one second by changing the values of the default timers [Iannac2005]. However changing timers may cause router processor overload or routing instabilities. BGP (an inter-domain routing protocol) may take much longer to converge to a new stable route than IS-IS. It was shown [LABJ00] that it takes an average of 3 minutes for BGP routes to stabilize. During this period end-to-end paths may experience intermittent loss of connectivity, as well as increased packet loss and latency. It was observed that during path restoral, measured packet loss grows by a factor of 30 and latency by a factor of 4. Therefore route changes can cause user-perceived impairments.

Congestion also causes burst losses, increases end-to-end delay, variation of delay and random loss rate. Congestion is known to occur more commonly in access links than in backbone links [KPD03] and [KPH04]. However congestion may also occur in over-provisioned backbone links. It was observed in [Iyer2003] that about 80% of all congestion events in backbone links were preceded by link failure. This phenomena was also observed in [BJFD05]. Since congestion and failures may cause packet losses, increase latency, and latency variation, these events may be observable to end-users in the form of application impairments. Service providers and end-user applications can benefit if they are able to reliably detect these events using end-to-end observations. Packet losses occur and are measurable on an end-to-end basis; however, it has been observed that probe

packets are rarely lost and thus a large number of probes are needed before loss-based metrics become reliable. Therefore the proposed research will focus on delay measurements.

1.4.2 Performance of RTM applications over the Internet

Network events are most important for RTM applications like voice over IP (VoIP), videoconferencing, virtual classroom and Internet gaming. Numerous measurement studies have reported assessments of quality of VoIP over Internet paths. An anomaly detection algorithm for VoIP was presented in [MMS05]. VoIP performance is also influenced by factors like clock skew, silence suppression, and echo cancellation behavior of the end points [WJS03] and on the specific codec, loss concealment, loss correction and playout schemes used. A mouth-to-ear delay less than 150 ms is considered acceptable for most VoIP [G.103] applications. However, if this delay is greater than 400 ms, then most end-users are dissatisfied with the service. In [MTK03] the Emodel was used to translate Internet measurements to VoIP mean opinion score (MOS). MOS is widely used as a metric to rate voice calls. MOS ranges from 0 to 5 with 5 being the best possible. A MOS below 3.6 is considered unacceptable for toll quality. Internet measurements were conducted over 43 different backbone paths in the United States continuously for a period of about 3 days. Loss durations varied from 10 ms to 167 seconds on these paths. Periods of high mean delay lasting from several seconds to several minutes were also observed on some paths. The MOS drops below 3.6 when the delay increases for all three playout delay techniques studied in [MTK03]. The findings of [WJS03] indicate that although voice services can be adequately provided by some ISPs, a significant number of backbone paths lead to poor performance. A

similar measurement study was reported in [CBD02]. But unlike the previous study, IS-IS protocol messages were also recorded to correlate route changes to drops in voice quality. One of the route change events reported in this work caused intermittent periods of 100% packet loss for about 50 minutes. One of the 100% packet loss events lasted for 12 minutes. The intermittent loss periods were attributed to router operating system problems and to the router not setting the "infinity hippity cost" bit which caused the other routers to send packets to the faulty router even when it did not know the route to the destination. Similar findings are reported in [CJT04], [TKM98] and [JJG04].

Effects of jitter and packet loss on perceptual quality of video were studied in [CT99]. Five traces were used in this study: perfect (no loss and no jitter), low loss (8% loss rate), high loss (22% loss rate), low jitter and high jitter (3 times the jitter in low jitter trace). To evaluate the perceptual quality, the authors in [CT99] used the quality opinion score in which subjects were asked for an explicit rating after watching the video clips. Test subjects entered their evaluations by means of a slider with values ranging from 1 (worst) to 1000 (best). In [CT99] the perceptual quality drops by over 50% in the presence of jitter or loss.

Several studies on multiplayer interactive network games found that end-to-end delays greater than 200 ms are "noticeable" and "annoying" to end-users of these games [NC04] [PW02] [BCL$^+$04]. While users of strategy games are more tolerant to latency, even modest delays of 75-100 ms are noticeable in first person shooter and car racing games [BCL$^+$04], [NC04]. From the above discussion it is clear that losses and significant deviations in latency may cause observable impairments to occur in all types of RTM applications. While a small number of losses or latency deviations may be tolerable (because of loss concealment and

forward error correction), a large number of consecutive losses or delay events will cause observable impairments. In [ABBM03] degradations were defined to be losses or significant deviations in RTT. Statistics of degradation events observed in the measurements were reported and methods to predict degradations were also presented. However, degradations were not defined the same way as impairments that will be observable to end-users.

Efforts by the IP performance metrics working group has lead to the development of loss distance and loss period metrics [KR02]. Events that have a loss period longer than some threshold may be classified as impairments. A impairment metric for RTM application users was introduced in [Fro03], where the time between congestion events was predicted and used to indicate the time between user-perceived impairments.

1.5 Main contributions

The main contributions of this dissertation are summarized below.

1. New methods for detecting RTM impairment events. Burst loss, disconnect, random loss and delay RTM impairments are defined in this dissertation. Also, methods to detect these impairments from end-to-end measurements are developed and evaluated using PlanetLab data.

2. New heuristics based methods for detecting congestion events. Two new methods for detecting congestion events are proposed and evaluated using PlanetLab measurements in this dissertation.

3. New heuristics based method for detecting route changes. A new heuristics based method for route change detection is also proposed and evaluated

using PlanetLab measurements. It is observed that this heuristics based route change detector is able to detect both layer 2 and layer 3 route changes.

4. Model-based optimal route change detector. Developed optimal model-based detector (parameter aware detector (PAD)) and analysed its performance. Although this detector may not be realizable in practice, the analysis developed here can be used to predict the best possible performance and then the performance of any detector can be compared to this performance to determine how far it is from the ideal.

5. Model-based parameter unaware detector (PUD). Developed a practical implementation of the route change detector based on PAD and determined its performance with respect to the optimal detector.

6. Performance comparison of various route change detectors. Extensive simulations were conducted to compare the performance of the three route change detectors: PAD, PUD and heuristics-based detectors. It is found that the acceptable performance region of PUD is bigger than that of the heuristics based detector. The PAD (or the ideal detector) has the biggest acceptable performance region amongst all three detectors as expected.

7. New scheduler. Another important contribution of this work is the finding that the widely deployed proportional fair (PF) scheduler causes RTM impairments. A new scheduler that mitigates the starvation and therefore the RTM impairment problem of the PF scheduler is proposed and evaluated in this dissertation.

1.6 Organization

This dissertation is organized as follows. Heuristics based methods for detecting RTM impairment events are developed in Chapter 2. Heuristic methods for detection the causes of RTM impairments namely congestion and route changes are also developed in Chapter 2. These methods are then evaluated using PlanetLab measuerements in Section 2.4. The PlanetLab measurements were conducted for about 26 days on 9 different node pairs. On two paths, congestion persisted for six to eight hours during the day on weekdays. A total of 96 layer 2 route changes were manually found in the traces. The heuristics based route change detector was able to detect 71.8% of these route changes. Four events detected by the heuristics based route change detector were false alarms. The performance of heuristics-based detector can be improved by using model-based detectors. The parameter aware detector (PAD) or the ideal detector and its practical implementation, namely the parameter unaware detector (PUD) are introduced in chapter 3. The analysis that can be used to predict the probabilities of detection and false alarm for the PAD is also developed in Chapter 3. This analysis is validated using simulations in Chapter 4. This analysis is then used in Chapter 4 to define the parameter space over which PAD has acceptable performance (defined here as a probability of detection (P_D)$\geq$ 0.999 and probability of false alarm (P_F)$\leq$0.001). Performance of the practical implementation of the ideal detector, i.e., PUD, is presented in Chapter 5. It is shown using receiver operating characterisitics that PUD performs poorly as compared to the ideal detector PAD. Also, extensive simulations were conducted to map the parameter space over which PUD and heuristics-based detectors have acceptable performance. These acceptable performance regions for all three detectors are presented in Chapter 5 and it is shown

that PAD has the biggest acceptable performance region followed by PUD and then by the heuristic detector. Finally, in Chapter 5, PUD is applied to RTT traces from PlanetLab. Finally, it is shown in Chapter 6 that the widely deployed proportional fair scheduler can cause RTM impairments. It is shown using both in laboratory and in deployed commercial 1xEVDO networks that RTM impairments are induced by this scheduler. A new scheduler that mitigates the starvation problem is proposed and evaluated using simulations in Chapter 6. Conclusions and future work are discussed in Chapter 7.

Chapter 2

Detection of RTM Impairment, Route change and Congestion Events

2.1 Introduction

Ad hoc methods for detecting user-perceived impairment events from end-to-end observations have been developed and are presented in Section 2.2. These are followed by methods for detecting congestion and route change in Section 2.3. Two procedures for detecting congestion from RTT and packet loss observations are discussed. Finally, Section 2.4 presents end-to-end measurement that were conducted using the Planet-lab infrastructure for about 26 days on 9 different node pairs. Statistics of the observed impairment, congestion and route change events are discussed here. Most of the ad-hoc methods presented in this section are reported in [BJFD05].

2.2 Detecting user-perceived impairment events

Effective quality of service (QoS) metrics must relate to end-user experience. For real-time multimedia (RTM) services these metrics should focus on phenomena that are observable by the end-user. Long bursts of packet losses, high delays and a high random packet loss rate are all observable impairments. Metrics such as long term average delay, loss and jitter may have little direct meaning to end-users of rapidly changing multimedia applications because knowledge of the specific coding, adaptive playout and PLC techniques is required to translate delay and loss into the user-perceived performance. A user-perceived impairment event as defined here will impact the customer's QoS independent of the specific coding mechanism or of attempts to mask and/or adaptively compensate for its effects. The QoS metric, that is a rate of user-perceived impairment events, is easily understood by end-users and captures the network performance that is observable by network customers. Impairments arise from a variety of phenomena including long bursts of packet losses, random packet losses and high delays. These anomalous connection states are discussed below along with methods to detect them from end-to-end observations.

2.2.1 Burst loss state

Long bursts of packet losses are known to be present in the Internet [BSUB98] [MT00] [JS00]. While loss concealment and channel coding techniques can improve overall performance in some cases, long sequences of packet losses causes a significant impairment. For example, when using the G.723.1 recommendation for compressed voice over IP networks (VoIP), only slight static and clipping result from one-to-four consecutive packet losses. However longer bursts of packet losses

will significantly degrade the QoS delivered to the user. PLC and channel coding techniques attempt to hide the impact of a small number of losses. However, these techniques do not work when a large number of consecutive VoIP packets are lost. Thus, an impairment event occurs when a large number of consecutive packets are lost. When all transmitted probe packets are lost for more than ξ (e.g., $\xi = 6$) seconds (but less than ψ seconds (Section 2.2.2)) then the connection is in the burst loss state.

2.2.2 Disconnect state

When all transmitted consecutive packets are lost for a very long period, then an event of a different nature (e.g., other than congestion) is directly responsible for the losses. If all transmitted probe packets are lost for ψ or more seconds (e.g., $\psi = 300$) then the connection is defined to be in the disconnected state. Such outages can be caused by failures at the edge or in the core of the network [YT03]. Failures can be caused by many events, e.g., scheduled maintenance, loss of power, fiber cut, hardware failure, malicious attack, software bugs, configuration errors etc. [Don01] [Gil03] [LAJ98]. At the edge, where the end customer connects to its service provider, traffic cannot be routed around the failure and the outage persists until the problem is resolved. In the core, traffic can be routed around the failure but routing protocols take from several seconds to several minutes to converge [LABJ00]. In the meantime, routing errors occur, causing outages for the end-user.

2.2.3 High random loss state

While long bursts of losses definitely cause user-perceived impairments, perceived quality also drops as random loss rate increases [JBG04]. The minimum loss rate at which perceived quality becomes unacceptable for a majority of the users depends on the coding and loss concealment technique in use. For RTM applications, channel coding is typically used in terms of block codes [WHZ00]. Specifically, for video streams a block code (e.g., Tornado code) is applied to a segment of k packets to generate a n packet block, where $n > k$. The channel encoder places k packets in a group and creates additional packets from them so that the total number of packets is n. This group of packets is transmitted to the receiver, which receives K packets ($n - K$ packets are lost). To perfectly recover a segment, a user must receive at least k packets (i.e., $K \geq k$) in the n packet block. If more than $n - k$ packets are lost then channel coding cannot recover any portion of the original segment. Some video coders adaptively increase $n - k$ when the packet loss rate is high. However, $n - k$ cannot be made arbitrarily large because coding delay and required capacity also increase with an increase in n. Moreover, many transport protocols decrease the rate when packet loss rate increases (to avoid congestion collapse) [FHPW00]. In this work, if the random packet loss rate is greater than some fixed threshold, then an impairment event is determined to have occurred.

For random losses, i.e., non consecutive losses, let the threshold packet loss probability be τ. Then, if loss probability is greater than τ it can be inferred that the connection is in high random loss state. The procedure to detect high random loss state is based on the premise that at least M (e.g., $M = 10$) loss events are needed to obtain an acceptable estimate of loss probability [SB88], i.e.,

for the standard deviation of the estimate for the loss probability to be on the order of 0.1×(loss probability) approximately 10 loss events must be observed. In this algorithm, the trace is scanned for packet losses in an increasing order of sequence numbers until M loss events are found. Loss probability is then inferred from the distance between first and M^{th} lost packet's sequence numbers. If the first and M^{th} lost packets are very far apart then loss probability is low. If the losses are close to each other then loss probability is high. A threshold distance $\zeta = \lfloor \frac{M}{\tau} \rfloor$ corresponds to loss probability τ. If the difference between M^{th} lost packet's sequence number and first lost packet's sequence number is greater than ζ, then loss probability is less than τ; otherwise if this difference is less than ζ, then loss probability is greater than τ. When the loss probability is greater than τ, connection is in high random loss state. The above procedure to detect high random loss state is then repeated for 2^{nd} and $(M+1)^{th}$ lost packets, 3^{rd} and $(M+2)^{th}$ lost packets and so on.

VoIP MOS is a function of loss probability and it decreases as random loss probability increases. It is evident from the discussion in [MTK03] that the shape of the MOS curve depends on a number of factors such as codec used, PLC technique used and whether packet losses are bursty or uniform. For most codecs and packet loss concealment (PLC) techniques, MOS is below 3.6 when random loss probability is greater than 0.1 (see [MTK03]). MOS below 3.6 is considered unacceptable. Three values of τ are evaluated here: $\tau = 0.05$, $\tau = 0.1$ and $\tau = 0.15$.

2.2.4 High delay state

High delays can also cause user-perceived impairments. A mouth-to-ear delay less than 150 ms is considered acceptable for most VoIP [G.103] applications. However, if the mouth-to-ear delay is greater than 400 ms, then most end-users are dissatisfied with the service. For multiplayer interactive network games, end-to-end delays greater than 200 ms are "noticeable" and "annoying" to end-users [BCL+04] [NC04] [PW02]. While end-users of sports and real-time strategy games are more tolerant to latency, even modest delays of 75-100 ms are noticeable in first person shooter and car racing games [BCL+04] [NC04]. RTM applications employ playout delay buffers at the receiver to compensate for network jitter. When the jitter is very high, a large playout buffer is needed to avoid excessive packet losses due to late arrivals. Playout buffer delay however is added to the total delay (e.g., mouth-to-ear delay for VoIP). Thus, when the network jitter is high, playout delay buffer size is increased at the cost of increased total delay. In addition to the playout delay, source/channel coding/decoding delays also contribute to the total delay. In this work, when the sum of mean estimated one-way delay and playout buffer delay are greater than some threshold delay (such that interactivity is impacted), then an impairment event is inferred.

Adaptive playout delay techniques attempt to minimize the playout delay while avoiding excessive packet loss due to late arrival of packets at the receiver [MKT98]. Given the observable RTT data, an estimate is made of the minimum playout delay buffer size that is needed to avoid excessive packet losses. Most adaptive playout schemes will likely have a playout buffer that is larger than this minimum. Since RTT measurements and not one-way delay measurements are collected, it is necessary to first form the one-way delays. Round trip propa-

gation delay is simply the minimum RTT of the current route or $MinRTT$ (more details in the discussion of Congested State). A simplifying assumption is made that the forward and the reverse paths are symmetric and the one-way propagation delay is one half $MinRTT$. Subtracting one-way propagation delay from RTTs gives an approximation for the one-way delays. As is evident, simplifying assumptions are used to form one-way delays from round trip times, however if one-way delays are available the procedure discussed below to estimate minimum playout delay can be applied directly.

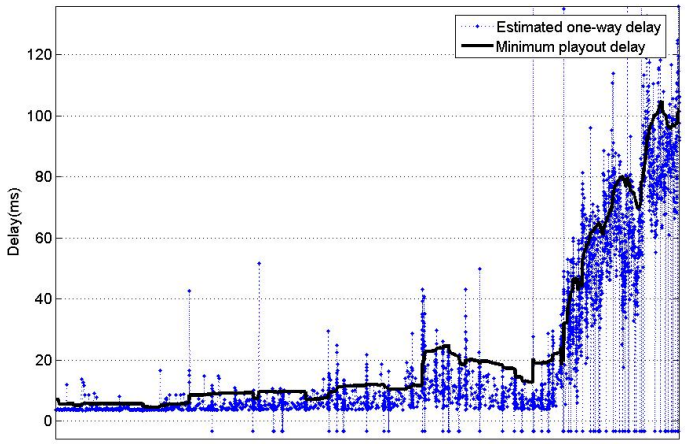

Figure 2.1. Estimated one-way delays and minimum playout delay (planetlab2. ashburn.equinix.planet-lab.org and planet-lab1.comet.columbia.edu in Feb, 2004)

Let the one-way delay estimate for RTT_i be OWD_i and let $jWindow$ be the window size (e.g. 160 samples). Then, M_i^O is the sample mean of all one-way delay samples in a window of $jWindow$ samples and S_i^O is the sample standard deviation, i.e.,

$$M_i^O = \text{mean}\{OWD_{i-jWindow+1}, OWD_{i-jWindow+2}, ..., OWD_i\}$$

$$S_i^O = \text{standard deviation}\{OWD_{i-jWindow+1}, OWD_{i-jWindow+2}, ..., OWD_i\}$$

Then, $M_i^O + S_i^O$ is one possible estimate of the minimum playout delay that is needed to avoid excessive packet losses due to late arrivals. Most playout schemes will likely have a playout delay greater than this minimum. Estimated one-way delays and minimum playout delays are shown in Figure 2.1. When this minimum playout delay exceeds a threshold delay (i.e., $M_i^O + S_i^O > D^{max}$) then it is inferred that interactivity for RTM applications is impacted (regardless of the type of playout scheme really in use) and the connection is defined to be in delay impairment state. To evaluate this approach, three different thresholds for our measurements: 100 ms, 150 ms and 200 ms are evaluated.

2.3 Detecting congestion and route changes

Methods for detecting congestion and route changes from end-to-end observations are presented in this section. The two methods for detecting congestion use RTT and loss information to infer congestion. Only method 1 is used for detecting congestion events from end-to-end measurements collected over Planet-Lab nodes. A new method for detecting route changes using only RTT information is also presented and evaluated using measurements.

2.3.1 Congested state

Congestion is a state of sustained network overload, where demand for resources exceeds the supply for an extended period of time. A congestion event may cause a number of consecutive packet losses. Congestion may also cause the random packet loss rate, mean delay and variation of delay to increase signifi-

cantly, thus resulting in impairment events. When one or more queues in the end-to-end connection are congested, the connection is in a congested state. This section presents two methods for detecting congestion events.

2.3.1.1 Method 1

It is well known that as the load increases, the mean and the variance of waiting times in queue increase. Specifically, for an M/M/1 queuing system [Kle75], the mean and the variance of waiting times in queue are given by:

$$M_W = \frac{\rho}{\mu - \lambda} \qquad \sigma_W^2 = \frac{\rho(2-\rho)}{(\mu-\lambda)^2}$$

where λ is the arrival rate, μ service rate and $\rho = \frac{\lambda}{\mu}$ is the load.
Let the ratio $\eta = \frac{\sigma_W}{M_W}$ (η is the coefficient of variation). Simplifying for η, it follows that

$$\eta = \sqrt{\frac{2-\rho}{\rho}}$$

Solving for ρ, there is the equality

$$\rho = \frac{2}{\eta^2 + 1} \tag{2.1}$$

Thus, given a set of waiting time samples from an M/M/1 queue, ρ can be estimated using the above equation. Clearly, real-world router queues are not accurately modeled as M/M/1 queues. Moreover, waiting time samples from each individual queue along an end-to-end connection are not observable at the end nodes. However, equation (2.1) suggests a decision variable that should be correlated to the congestion along an end-to-end path. The pseudo waiting times are extracted from the RTT samples and used to estimate the value of the decision

variable $\widetilde{\rho}$.

Let RTT_i be the i^{th} RTT sample in ms, then the pseudo waiting time w_i is given by:

$$w_i = RTT_i - MinRTT$$

where $MinRTT$ is the minimum of all RTT samples collected on the current route. Thus, if j and k are sequence numbers where route change events nearest to sequence number i occurred (route change detection is discussed later) and $j < i < k$, then

$$MinRTT = min\{RTT_j, RTT_{j+1}, ..., RTT_{i-1}, RTT_i, RTT_{i+1}, ..., RTT_k\}$$

However, the minimum RTT of the current route computed using the above procedure is not always accurate because of the timing issues on Planet-lab nodes [pla04]. Apparently, the minimum RTT drops to a very low value momentarily during network time protocol (NTP) resynchronization events. To remove these minimum RTT outliers caused by timing mechanisms, all RTT samples are removed that have a value less than a 1 percentile value of RTT samples from the current route. The minimum RTT is then computed using the remaining RTT samples.

The mean and the standard deviation of the waiting times are estimated over a window of $cWindow$ samples.

$$\widetilde{M_i} = mean\{w_i, w_{i-1}, ..., w_{i-cWindow+1}\}$$

$$\widetilde{\sigma_i} = standard\ deviation\{w_i, w_{i-1}, ..., w_{i-cWindow+1}\}$$

Then, the decision variable $\widetilde{\rho}_i$ is formed by

$$\widetilde{\rho}_i = \frac{2}{\widetilde{\eta}_i^2 + 1} \qquad \text{where } \widetilde{\eta}_i = \frac{\widetilde{\sigma}_i}{\widetilde{M}_i}$$

RTTs that are collected over a period of one day are shown along with the decision variable $\widetilde{\rho}$ in Figure 2.2(a). For a period of about 7 to 8 hours during the day, RTT is much longer than the mean RTT of 15 ms. Variation of RTTs and packet loss rate also increase substantially during this period. Possibly, one of the router queues in the end-to-end connection is congested. It is clear from this figure that the decision variable $\widetilde{\rho}$ is correlated with congestion as $\widetilde{\rho}$ is higher during the congestion event.

At first, it might seem that choosing a constant threshold ρ_T and checking for the condition $\widetilde{\rho}_i > \rho_T$ is sufficient to detect congestion. But this method results in many false positives as $\widetilde{\rho}$ is high not only during congestion but also when queues in the end-to-end path are very lightly loaded. This is illustrated in Figure 2.2(b) where RTTs are almost the same. Mean and standard deviation of waiting times are close to zero. However, the decision variable $\widetilde{\rho}$ has a value close to 1 for a significant portion of the trace. This happens because when the queues in the end-to-end path are very lightly loaded, waiting times w are close to 0. In that case, the variation in delay is small (e.g. from processing delays in routers, Ethernet contention delays, etc.). Thus, often $\widetilde{\sigma}$ is less than $\widetilde{M}$, i.e., the ratio $\widetilde{\eta}$ is less than 1 and as a result $\widetilde{\rho}$ is greater than 1.

Therefore, to remove the false positives two more conditions are checked. First, false positives occur when the mean waiting time is small. Thus, if $\widetilde{M}_i < M_T$ (e.g. $M_T = 5$ ms) then the event is a false positive. Second, during congestion when arrival rate exceeds service rate for an extended period of time, packet losses are

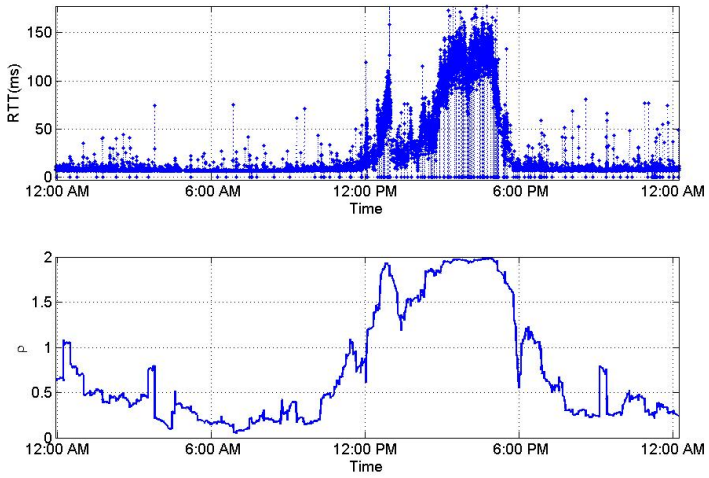

(a) A case where $\widetilde{\rho}$ is high when the load is high (planetlab2.ashburn.equinix.planet-lab.org and planet-lab1.comet.columbia.edu, Feb. 2004)

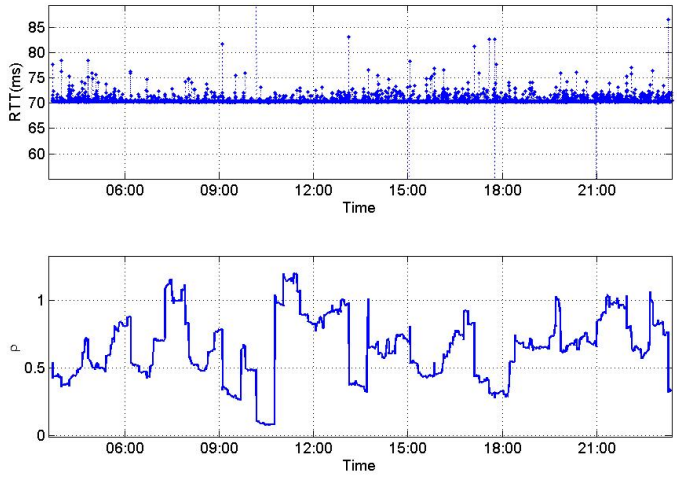

(b) A case where $\widetilde{\rho}$ is high when the load is very low (planet2.berkeley.intel-research.net and planet2.pittsburgh.intel-research.net, August 2004)

Figure 2.2. RTTs and decision variable $\widetilde{\rho}$

observed. Let $\widetilde{L}_i$ be the observed percentage packet loss, i.e.,

$$\widetilde{L}_i = \frac{\text{number of losses from sequence numbers } (i - cWindow + 1) \text{ to } i}{cWindow}$$

If $\widetilde{L}_i < L_T$ (e.g. $L_T = 0.016$) then the event is a false positive.

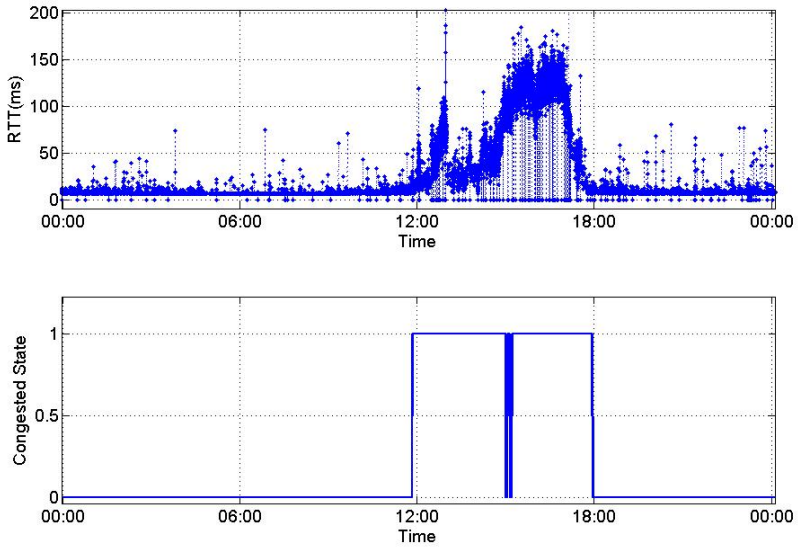

Figure 2.3. RTTs and a congestion event detected using the discussed procedure (planetlab2.ashburn.equinix.planet-lab.org and planetlab1.comet. columbia.edu, Feb. 2004)

To summarize, if $(\widetilde{\rho}_i > \rho_T)$ and $(\widetilde{M}_i \geq M_T)$ and $(\widetilde{L}_i \geq L_T)$ then a congestion event is detected. Figure 2.3 illustrates a congestion event detected using the above procedure with $cWindow$ set to 160 samples and ρ_T set to 0.75.

2.3.1.2 Method 2

The second method for detecting congestion uses an estimate of load of the queue with maximum load amongst all queues in the path[1]. If the load estimate

[1]This method was not included in [BJFD05]

is close to 1 and the loss rate is greater than some threshold, then the connection is in congested state. Load is defined as follows :-

$$\rho = \frac{\lambda}{\mu} = P\,(\text{server is busy})$$

$$\rho = 1 - P\,(\text{server is idle}) \tag{2.2}$$

Equation 2.2 can be used to form an estimate of the load from end-to-end measurements as follows. Let $MinRTT_{cW}$ be the minimum of $cWindow$ RTT samples, i.e.,

$$MinRTT_{cW} = min\{RTT_i, RTT_{i-1}, ..., RTT_{i-cWindow+1}\}$$

Also, let $MinCount$ be the number of RTT samples in the window of $cWindow$ samples, that have a RTT value less than $MinRTT_{cW} + \epsilon$, where ϵ is the error term (e.g., $\epsilon = 0.5ms$). Then it is conjectured that amongst the $cWindow$ RTT samples, $MinCount$ samples found the queue empty on arrival[2]. Then $\frac{MinCount}{cWindow}$ is an estimate of the probability: $P\,(\text{server is idle})$. From Equation 2.2 load can be estimated as follows,

$$\widetilde{\rho} = 1 - \frac{MinCount}{cWindow} \tag{2.3}$$

In the above discussion it is assumed that there is only one queue in the path. However, this method may be used to estimate the load of the queue with maximum load in the path under certain conditions[3]. Note that this load estimation procedure does not assume any traffic model.

[2] ϵ represents the small variable delays like link layer contention delays, processing delays etc.

[3] Future work will include an investigation of these conditions and this could lead to improvements in the load estimation procedure.

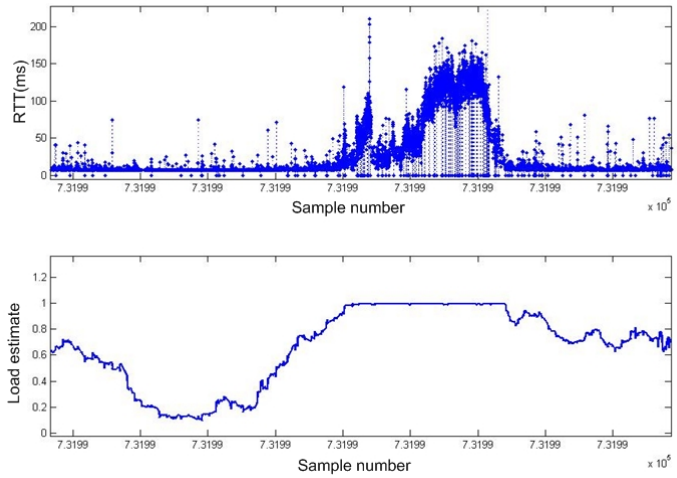

(a) RTT samples and $\widetilde{\rho}$ (planetlab2.ashburn.equinix.planet-lab.org and planetlab1.comet.columbia.edu, Feb. 2004)

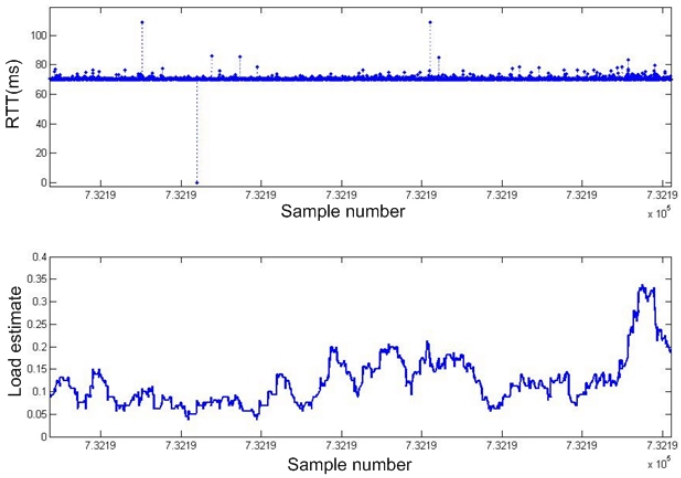

(b) RTT samples and $\widetilde{\rho}$ (planet2.berkeley.intel-research.net and planet2.pittsburgh.intel-research.net, August 2004)

Figure 2.4. RTTs and load estimate $\widetilde{\rho}$

RTTs collected over a period of one day that were shown earlier in Figures 2.2(a) and 2.2(b) are shown again in Figures 2.4(a) and 2.4(b) along with the load estimate $\widetilde{\rho}$. In Figure 2.4(a) mean RTT, variation of RTT and loss rate is very high for a $7-8$ hour period. It is conjectured that one of the queues in the end-to-end path is congested. Note that the load estimate $\widetilde{\rho}$ is very close to 1 during this entire period of time and is less than 0.95 at all other times. Also, in Figure 2.4(b) load estimate $\widetilde{\rho}$ is less than 0.35 for the entire duration of the trace. These plots suggest that to detect congestion, it may be sufficient to compare $\widetilde{\rho}$ to a load threshold (say $\rho_T^{[2]} = 0.98$). However, if events other than congestion cause the RTT variation to increase then the load may be overestimated using this method. To avoid false positives that may be caused by such events, loss rate can also be compared to a threshold loss rate in addition to comparing the load estimate to a load threshold. Thus, the connection is in congested state if $(\widetilde{\rho} \geq \rho_T^{[2]})$ and $(\widetilde{L}_i \geq L_T)$.

2.3.2 Route change state

Layer 3 route changes can be detected by comparing routes returned by traceroute. If the route returned by current traceroute is not the same as the route returned by the previous traceroute then the route changed. Route changes can also be detected by comparing values stored in IP TTL field of arriving probe packets. If the TTL value of arriving packet is different from the TTL value of a packet that arrived immediately before the current packet, then it is inferred that there has been a Layer 3 route change. Since probe packets are sent at a higher rate than traceroute measurements are performed, route changes are detected faster using the TTL change method. However, not all route changes cause a TTL change

(e.g., when the new route has same number of hops as the old route). Layer 3 route changes may also be detected using the minimum RTT change algorithm discussed below.

Layer 2 route changes can also be detected from end-to-end observations using the minimum RTT change algorithm. Figure 2.5 shows the graph of RTTs observed on 12 August, 2004 between planet2.berkeley.interl-research.net and planet2.pittsburgh.intel-research.net. The minimum RTT increases from 68 ms to 75 ms initially and then subsequently decreases to 68 ms. Neither the TTLs nor the routes returned by traceroute changed during this period. Thus, it can be inferred that there was a Layer 2 route change. The algorithm that follows, detects such Layer 2 route changes from the RTT pattern under certain conditions.

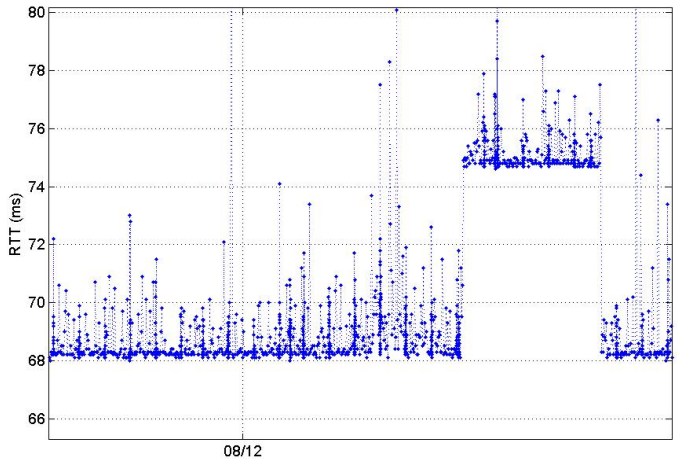

Figure 2.5. Layer 2 route change observed between planet2.berkeley.intel-research.net and planet2.pittsburgh.intel-research.net on 12 August, 2004

First, RTTs are grouped into non-overlapping windows and minimum RTT of each window is calculated. The minimum RTT of the most recent window is then compared to minimum RTTs of previous windows to answer two questions. First,

is the utilization of queues low enough for the Layer 2 route change detection algorithm to work (see Figure 2.6(a))? If the answer to the first question is yes, then second, has the minimum RTT changed? A change in the minimum RTT is either due to a route change or due to random delays possibly arising from queuing (see Figure 2.6(b)). When the minimum RTT changes, the algorithm tries to determine whether or not it was caused by a route change.

Minimum RTT is computed as follows. W is the route change window size, e.g., $W = 40$ samples. i is the sequence number of the most recent RTT sample. S_i is the set of W sequence numbers, $S_i = \{i, i-1, i-2, ..., i-W+1\}$. RTT^{S_i} is the set of W RTT samples: $RTT^{S_i} = \{RTT_i, RTT_{i-1}, RTT_{i-2}, ..., RTT_{i-W+1}\}$. $min[RTT^{S_i}]$ is minimum of all RTTs in the set RTT^{S_i}. Then $min[RTT^{S_i}]$ is the minimum RTT of the current window.

Minimum RTT of the current window is compared to minimum RTTs of the previous windows. The set $prevMins_i$ stores minimum RTTs of previous windows. $numPrevWindows_i$ is the number of windows since the most recent route change. If the most recent route change occurred at sequence number j ($j < i$), then $numPrevWindows_i = \lfloor \frac{i-j+1}{W} \rfloor$. $prevMins_i$ is the set of minimum RTTs of previous $numPrevWindows_i - 1$ windows, i.e.,

$prevMins_i = \{min[RTT^{S_{i-W}}], min[RTT^{S_{i-2W}}], ..., min[RTT^{S_{i-(numPrevWindows-1)W}}]\}$

The first step in the process is to compare the minimum RTT of the current window to minimum RTTs of previous windows to determine whether or not variation in RTTs is low enough for Layer 2 route changes to be detected. Figure 2.6(a) illustrates the case where delay variation is high and Layer 2 route changes cannot be reliably inferred from the observations. $RTT_k = FixedDelay_k + VariableQueuingDelay_k + VariableOtherDelays_k$, where $FixedDelay_k$ is the

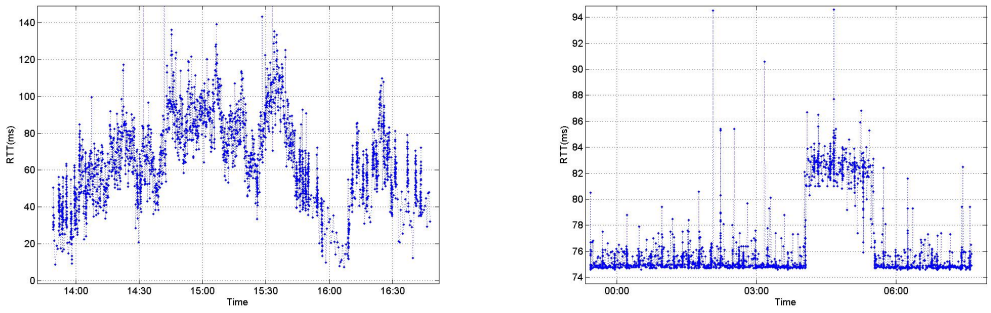

(a) An example case where Layer 2 route changes cannot be detected because queuing delays are very large (ashburn-columbia, Feb. 2004)

(b) An example of minimum RTT change caused by a heavily loaded queue (berkeley-pittsburgh, August 2004)

Figure 2.6. Detecting Layer 2 route changes: special cases

sum of fixed propagation and transmission delays, $VariableQueuingDelay_k$ is the sum of all queuing delays experienced by packet k and $VariableOtherDelays_k$ is the sum of all other variable delays (e.g., link layer contention delay). It is assumed that $VariableOtherDelays_k$ are less than ϵ (e.g., $\epsilon = 0.5$ ms). If all queues in the end-to-end path have low utilization, then it is likely that at least one of the W RTT probe packets experiences zero queuing ($min[RTT^{S_k}] = FixedDelay_m + VariableOtherDelays_m$,$m \in S_k$). In that case, minimum RTTs in the set $prevMins_i$ differ from each other by an amount less than ϵ, i.e., $max[prevMins_i] - min[prevMins_i] < \epsilon$. If however, one or more queues in the end-to-end path have significant utilization then it is likely that none of the W RTT probe packets experience zero queuing ($min[RTT^{S_k}] = FixedDelay_m + VariableQueuingDelay_m + VariableOtherDelays_m$, $m \in S_k$). In that case, minimum RTTs in the set $prevMins_i$ usually have a range greater than ϵ ($max[prevMins_i] - min[prevMins_i] > \epsilon$).

Thus, if $std[prevMins_i] < \epsilon$ then the delay variation is not significant and Layer 2 route changes can be detected. Otherwise one or more queues in the end-

to-end path may be congested and Layer 2 route changes cannot be accurately detected using this approach.

Next, minimum RTT of current window is compared to minimum RTTs of previous windows to determine whether or not the minimum RTT has changed. If either $min[RTT^{S_i}] < (median[prevMins_i] - \epsilon)$ or if $min[RTT^{S_i}] > (median[prevMins_i] + \epsilon)$ then it is inferred that the minimum RTT has changed.

This minimum RTT change is either caused by a route change or delay variation possibly caused by queuing in a heavily loaded router queue. Figure 2.6(b) illustrates minimum RTT change caused by a large delay variation. Minimum RTT changes from 74 ms to a little over 80 ms in this case. If $(median[RTT^{S_i}] - min[RTT^{S_i}]) < \kappa$ (e.g., $\kappa = 1ms$) then it is inferred that the minimum RTT change is caused by a route change. However, it is possible that there is a Layer 2 route change and one of the switches in the new route is heavily loaded. To detect that condition, examine $\gamma \times W$ (e.g.$\gamma = 3$) more RTT samples. If $(median[RTT^{S_i}] - min[RTT^{S_i}]) > \kappa\ ms$ then $\gamma \times W$ more RTT samples are collected before it can be decided whether or not it was a route change that caused the minimum RTT change. Let $n = i + (\gamma \times W)$, where i is the sequence number of most recent RTT probe packet. $S_{i:n}$ is the set of sequence numbers from i to n, i.e., $S_{i:n} = \{i, i+1, ..., n-1, n\}$. $RTT^{S_{i:n}}$ is the set of RTT samples $RTT^{S_{i:n}} = \{RTT_i, RTT_{i+1}, ..., RTT_{n-1}, RTTn\}$. $min[RTT^{S_{i:n}}]$ is the minimum of all RTTs in the set $RTT^{S_{i:n}}$. If for each p, $p \in S^{i:n}$, $min[RTT^{S_p}] \leq (min[RTT^{S_{i:n}}] + \epsilon)$, then it is inferred that the minimum RTT change is caused by a route change. Otherwise it is inferred that delay variation caused the minimum RTT change.

If a route change is detected, routes returned by traceroute and TTLs are compared. If neither traceroutes nor TTLs change, then it is inferred that there

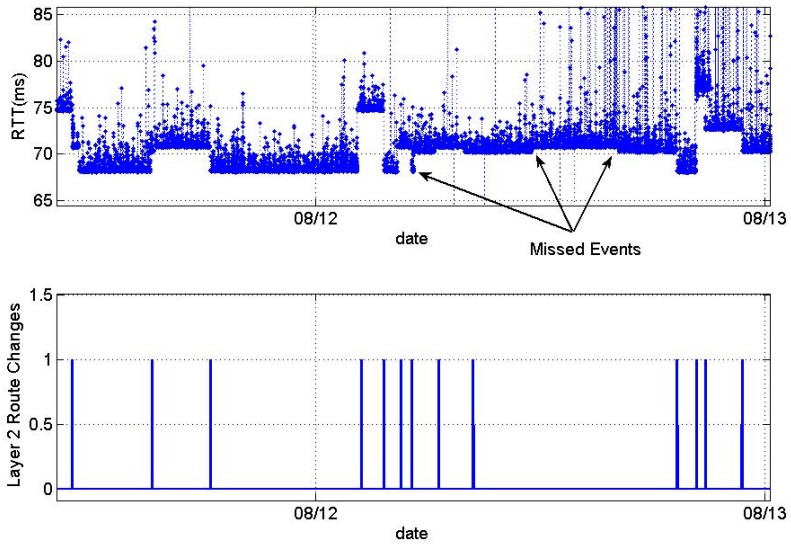

Figure 2.7. Layer 2 route change detected using the discussed procedure (planet2. berkeley.intel-research.net and planet2.pittsburgh.intel-research.net, August 2004)

was a Layer 2 route change. Figure 2.7 illustrates Layer 2 route changes detected using the above procedure. The RTTs were collected in August 2004 between planet2.berkeley.intel-research.net and planet2.pittsburgh.intel-research.net. While the algorithm successfully detected most of the Layer 2 route changes, it failed to detect the three marked as missed events. Note that when the first missed event occurred, very few RTT samples (less than $(\nu + 1) \times W$ samples) were collected since the most recent successfully detected route change. The set $prevMins_i$ should have at least ν (e.g., $\nu = 3$) elements before minimum RTT changes can be detected. Since, less than W RTT samples were collected in the new route before another route change occurred, and since the set $prevMins$ was empty, this route change was not detected. For the second and third missed events, the minimum RTT changed by 0.4 ms and ϵ was set to 0.5 ms. Since the algorithm can detect route changes only when the minimum RTT changes by more than ϵ

ms, these route changes were not detected. In the measurements collected over the Internet for about 26 days on 9 different node pairs, 96 events were manually found by visual analysis of RTT data that looked like route changes. The Layer 2 route change algorithm detected 71.8% of these 96 events. The other events were not detected either because the minimum RTT changed by a value less than ϵ or because after the first route change, very few RTT samples were collected in the new route before the route changed again. The algorithm also generated some false positives (detected a route change when visually we could not find any route changes). About 4% of the detected events were false positives.

The minimum RTT of a path can change not only when there is a Layer 2 route change but also due to a Layer 3 route change. Thus, this algorithm for detecting Layer 2 route changes can also be used to detect Layer 3 route changes. This is useful when administrators restrict ICMP response from routers and traceroute cannot be used to detect Layer 3 route changes. For the measurements that were conducted, Layer 3 route changes detected using the RTT based algorithm were compared with the ones detected using traceroute or TTL changes. For 38.7% of all Layer 3 route changes detected using traceroute or TTL changes, minimum RTT change was not significant (less than ϵ ms) and hence the RTT based algorithm did not detect these route changes. About 38.1% of the Layer 3 route changes detected using traceroute or TTL changes were either preceded by another Layer 3 route change (with less than $\nu \times W$ RTT samples between the two route changes) or followed by another Layer 3 route change (with less than W RTT samples between the two route changes). These route changes were also not detected by the RTT based algorithm. We expect the proposed RTT based algorithm to detect a Layer 3 route change when there are enough RTT samples

and the change in RTT is significant; in those cases the technique detected 89.7% of the route changes. The algorithm missed 10.3% of those Layer 3 route changes. Future work could lead improvements in the algorithm to increase the probability of detecting route changes.

2.4 Measurement results

End-to-end measurements were conducted for 26 days on 9 different end-node pairs connected to the Planet-Lab infrastructure. This section discusses the characteristics of impairment events that were observed in these measurements. Paths on which congestion events were observed had a large number of high random loss and burst loss events. Congestion events were observed on two out of the nine pairs[4]. Characteristics of these congestion events are discussed. Layer 3 route changes were observed on all the 9 pairs and Layer 2 route changes on 6 pairs.

Table 2.1 lists the location of end nodes, dates and number of days on which data was collected. Node pairs for which both end nodes are within the United States are labeled DC (for Domestic-Commercial) since at least one of the two end nodes is a non-Internet2 node. When both end nodes are Internet2 nodes (nodes in a university or a research center), then traffic is routed through Internet2 routers that have a very low load. For this reason, only pairs were used for which at least one node is a non-Internet2 node. Node pairs labeled I (International) have either one or both end nodes outside the United States. There is 21 days of data for node pairs DC1 and I2, 24 days for DC2 and 26 days for the remaining node pairs.

Statistics of all detected impairment events are listed in Table 2.2. Rate of

[4]Method 1 was used to detect congestion

Table 2.1. Measurement sites, dates and number of days on which data was collected

Label	Node pair	Dates	Number of days
DC1	Ashburn(Virginia) planetlab2.ashburn.equinix.planet-lab.org - Columbia Univ. (New York) planet-lab1.comet.columbia.edu	Feb. 6 to Feb. 27, 2004	21
DC2	Columbia Univ. (New York) planet-lab2.comet.columbia.edu - Sanjose (California) planetlab2.sanjose.equinix.planet-lab.org	Feb. 18 to Feb. 27; March 5 to March 18, 2004	10 14
DC3	Berkeley (California) planet2.berkeley.intel-research.net - Pittsburgh (Pennsylvania) planet2.pittsburgh.intel-research.net	Aug 8 to Sep 2, 2004	26
DC4	Seattle (Washington) planet1.seattle.intel-research.net - Santa Clara (California) planetlab-2.scla.nodes.planet-lab.org	Aug 8 to Sep 2, 2004	26
DC5	Seattle (Washington) planet2.seattle.intel-research.net - Sterling (Virginia) planetlab-2.stva.nodes.planet-lab.org	Aug 8 to Sep 2, 2004	26
I1	Cambridge (United Kingdom) planetlab1.cambridge.intel-research.net - Berkeley (California) planet1.berkeley.intel-research.net	Aug 8 to Sep 2, 2004	26
I2	Athens (Greece) planet-lab1.cslab.ece.ntua.gr - Cornell Univ. (New York) planetlab1.cs.cornell.edu	Aug 13 to Sep 2, 2004	21
I3	Zurich (Switzerland) planetlab02.ethz.ch - Copenhagen (Denmark) planet-lab1.diku.dk	Aug 8 to Sep 2, 2004	26
I4	Durham (North Carolina) planet-lab1.cs.duke.edu - Taipei (Taiwan) plan-etlab1.iis.sinica.edu.tw	Aug 8 to Sep 2, 2004	26

impairments is higher for DC1 and DC2 than for the rest of the pairs. For DC1 and DC2, impairment events occur at an average once every five hours or less. For all other pairs except I1, mean time between events is more than 60 hours. Mean duration of impairment events that occur in DC1 and DC2 is also longer than the mean duration of events in other paths. Mean duration of events for DC1 and DC2 ranges from 35 minutes to 92.5 minutes, while the mean duration of impairments for the other sites ranges from 4 minutes to 28 minutes. No impairments were observed on I4. Mean duration of impairment events for all sites combined is 40 minutes and mean time between impairment events is 9.8 hours.

Table 2.2. Statistics of user-perceived impairments

Data Set	Mean duration of impairments (minutes)	Mean time between impairments (hours)	Mean number of impairments per day
DC1	35.9	3.52	7
DC2 (Feb)	92.5	5.22	4
DC2 (March)	37.3	4.95	4.78
DC3	9.7	62.97	0.23
DC4	4.4	89.44	0.115
DC5	15.61	268	0.004
I1	14.5	15.2	1.38
I2	28.4	121.17	0.19
I3	4.62	122.47	0.15
I4	-	-	0

Table 2.3 lists the observed mean number of burst loss events, high random loss events (loss probability > 0.05), congestion events and delay impairment (>100 ms) events per day for each data set. Congestion and high random loss events occurred only in data sets DC1 and DC2. Mean number of burst loss events per day in DC1 and DC2 are greater than number of burst loss events in other data sets.

Table 2.3. Mean number of loss, congestion and delay impairment events per day

Data set	Mean number of burst loss events per day	Mean number of high random loss events (loss rate>5%) per day	Mean number of congestion events per day	Mean number of delay impairment (100 ms) events per day
DC1	7	6.7	2.5	2.28
DC2	1.125	4.08	1.66	2
DC3	0.11	0	0	0.07
DC4	0	0	0	0.07
DC5	0	0	0	0.07
I1	0.8	0	0	1.57
I2	0	0	0	4.76
I3	0.07	0	0	3.42
I4	0	0	0	0

An interesting trend is observed in both data sets DC1 and DC2. Connection state alternates between congested and normal states for six to eight hours during day time on weekdays. This is illustrated using one week of data from DC1 in Figure 2.8 (day labels on time axes correspond to start of that day). Except for Sunday night, congestion events started at about 11 AM and lasted until 6 or 7

PM on weekdays. On this particular week, congestion events were also observed on late Sunday night and early Monday morning. Histograms of duration and time between congestion events for DC1 and DC2 are shown in Figures 2.9(a) and 2.9(b). Mean duration of congestion is 42.6 minutes and mean time between congestion events is 4.4 hours.

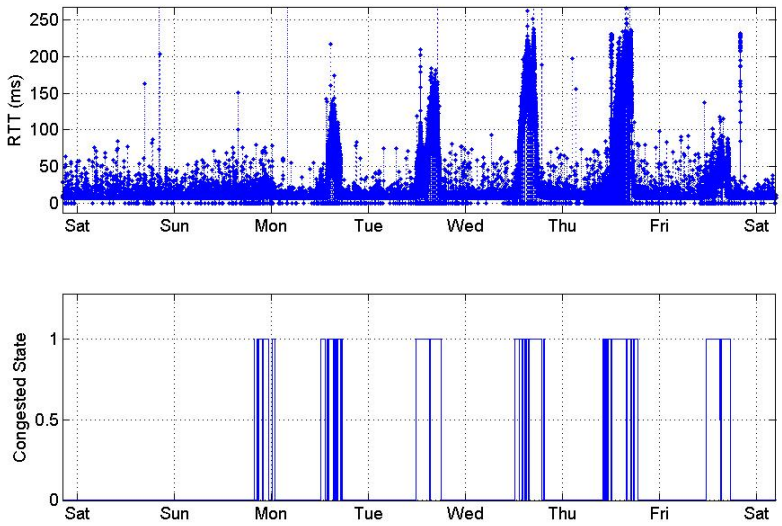

Figure 2.8. Congestion events observed over a period of one week (DC1)

For DC1 and DC2, burst loss, high random loss and high delay impairments occurred when the connection was in congested state. For DC1, delay and random loss impairments occurred for 59.2% of the time while connection was in the congested state. For DC2, impairments occurred for more than 90% of the time the connection was in the congested state. Table 2.4 lists the impairment time during which the connection is not in the congested state. It is clear that most of the delay and high random loss impairments in DC1 and DC2 occur when the connection is in the congested state. From a total of 174 burst loss events that occurred in DC1 and DC2, 61% occurred when the connection was in the congested

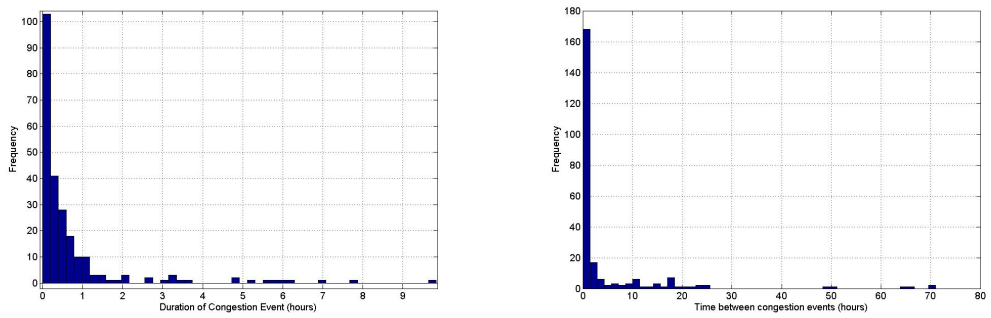

(a) Histogram of duration of congestion events (b) Histogram of time between congestion events

Figure 2.9. Duration and time between Congestion events on DC1 and DC2

state. Mean time between burst loss events that occur when the connection is in the congested state is 14 minutes and the mean duration is 22.64 seconds. About 75% of all burst loss events that occur when the connection is in the congested state are less than 8 minutes apart and 50% are less than 2.5 minutes apart. Therefore impairments are more likely to occur when the connection is in the congested state as defined here.

Table 2.4. Percentage of impairment state time during which connection was not in congested state

Impairment	DC1	DC2(Feb)	DC2(March)
High random loss	46.4	23.4	48.1
High delay	19.9	11.2	17.7

Mean and standard deviation of duration and time between high random loss, delay impairment and congestion events are listed in Table 2.5. These statistics were computed using data from all the nine node pairs. But since congestion and high loss events occur only in data sets DC1 and DC2, mean and standard deviation for these events were computed using data only from data sets DC1 and DC2.

Table 2.6 lists the mean number of Layer 2 and Layer 3 route changes per day

Table 2.5. Mean and standard deviation of duration and time between events

Event	Mean duration (minutes)	St. dev. of duration (minutes)	Mean time between events (minutes)	Std. dev. of time between events (minutes)
Congestion	42.63	82.3	264	648
High random loss (5%)	119.8	180.8	666	822
High random loss (10%)	45.16	58.32	522	1206
High random loss (15%)	13.9	38.1	355.2	1128
Delay impairment (100 ms)	37.07	76.9	685.8	2063.4
Delay impairment (150 ms)	39.06	120.85	2295.6	4434
Delay impairment (200 ms)	24.99	16.42	4222.2	5987.4

for all the data sets. The CDF of time (in hours) between Layer 3 route changes is shown in Figure 2.10(a). About 80% of all Layer 3 route changes are less than 45 minutes apart and mean time between Layer 3 route changes is 7.23 hours. Figure 2.10(b) shows the histogram of time (in seconds) between Layer 3 route changes. About 18% of all Layer 3 route changes are 1 second apart and about 15% are 2 seconds apart. These are caused by frequent route changes that occur when routers are trying to converge to a new route. Since the measurement client sent probe packets once every second on detecting a TTL change, frequency of 1 and 2 second times is high in the histogram. Histogram of time (in hours) between Layer 2 route changes is shown in Figure 2.11. Time between route changes for about 40% of Layer 2 route changes is less than 3 hours. Mean time between Layer 2 route changes is 58.22 hours.

Since route changes occur when a network component fails, they are often preceded by packet losses. About 8% of all Layer 3 route changes were preceded by burst or disconnect loss events. Mean duration of loss events that precede Layer 3 route changes is 113.5 seconds. This is about five times the mean duration of burst

Table 2.6. Observerved number of route changes per day

Data set	Mean number of Layer 2 route changes per day	Mean number of Layer 3 route changes per day
DC1	0	0.428
DC2	0.041	4.08
DC3	0.69	2.76
DC4	0	1
DC5	0.34	0.115
I1	0.23	5.84
I2	0.095	1.14
I3	0	3.8
I4	0.146	3.76

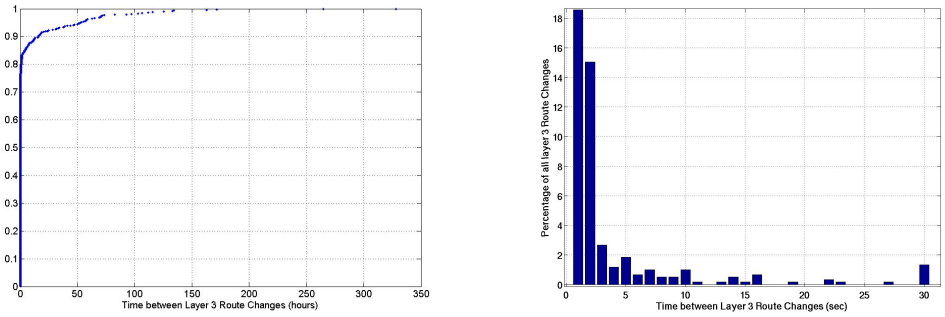

(a) CDF of time between Layer 3 route changes (b) Histogram of time between Layer 3 route changes

Figure 2.10. Time between Layer 3 route changes

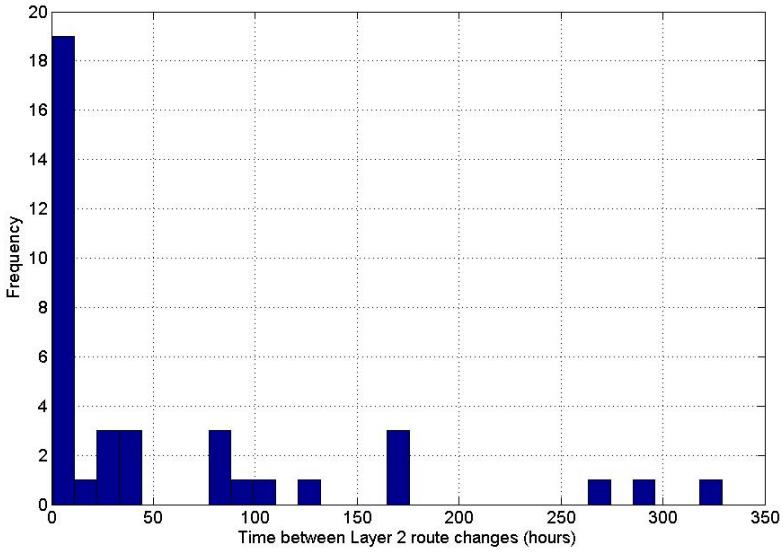

Figure 2.11. Histogram of time between Layer 2 route changes

loss impairment events that occur during the congestion state (22.64 sec). Mean time between burst loss events that precede Layer 3 route changes is more than 7.23 hours while the mean time between burst loss events during congestion was only 14 minutes. No correlation between Layer 2 route changes and packet losses was observed. The fact that there were no burst or disconnect loss events preceding Layer 2 route changes reinforces the idea that Layer 2 restoration is faster than restoration at Layer 3. Histogram of duration of the loss events preceding a Layer 3 route change are shown in Figure 2.12. Maximum duration for which there were packet losses before a route change event is 5.45 minutes.

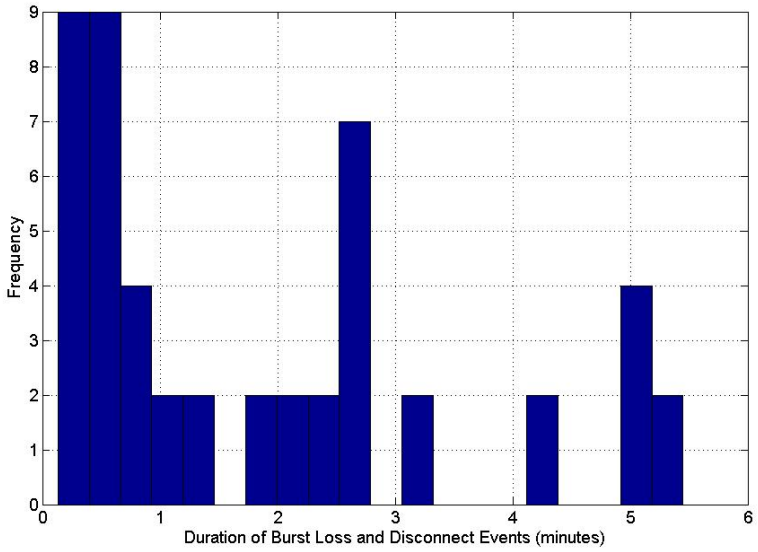

Figure 2.12. Histogram of duration of burst loss and disconnect events that precede Layer 3 route changes

A total of seven disconnect events were observed. For five out of the seven disconnect events at least one traceroute was performed during the disconnect event. Examination of these traceroutes reveals that in all five cases the problem was in a router 3 or 4 hops from one of the end nodes. Either there was a routing loop or traceroute packets did not return from the problem router. The two

disconnect events for which traceroute was not performed during the disconnect event occurred during congestion. Figure 2.13 illustrates one of the two events. The other disconnect event looks similar to this one. At approximately time 14:00, a disconnect event occurred. Since mean delay drops substantially after the disconnect event (and slowly starts increasing again), it seems that the disconnect event occurred due to a problem in the congested router. Although no traceroutes were performed during the disconnect event, the TTL changed for the first two packets that were sent immediately after the disconnect event.

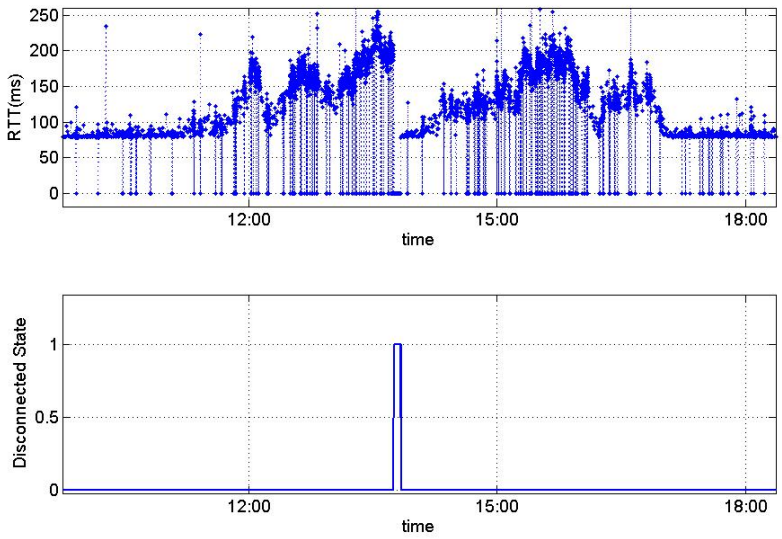

Figure 2.13. Disconnect event due to problem in congested router

2.5 Conclusion

Methods for detecting user-perceived impairment events from end-to-end observations were presented in this chapter. Also, ad hoc techniques for detecting congestion and route changes were presented. In the measurements conducted

using the Planet-Lab infrastructure, it was observed that the route change detection algorithm detected about 71% of all layer 2 route changes. The accuracy of the ad hoc algorithms discussed in this chapter may be improved by using the model-based approach. Model-based algorithms for detecting route chages are presented in the next few chapters. It will be shown in the next few chapters that the model-based route change detection algorithm has acceptable performance for a larger region of the parameter space than the heuristics based route change detection algorithm.

Chapter 3

Model-Based Approach: Analysis

3.1 Introduction

A heuristic algorithm for detecting route changes from the RTTs was proposed and applied to trace data in Chapter 2. Although this algorithm successfully detected a large percentage of the visible route changes, the heuristic nature of this algorithm precludes the prediction of the expected probabilities of false alarm and detection. Moreover, this algorithm's performance cannot be quantifiably tuned. The probabilities of false alarm and detection measured in Chapter 2 by applying the detection algorithm on the PlanetLab data are not representative of this detection algorithm's performance in general. The heuristic detection algorithm's performance depends on the RTTs and the values of its parameters and a user cannot predict the false alarm and detection probability when this algorithm is applied on a given data.

This chapter proposes a new model-based algorithm for detecting route changes whose performance can be predicted. Here RTTs are modeled using a Gamma distributed random variable (as suggested in [Muk92]). A likelihood ratio pro-

vides the foundation for the proposed algorithm. Here, a hypothesis test is used to determine which of the two alternatives (route change or no route change) is true when presented with real data. This algorithm for detecting route changes is named the parameter unaware detector (PUD) because the parameters of the associated Gamma distributions are not known. PUD estimates these parameters from the RTT samples and then uses these estimates in the likelihood ratio test to detect route changes. Closed form expressions that define the PDF of the likelihood ratio under each of the two hypothesis are needed to predict the probabilities of false alarm and detection. Since PUD uses the estimates of the Gamma distribution parameters in the likelihood ratio test (and not the actual parameters), it is difficult to derive closed form expressions for PDF of likelihood ratio and thus predict its performance. Instead of deriving an expression for PDF of likelihood ratio for PUD, the approach used in this dissertation is to derive expressions for PDF of likelihood ratio of the parameter aware detector (PAD). Here the values of the parameters of the associated distribution are assumed to be known. It is expected that the performance of PUD as a function of the parameters will follows the same trends as performance of PAD. Also, the PAD is the optimum detector in the likelihood ratio sense and thus provides the theoretical upper bound for the performance of any detection algorithm. Any detection algorithm proposed in the future can be compared to PAD. Deriving the performance of the optimum detector which provides the performance bound for all algorithms is one of the contributions of this research. PUD is discussed in section 3.2 followed by PAD in section 3.3. Expressions for the first two moments of the likelihood ratio for PAD are also obtained in this chapter in sections 3.4 and 3.5. Chapter 4 illustrates how these expressions for the first two moments of the likelihood ratio combined with

a distribution assumption can be used to predict the probabilities of detection and false alarms.

3.2 Parameter unaware detector

Round trip time (t) can be modeled by the Gamma distributed random variable [Muk92] that has the following PDF,

$$f_T(t|\alpha,\beta,\gamma) = \begin{cases} \frac{1}{\Gamma(\alpha)\beta^{\alpha}}(t-\gamma)^{(\alpha-1)}e^{-\frac{(t-\gamma)}{\beta}} & \text{if } \gamma \leq t < \infty \\ 0 & \text{otherwise} \end{cases} \tag{3.1}$$

Given n samples $(t_1, t_2, ..., t_n)$, the problem is to determine whether or not there was a route change when these n samples were collected. Let the composite[1] null hypothesis H_0 be that all n samples are drawn from Gamma distributed random variable with parameters α_0, β_0 and γ_0. Also, let the alternative composite hypothesis H_1 be that the first $\lfloor \frac{n}{2} \rfloor$ samples are drawn from a Gamma distributed random variable with parameters α_1, β_1 and γ_1, and the last $\lceil \frac{n}{2} \rceil$ samples are drawn from a Gamma distributed random variable with parameters α_2, β_2 and γ_2. Since the parameters α_0, β_0, γ_0, α_1, β_1, γ_1, α_2, β_2 and γ_2 are not known, they have to be estimated first before the likelihood ratio test can be used. Parameter $\hat{\gamma_0}$ is simply the minimum of n samples. Parameters $\hat{\alpha_0}$ and $\hat{\beta_0}$ are estimated from all n samples by using the iterative maximum likelihood estimation method ([MEP93], [Law82], [ME98]). Similarly, $\hat{\alpha_1}, \hat{\beta_1}, \hat{\gamma_1}$ are the estimates formed using first $\lfloor \frac{n}{2} \rfloor$ samples and $\hat{\alpha_2}, \hat{\beta_2}, \hat{\gamma_2}$ are the estimates formed using last $n - \lfloor \frac{n}{2} \rfloor$ samples.

[1] The hypothesis is composite because values of the parameters are not known.

Likelihood ratio L is then defined as follows

$$L = Log \frac{\prod_{i=1}^{n} f_T(t = t_i|\hat{\alpha_0}, \hat{\beta_0}, \hat{\gamma_0})}{\prod_{i=1}^{\lfloor \frac{n}{2} \rfloor} f_T(t = t_i|\hat{\alpha_1}, \hat{\beta_1}, \hat{\gamma_1}) \prod_{i=\lfloor \frac{n}{2} \rfloor + 1}^{n} f_T(t = t_i|\hat{\alpha_2}, \hat{\beta_2}, \hat{\gamma_2})} \tag{3.2}$$

where $f_T(t = t_i|\hat{\alpha_0}, \hat{\beta_0}, \hat{\gamma_0})$ represents the value obtained by evaluating the function in Equation 3.1 at t_i. Since $t_i \geq \hat{\gamma_0}, \forall i \in \{1..n\}$; $t_i \geq \hat{\gamma_1}, \forall i \in \{1..\lfloor \frac{n}{2} \rfloor\}$ and $t_i \geq \hat{\gamma_2}, \forall i \in \{\lfloor \frac{n}{2} \rfloor + 1..n\}$, Equation 3.2 can be rewritten as follows: -

$$L = Log \frac{\left(\frac{1}{[\Gamma(\hat{\alpha_0})]^n \hat{\beta_0}^{n\hat{\alpha_0}}} \prod_{i=1}^{n} (t_i - \hat{\gamma_0})^{(\hat{\alpha_0}-1)} e^{-\frac{(t_i - \hat{\gamma_0})}{\hat{\beta_0}}} \right)}{\left(\frac{1}{[\Gamma(\hat{\alpha_1})]^{\lfloor \frac{n}{2} \rfloor} \hat{\beta_1}^{\lfloor \frac{n}{2} \rfloor \hat{\alpha_1}}} \prod_{i=1}^{\lfloor \frac{n}{2} \rfloor} (t_i - \hat{\gamma_1})^{(\hat{\alpha_1}-1)} e^{-\frac{(t_i - \hat{\gamma_1})}{\hat{\beta_1}}} \right) \times \left(\frac{1}{[\Gamma(\hat{\alpha_2})]^{\lceil \frac{n}{2} \rceil} \hat{\beta_2}^{\lceil \frac{n}{2} \rceil \hat{\alpha_2}}} \prod_{i=\lfloor \frac{n}{2} \rfloor + 1}^{n} (t_i - \hat{\gamma_2})^{(\hat{\alpha_2}-1)} e^{-\frac{(t_i - \hat{\gamma_2})}{\hat{\beta_2}}} \right)} \tag{3.3}$$

If the likelihood ratio is greater than some threshold λ then the decision is in favor of H_0, otherwise the decision is in favor of H_1. The model-based detection algorithm discussed above was implemented to determine its utility. RTT samples were generated from a Gamma distributed random variable with parameters: $\alpha = 0.12, \beta = 1.99$. These parameters were estimated from Internet RTT measurements between planck227.test.ibbt.be (Ghent University, Belgium) and planetlab1.larc.usp.br (University of Sao Paulo, Brazil) on October 21, 2006. Minimum RTT is a uniformly distributed random variable between 0 and 10 ms and this minimum RTT was changed once every 200 samples. The detection algorithm discussed above was applied to this data with its window size (n) fixed at 30 samples. Figure 3.1 illustrates that there is a sharp decrease in the likelihood ratio whenever there is a route change. There is a significant change in the likelihood ratio even when the RTT changes by less than 1 ms. All of the route changes in

this example can be detected by choosing a suitable threshold (e.g., $\lambda = -40$). The RTTs shown in Figure 3.1 are not the actual measured RTTs but instead are samples from Gamma distributed model of the measured RTT data. The evaluation procedure described above was repeated with with measured RTTs that were collected between Ghent University, Belgium and University of Sao Paulo, Brazil on October 21, 2006. Since no route changes were observed when this data was collected, route changes were introduced by changing the minimum RTT once every 200 samples. The likelihood ratio decreased sharply during a route change in this case too as illustrated in Figure 3.2. For the first route change visible in Figure 3.2, a minimum RTT change of -0.1ms caused the likelihood ratio to drop to -60. From this preliminary evaluation of the detection algorithm, it is clear that the algorithm is sensitive to minimum RTT changes and can possibly pick up changes as low as 0.1ms for a randomly selected data set of RTTs collected between nodes in Belgium and Brazil.

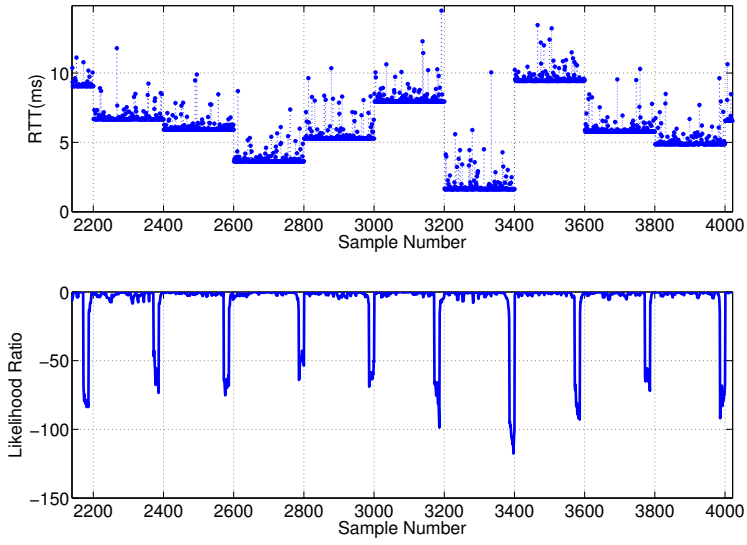

Figure 3.1. Likelihood ratio as a function of the model-based RTTs ($n = 30$)

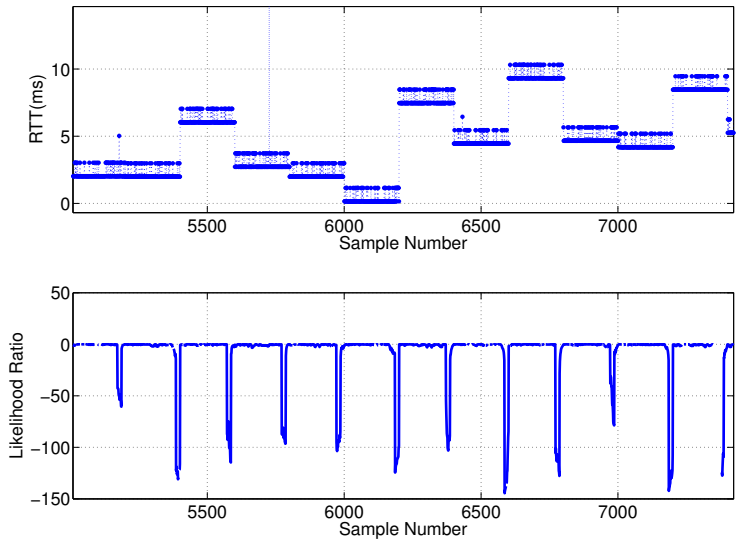

Figure 3.2. Likelihood ratio as a function of the measured RTTs ($n = 30$)

In the example considered above, it is very easy to choose a threshold such that all the route changes are detected and there are no false alarms. However, with a different set of parameter values (e.g., higher α), the decrease in the value of likelihood ratio L may not be as significant and it may not be possible to choose a threshold such that the detection probability is close to 1 and false alarm probability is small. A high value of the threshold results in high detection probability but then the false alarm probability is also high. Similarly, a low value of the threshold reduces the false alarm probability but then the detection probability also reduces. Figure 3.3 illustrates the case where high load in a router queue is modeled by chosing the parameter values of $\alpha = 1.2$ and $\beta = 6$. The detector window size was increased to 50 samples. A threshold of -10 will result in a high detection probability but the false alarm probability is also non-zero. Decreasing the threshold to -15 may reduce the false alarm probability to 0 but the detection probability will also reduce.

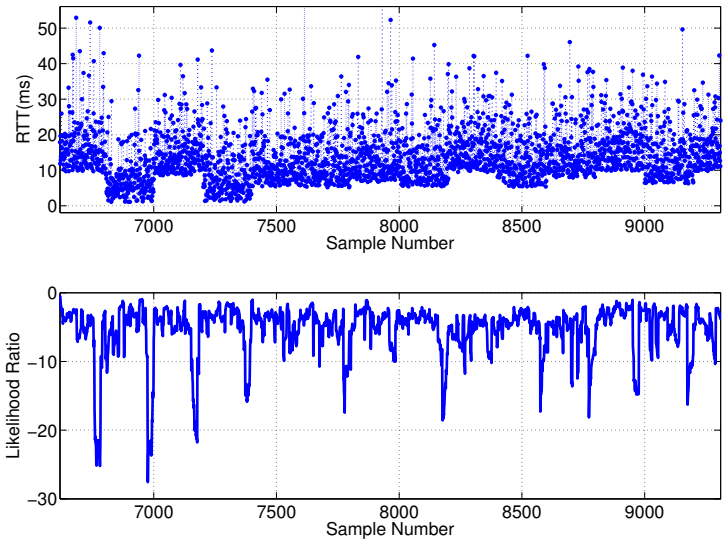

Figure 3.3. Likelihood ratio as a function of the model-based RTTs ($\alpha = 1.2, \beta = 6, n = 50$)

It is clear from the examples above that the sensitivity of this detection algorithm depends on parameters of the Gamma distribution, the change in minimum RTT, the window size (n) and the threshold (λ) and there is a need for a mapping function that can transform these parameters into probabilities of detection and false alarms. Since it has not been possible to derive such a mapping function for PUD, a mapping function will be derived for PAD in this chapter. The PAD is optimum and provides an upper bound on performance.

3.3 Parameter aware detector

PAD is similar to PUD except that the parameters α_0, β_0, γ_0, α_1, β_1, γ_1, α_2, β_2 and γ_2 are assumed to be known. Given n samples $(t_1, t_2, ..., t_n)$, the problem is to determine whether or not there was a route change when these n samples

were collected. The simple[2] null hypothesis H_0 is that all n samples are drawn from Gamma distributed random variable with parameters α_0, β_0 and γ_0. The alternative simple hypothesis H_1 is that the first $\lfloor \frac{n}{2} \rfloor$ samples are drawn from a Gamma distributed random variable with parameters α_1, β_1 and γ_1, and the last $\lceil \frac{n}{2} \rceil$ samples are drawn from a Gamma distributed random variable with parameters α_2, β_2 and γ_2. Since it is assumed that the parameters α_0, β_0, γ_0, α_1, β_1, γ_1, α_2, β_2 and γ_2 are known, there is no need to estimate these parameters. The likelihood ratio can then be evaluated using the following equation.

$$L = Log \frac{\prod_{i=1}^{n} f_T(t = t_i|\alpha_0, \beta_0, \gamma_0)}{\prod_{i=1}^{\lfloor \frac{n}{2} \rfloor} f_T(t = t_i|\alpha_1, \beta_1, \gamma_1) \prod_{i=\lfloor \frac{n}{2} \rfloor + 1}^{n} f_T(t = t_i|\alpha_2, \beta_2, \gamma_2)} \tag{3.4}$$

If the value of L obtained from Equation 3.4 above is greater than threshold λ then hypothesis H_0 (no route change) is true, otherwise hypothesis H_1 (rotue change) is true. PAD is an ideal detector because it is assumed that the values of the parameters are known and with this knowledge, PAD has the best performance amongst all possible detectors in the likelihood ratio sense.

If the PDF of L when H_0 is true and the PDF of L when H_1 is true are known then the probability of false alarms and detection can be predicted for a given value of the threshold. The first two moments of L as a function of the 10 parameters α_0, β_0, γ_0, α_1, β_1, γ_1, α_2, β_2, γ_2 and n are derived in sections 3.4 and 3.5 for hypothesis H_0 and H_1 respectively. To determine an appropriate threshold and associated probabilities of detection and false alarms, it is assumed that the conditional PDFs are Gaussian. This assumption is validated using simulation.

[2]The hypothesis is simple because the values of the parameters are known.

3.4 Moments of L: H_0 true

In this section, expressions for the first two moments of L when H_0 is true are derived. It is very difficult to derive an expression for PDF of L and for this reason only the first two moments are derived and then a Gaussian distribution is assumed. The base parameter space can be partitioned into two subspaces and the moments of L are found using different methods for each of the two subspaces. The two parameter subspaces are named *L-finite* subspace and *L-infinite* subspace and section 3.4.1 discusses why the parameter space is partitioned. Expressions for expected value of L and variance of L when parameters are in the *L-finite* subspace are derived in Sections 3.4.2 and 3.4.3 respectively. Expressions for expected value of L and variance of L when parameters are in the *L-infinite* subspace are derived in Sections 3.4.4 and 3.4.5 respectively.

3.4.1 Parameter subspaces

When parameter values are such that $\gamma_0 \geq \text{Max}(\gamma_1, \gamma_2)$, the parameters are in the *L-finite* subspace because L is always finite in this subspace. However, when parameter values are such that $\gamma_0 < \text{Max}(\gamma_1, \gamma_2)$, the parameters are in the *L-infinite* subspace because L may be either finite or infinite. When parameters are in the *L-infinite* subspace the probability that L is infinite is nonzero. Since it is assumed that hypothesis H_0 is true, all of the n samples are from a Gamma distribution with parameters α_0, β_0 and γ_0. When $\gamma_0 < \text{Max}(\gamma_1, \gamma_2)$, one of the following is true: ($\gamma_0 < \gamma_1$,$\gamma_0 \geq \gamma_2$) or ($\gamma_0 \geq \gamma_1$,$\gamma_0 < \gamma_2$) or ($\gamma_0 < \gamma_1$,$\gamma_0 < \gamma_2$). When $t_i < \gamma_1, i \in \{1..\lfloor \frac{n}{2} \rfloor\}$ or $t_i < \gamma_2, i \in \{\lfloor \frac{n}{2} \rfloor + 1..n\}$ for one or more samples t_i, then $L = \infty$ (See Equations 3.1 and 3.4). When $L = \infty$, there is no ambiguity in deciding in favor of H_0 because $P(L = \infty | H_1) = 0$. The probability that L is finite

when parameters are in the *L-infinite* subspace will be derived in this section. This probability will be useful later when expressions for probability of false alarms and detection are derived. When parameters are in *L-infinite* subspace, then one of the following is true: -

- $\gamma_2 > \gamma_0 \geq \gamma_1$
- $\gamma_1 > \gamma_0 \geq \gamma_2$
- $\gamma_2 > \gamma_0$ and $\gamma_1 > \gamma_0$

Expressions for the probability that L is finite (or infinite) will be obtained for each of the three cases. Probability that $t_i > \xi, \forall i : i \in \{1..n\}$ (ξ is a constant, $\xi \geq \gamma_0$) can be evaluated as follows

$$P(t_i > \xi, \forall i : i \in \{1..n\}) = P(\text{Min}[t_i, i \in \{1..n\}] > \xi) \tag{3.5}$$

The probability $P(\text{Min}[t_i, i \in \{1..n\}] > \xi)$ can be computed using order statistics. PDF of the k^{th} order statistic is as follows (from [HC95])

$$g_k(y_k) = \begin{cases} \frac{n!}{(k-1)!(n-k)!} \left[F(y_k)\right]^{(k-1)} \left[1 - F(y_k)\right]^{(n-k)} f(y_k) & 0 \leq y_k < \infty \\ 0 & \text{otherwise} \end{cases}$$

Here $F(y)$ is the CDF and $f(y)$ is the PDF of the random variable from which samples are drawn. For a two parameter ($\gamma = 0$) Gamma distributed random variable, PDF of the first order statistic is as follows

$$g_1(y_1) = \begin{cases} \frac{n y_1^{(\alpha-1)} e^{-\frac{y_1}{\beta}}}{[\Gamma(\alpha)]^n \beta^\alpha} \left[\Gamma\left(\alpha, \frac{y_1}{\beta}\right)\right]^{n-1} & 0 \leq y < \infty \\ 0 & \text{otherwise} \end{cases}$$

The probability $P(\text{Min}[t_i, i \in \{1..n\}] > \xi)$ is then the integration of this PDF ($g_1(y_1)$) for y_1 ranging from $\xi - \gamma_0$ to ∞.

$$P(\text{Min}[t_i, i \in \{1..n\}] > \xi) = \frac{n}{[\Gamma(\alpha)]^n \beta^\alpha} \int_{\xi-\gamma_0}^{\infty} q^{\alpha_0-1} e^{-\frac{q}{\beta_0}} \left[\Gamma(\alpha_0, \frac{q}{\beta_0})\right]^{n-1} dq \quad (3.6)$$

Form Equation 3.5, it follows that

$$P(t_i > \xi, \forall i : i \in \{1..n\}) = \frac{n}{[\Gamma(\alpha_0)]^n \beta_0^{\alpha_0}} \int_{\xi-\gamma_0}^{\infty} q^{\alpha_0-1} e^{-\frac{q}{\beta_0}} \left[\Gamma(\alpha_0, \frac{q}{\beta_0})\right]^{n-1} dq \quad (3.7)$$

The expressions for the probability that L is finite for each of the three cases can be derived from Equation 3.7 as follows.

- $\gamma_2 > \gamma_0 \geq \gamma_1$

$$\begin{aligned} &P(L \neq \infty) = P_{LF|H_0} = P(t_i > \gamma_2, \forall i : i \in \{\lfloor \tfrac{n}{2} \rfloor + 1..n\}) \\ &= \frac{\lceil \frac{n}{2} \rceil}{[\Gamma(\alpha_0)]^{\lceil \frac{n}{2} \rceil} \beta_0^{\alpha_0}} \int_{\gamma_2-\gamma_0}^{\infty} q^{\alpha_0-1} e^{-\frac{q}{\beta_0}} \left[\Gamma(\alpha_0, \frac{q}{\beta_0})\right]^{\lceil \frac{n}{2} \rceil - 1} dq \end{aligned} \quad (3.8)$$

- $\gamma_1 > \gamma_0 \geq \gamma_2$

$$\begin{aligned} &P(L \neq \infty) = P_{LF|H_0} = P(t_i > \gamma_1, \forall i : i \in \{1..\lfloor \tfrac{n}{2} \rfloor\}) \\ &= \frac{\lfloor \frac{n}{2} \rfloor}{[\Gamma(\alpha_0)]^{\lfloor \frac{n}{2} \rfloor} \beta_0^{\alpha_0}} \int_{\gamma_1-\gamma_0}^{\infty} q^{\alpha_0-1} e^{-\frac{q}{\beta_0}} \left[\Gamma(\alpha_0, \frac{q}{\beta_0})\right]^{\lfloor \frac{n}{2} \rfloor - 1} dq \end{aligned} \quad (3.9)$$

- $\gamma_2 > \gamma_0$ and $\gamma_1 > \gamma_0$

$$
\begin{aligned}
&P(L \neq \infty) = P_{LF|H_0} \\
&= P([t_i > \gamma_2, \forall i : i \in \{\lfloor \tfrac{n}{2} \rfloor + 1..n\}] \text{ and } [t_i > \gamma_1, \forall i : i \in \{1..\lfloor \tfrac{n}{2} \rfloor\}]) \\
&= \left(\frac{\lceil \frac{n}{2} \rceil}{[\Gamma(\alpha_0)]^{\lceil \frac{n}{2} \rceil} \beta_0^{\alpha_0}} \int_{\gamma_2 - \gamma_0}^{\infty} q^{\alpha_0 - 1} e^{-\frac{q}{\beta_0}} \left[\Gamma(\alpha_0, \tfrac{q}{\beta_0}) \right]^{\lceil \frac{n}{2} \rceil - 1} dq \right) \times \\
&\left(\frac{\lfloor \frac{n}{2} \rfloor}{[\Gamma(\alpha_0)]^{\lfloor \frac{n}{2} \rfloor} \beta_0^{\alpha_0}} \int_{\gamma_1 - \gamma_0}^{\infty} q^{\alpha_0 - 1} e^{-\frac{q}{\beta_0}} \left[\Gamma(\alpha_0, \tfrac{q}{\beta_0}) \right]^{\lfloor \frac{n}{2} \rfloor - 1} dq \right)
\end{aligned}
\tag{3.10}
$$

Equations 3.8, 3.9 and 3.10 can be used to predict the probability that L is finite given that H_0 is true and parameters are in *L-infinite* subspace. These will be used later in Chapter 4 when receiver operating characteristics are discussed. An expression for expected value of L when parameters are in the *L-finite* subspace will be obtained next in section 3.4.2.

3.4.2 Expected value: *L-finite*

When the parameters are in the *L-finite* subspace (i.e., $\gamma_0 \geq \text{Max}(\gamma_1, \gamma_2)$), likelihood ratio L is always finite and can be expressed as follows (from Equations 3.4 and 3.1).

$$
L = Log \frac{\frac{1}{[\Gamma(\alpha_0)\beta_0{}^{\alpha_0}]^n} \prod_{i=1}^{n} (t_i - \gamma_0)^{(\alpha_0 - 1)} e^{-\frac{(t_i - \gamma_0)}{\beta_0}}}{\left(\frac{1}{[\Gamma(\alpha_1)\beta_1{}^{\alpha_1}]^{\lfloor \frac{n}{2} \rfloor}} \prod_{i=1}^{\lfloor \frac{n}{2} \rfloor} (t_i - \gamma_1)^{(\alpha_1 - 1)} e^{-\frac{(t_i - \gamma_1)}{\beta_1}} \right) \times \left(\frac{1}{[\Gamma(\alpha_2)\beta_2{}^{\alpha_2}]^{\lceil \frac{n}{2} \rceil}} \prod_{i=\lfloor \frac{n}{2} \rfloor + 1}^{n} (t_i - \gamma_2)^{(\alpha_2 - 1)} e^{-\frac{(t_i - \gamma_2)}{\beta_2}} \right)}
$$

This equation can be rewritten as follows

$$\begin{aligned} L = \; & -nLog[\Gamma(\alpha_0)] - n\alpha_0 Log[\beta_0] + \textstyle\sum_{i=1}^{n}(\alpha_0 - 1)Log(t_i - \gamma_0) - \sum_{i=1}^{n}\frac{(t_i-\gamma_0)}{\beta_0} \\ & + \lfloor \tfrac{n}{2} \rfloor Log[\Gamma(\alpha_1)] + \lfloor \tfrac{n}{2} \rfloor \alpha_1 Log[\beta_1] - \textstyle\sum_{i=1}^{\lfloor \frac{n}{2} \rfloor}(\alpha_1 - 1)Log(t_i - \gamma_1) \\ & + \textstyle\sum_{i=1}^{\lfloor \frac{n}{2} \rfloor}\frac{(t_i-\gamma_1)}{\beta_1} + \lceil \tfrac{n}{2} \rceil Log[\Gamma(\alpha_2)] + \lceil \tfrac{n}{2} \rceil \alpha_2 Log[\beta_2] \\ & - \textstyle\sum_{i=\lfloor \frac{n}{2} \rfloor+1}^{n}(\alpha_2 - 1)Log(t_i - \gamma_2) + \sum_{i=\lfloor \frac{n}{2} \rfloor+1}^{n}\frac{(t_i-\gamma_2)}{\beta_2} \end{aligned} \tag{3.11}$$

Expected value $E[L|H_0]$ can then be expressed as follows

$$\begin{aligned} E[L|H_0] = \; & -nLog[\Gamma(\alpha_0)] - n\alpha_0 Log[\beta_0] + \textstyle\sum_{i=1}^{n}(\alpha_0 - 1)E[Log(t_i - \gamma_0)] \\ & - \textstyle\sum_{i=1}^{n}\frac{(E[t_i]-\gamma_0)}{\beta_0} + \lfloor \tfrac{n}{2} \rfloor Log[\Gamma(\alpha_1)] + \lfloor \tfrac{n}{2} \rfloor \alpha_1 Log[\beta_1] \\ & - \textstyle\sum_{i=1}^{\lfloor \frac{n}{2} \rfloor}(\alpha_1 - 1)E[Log(t_i - \gamma_1)] + \sum_{i=1}^{\lfloor \frac{n}{2} \rfloor}\frac{(E[t_i]-\gamma_1)}{\beta_1} + \lceil \tfrac{n}{2} \rceil Log[\Gamma(\alpha_2)] \\ & + \lceil \tfrac{n}{2} \rceil \alpha_2 Log[\beta_2] - \textstyle\sum_{i=\lfloor \frac{n}{2} \rfloor+1}^{n}(\alpha_2 - 1)E[Log(t_i - \gamma_2)] \\ & + \textstyle\sum_{i=\lfloor \frac{n}{2} \rfloor+1}^{n}\frac{(E[t_i]-\gamma_2)}{\beta_2} \end{aligned} \tag{3.12}$$

Since it is assumed that H_0 is true, $E[t_i] = \gamma_0 + \alpha_0\beta_0$. Substituting, there is the equality

$$\begin{aligned} E[L|H_0] = \; & -nLog[\Gamma(\alpha_0)] - n\alpha_0 Log[\beta_0] + \textstyle\sum_{i=1}^{n}(\alpha_0 - 1)E[Log(t_i - \gamma_0)] - n\alpha_0 \\ & + \lfloor \tfrac{n}{2} \rfloor Log[\Gamma(\alpha_1)] + \lfloor \tfrac{n}{2} \rfloor \alpha_1 Log[\beta_1] - \textstyle\sum_{i=1}^{\lfloor \frac{n}{2} \rfloor}(\alpha_1 - 1)E[Log(t_i - \gamma_1)] \\ & + \lfloor \tfrac{n}{2} \rfloor \frac{\gamma_0+\alpha_0\beta_0-\gamma_1}{\beta_1} + \lceil \tfrac{n}{2} \rceil Log[\Gamma(\alpha_2)] + \lceil \tfrac{n}{2} \rceil \alpha_2 Log[\beta_2] \\ & - \textstyle\sum_{i=\lfloor \frac{n}{2} \rfloor+1}^{n}(\alpha_2 - 1)E[Log(t_i - \gamma_2)] + \lceil \tfrac{n}{2} \rceil \frac{\gamma_0+\alpha_0\beta_0-\gamma_2}{\beta_2} \end{aligned} \tag{3.13}$$

Expressions for $E[Log(t_i - \gamma_0)]$, $E[Log(t_i - \gamma_1)]$ and $E[Log(t_i - \gamma_2)]$ are needed to solve the above equation further. While there are no known expressions for $E[Log(t_i - \gamma_1)]$ and $E[Log(t_i - \gamma_2)]$, the term $E[Log(t_i - \gamma_0)]$ can be solved further as follows. Let T is a Gamma distributed random variable with parameters α_0,

β_0 and γ_0 (RTTs). Also, let Y be a random variable such that $Y = T - \gamma_0$. Random variable Y is then a 2 parameter Gamma distributed random variable with parameters α_0 and β_0. Expected value $E[logY]$ then is same as the expected value $E[Log(t_i - \gamma_0)]$. The moment generating function of Y can be obtained as follows.

$$\begin{aligned} M(u) = E(e^{uLog(y)}) = & \ \frac{1}{\Gamma(\alpha_0)\beta_0^{\alpha_0}} \int_0^\infty e^{uLog(y)} y^{(\alpha_0-1)} e^{(-\frac{y}{\beta_0})} dy \\ & = \frac{1}{\Gamma(\alpha_0)\beta_0^{\alpha_0}} \int_0^\infty y^u y^{(\alpha_0-1)} e^{(-\frac{y}{\beta_0})} dy \\ & = \frac{\beta_0^u \Gamma(u+\alpha_0)}{\Gamma(\alpha_0)} \end{aligned}$$

The cumulant generating function is then

$$K(u) = Log[M(u)] = uLog(\beta_0) + Log[\Gamma(u + \alpha_0)] - Log[\Gamma(\alpha_0)]$$

Hence, the first cumulant is

$$\begin{aligned} \kappa_1(LogY) & = Log(\beta_0) + \tfrac{d}{du} Log[\Gamma(u + \alpha_0)]\big|_{u=0} = Log(\beta_0) + \tfrac{d}{d\alpha_0} Log[\Gamma(\alpha_0)] \\ & = Log(\beta_0) + \psi(\alpha_0) \end{aligned}$$

where ψ denotes the digamma function [NJB94], [BK46]. Therefore,

$$\kappa_1(LogY) = E[LogY] = E[Log(T - \gamma_0)] = Log(\beta_0) + \psi(\alpha_0) \tag{3.14}$$

Although simplified expression for $E[Log(T - \gamma_0)]$ is derived above, to the best of our knowledge, there is no simple expression for $E[Log(T - \gamma_i)], i = \{1, 2\}$. For this reason, numerical integration is used to find the value of $E[Log(t - \gamma_i)], i = \{1, 2\}$. The value obtained using numerical integration will be denoted by the function

$I1(\alpha_0, \beta_0, \gamma_0, \gamma_1)$.

$$\begin{aligned} E[Log(t-\gamma_1)] = \;& I1(\alpha_0, \beta_0, \gamma_0, \gamma_1) \\ & = \tfrac{1}{\Gamma(\alpha_0)\beta_0^{\alpha_0}} \int_{\gamma_0}^{\infty} Log(t-\gamma_1)(t-\gamma_0)^{(\alpha_0-1)} e^{(-\frac{t-\gamma_0}{\beta_0})} dt \end{aligned} \tag{3.15}$$

Similarly, value obtained for $E[Log(T-\gamma_2)]$ using numerical integration is denoted by $I1(\alpha_0, \beta_0, \gamma_0, \gamma_2)$. Then Equation 3.13 can now be rewritten as follows.

$$\begin{aligned} E[L|H_0] \;& = -nLog[\Gamma(\alpha_0)] - n\alpha_0 Log[\beta_0] - n\alpha_0 + \lfloor \tfrac{n}{2} \rfloor Log[\Gamma(\alpha_1)] \\ & + \lfloor \tfrac{n}{2} \rfloor \alpha_1 Log[\beta_1] + \lfloor \tfrac{n}{2} \rfloor \tfrac{\gamma_0 + \alpha_0\beta_0 - \gamma_1}{\beta_1} + \lceil \tfrac{n}{2} \rceil Log[\Gamma(\alpha_2)] \\ & + \lceil \tfrac{n}{2} \rceil \alpha_2 Log[\beta_2] + \lceil \tfrac{n}{2} \rceil \tfrac{\gamma_0 + \alpha_0\beta_0 - \gamma_2}{\beta_2} + n(\alpha_0 - 1)\left(Log(\beta_0) + \psi(\alpha_0)\right) \\ & - \lfloor \tfrac{n}{2} \rfloor (\alpha_1 - 1)\left(I1(\alpha_0, \beta_0, \gamma_0, \gamma_1)\right) \\ & - \lceil \tfrac{n}{2} \rceil (\alpha_2 - 1)\left(I1(\alpha_0, \beta_0, \gamma_0, \gamma_2)\right) \end{aligned} \tag{3.16}$$

Equation 3.16 was validated using simulation and it accurately predicts the expected value of L when hypothesis H_0 is true and parameters are in the *L-finite* subspace. Formal validation results are presented in Chapter 4 where the expression in Equation 3.16 is used to predict the receiver operating characteristics. An expression for the second moment of L is derived in the next section.

3.4.3 Second moment: *L-finite*

An expression for second moment of L (i.e., $E[L^2]$) will be derived in this section. From Equation 3.4, it follows that

$$E[L^2] = E\left[\left(Log\, \frac{\prod_{i=1}^{n} f_T(t_i|\alpha_0, \beta_0, \gamma_0)}{\prod_{i=1}^{\lfloor \frac{n}{2} \rfloor} f_T(t_i|\alpha_1, \beta_1, \gamma_1) \prod_{i=\lfloor \frac{n}{2} \rfloor + 1}^{n} f_T(t_i|\alpha_2, \beta_2, \gamma_2)}\right)^2\right] \tag{3.17}$$

Right hand side of the above equation can be expanded as illustrated in the following steps.

$$E[L^2] = E\left[\left(\begin{array}{l} \sum_{i=1}^{n} Logf_T(t_i|\alpha_0,\beta_0,\gamma_0) - \sum_{i=1}^{\lfloor \frac{n}{2} \rfloor} Logf_T(t_i|\alpha_1,\beta_1,\gamma_1) \\ -\sum_{i=\lfloor \frac{n}{2} \rfloor+1}^{n} Logf_T(t_i|\alpha_2,\beta_2,\gamma_2) \end{array}\right)^2\right]$$

$$E[L^2] = E\left[\left(\begin{array}{l} \sum_{i=1}^{n} Logf_T(t_i|\alpha_0,\beta_0,\gamma_0) - \sum_{i=1}^{\lfloor \frac{n}{2} \rfloor} Logf_T(t_i|\alpha_1,\beta_1,\gamma_1) \\ -\sum_{i=\lfloor \frac{n}{2} \rfloor+1}^{n} Logf_T(t_i|\alpha_2,\beta_2,\gamma_2) \end{array}\right) \times \left(\begin{array}{l} \sum_{i=1}^{n} Logf_T(t_i|\alpha_0,\beta_0,\gamma_0) - \sum_{i=1}^{\lfloor \frac{n}{2} \rfloor} Logf_T(t_i|\alpha_1,\beta_1,\gamma_1) \\ -\sum_{i=\lfloor \frac{n}{2} \rfloor+1}^{n} Logf_T(t_i|\alpha_2,\beta_2,\gamma_2) \end{array}\right)\right]$$

$$E[L^2] = E\left[\begin{array}{l} \sum_{i=1}^{n}\sum_{j=1}^{n} \left(Logf(t_i|\alpha_0,\beta_0,\gamma_0) \times Logf(t_j|\alpha_0,\beta_0,\gamma_0)\right) \\ -\sum_{i=1}^{n}\sum_{j=1}^{\lfloor \frac{n}{2} \rfloor} \left(Logf(t_i|\alpha_0,\beta_0,\gamma_0) \times Logf(t_j|\alpha_1,\beta_1,\gamma_1)\right) \\ -\sum_{i=1}^{n}\sum_{j=\lfloor \frac{n}{2} \rfloor+1}^{n} \left(Logf(t_i|\alpha_0,\beta_0,\gamma_0) \times Logf(t_j|\alpha_2,\beta_2,\gamma_2)\right) \\ -\sum_{i=1}^{n}\sum_{j=1}^{\lfloor \frac{n}{2} \rfloor} \left(Logf(t_i|\alpha_0,\beta_0,\gamma_0) \times Logf(t_j|\alpha_1,\beta_1,\gamma_1)\right) \\ +\sum_{i=1}^{\lfloor \frac{n}{2} \rfloor}\sum_{j=1}^{\lfloor \frac{n}{2} \rfloor} \left(Logf(t_i|\alpha_1,\beta_1,\gamma_1) \times Logf(t_j|\alpha_1,\beta_1,\gamma_1)\right) \\ +\sum_{i=1}^{\lfloor \frac{n}{2} \rfloor}\sum_{j=\lfloor \frac{n}{2} \rfloor+1}^{n} \left(Logf(t_i|\alpha_1,\beta_1,\gamma_1) \times Logf(t_j|\alpha_2,\beta_2,\gamma_2)\right) \\ -\sum_{i=1}^{n}\sum_{j=\lfloor \frac{n}{2} \rfloor+1}^{n} \left(Logf(t_i|\alpha_0,\beta_0,\gamma_0) \times Logf(t_j|\alpha_2,\beta_2,\gamma_2)\right) \\ +\sum_{i=1}^{\lfloor \frac{n}{2} \rfloor}\sum_{j=\lfloor \frac{n}{2} \rfloor+1}^{n} \left(Logf(t_i|\alpha_1,\beta_1,\gamma_1) \times Logf(t_j|\alpha_2,\beta_2,\gamma_2)\right) \\ +\sum_{i=\lfloor \frac{n}{2} \rfloor+1}^{n}\sum_{j=\lfloor \frac{n}{2} \rfloor+1}^{n} \left(Logf(t_i|\alpha_2,\beta_2,\gamma_2) \times Logf(t_j|\alpha_2,\beta_2,\gamma_2)\right) \end{array}\right] \tag{3.18}$$

Solving, there is the equality

$$E[L^2] = \left(\begin{array}{l} \sum_{i=1}^{n} \sum_{j=1}^{n} E\left[Logf(t_i|\alpha_0,\beta_0,\gamma_0) \times Logf(t_j|\alpha_0,\beta_0,\gamma_0)\right] \\ + \sum_{i=1}^{\lfloor \frac{n}{2} \rfloor} \sum_{j=1}^{\lfloor \frac{n}{2} \rfloor} E\left[Logf(t_i|\alpha_1,\beta_1,\gamma_1) \times Logf(t_j|\alpha_1,\beta_1,\gamma_1)\right] \\ + \sum_{i=\lfloor \frac{n}{2} \rfloor+1}^{n} \sum_{j=\lfloor \frac{n}{2} \rfloor+1}^{n} E\left[Logf(t_i|\alpha_2,\beta_2,\gamma_2) \times Logf(t_j|\alpha_2,\beta_2,\gamma_2)\right] \\ -2 \sum_{i=1}^{n} \sum_{j=1}^{\lfloor \frac{n}{2} \rfloor} E\left[Logf(t_i|\alpha_0,\beta_0,\gamma_0) \times Logf(t_j|\alpha_1,\beta_1,\gamma_1)\right] \\ -2 \sum_{i=1}^{n} \sum_{j=\lfloor \frac{n}{2} \rfloor+1}^{n} E\left[Logf(t_i|\alpha_0,\beta_0,\gamma_0) \times Logf(t_j|\alpha_2,\beta_2,\gamma_2)\right] \\ +2 \sum_{i=1}^{\lfloor \frac{n}{2} \rfloor} \sum_{j=\lfloor \frac{n}{2} \rfloor+1}^{n} E\left[Logf(t_i|\alpha_1,\beta_1,\gamma_1) \times Logf(t_j|\alpha_2,\beta_2,\gamma_2)\right] \end{array} \right) \tag{3.19}$$

In the next step, it is assumed that the samples t_i and t_j are independent identically distributed. This assumption is valid for RTT measurements considered here. Also, terms for which $i = j$ have been separated.

$$E[L^2] = \left(\begin{array}{l} \sum_{i=1}^{n} E\left[Log^2 f(t_i|\alpha_0,\beta_0,\gamma_0)\right] \\ + \sum_{i=1}^{n} \sum_{j=1,j\neq i}^{n} E\left[Logf(t_i|\alpha_0,\beta_0,\gamma_0)\right] \times E\left[Logf(t_j|\alpha_0,\beta_0,\gamma_0)\right] \\ + \sum_{i=1}^{\lfloor \frac{n}{2} \rfloor} E\left[Log^2 f(t_i|\alpha_1,\beta_1,\gamma_1)\right] \\ + \sum_{i=1}^{\lfloor \frac{n}{2} \rfloor} \sum_{j=1,j\neq i}^{\lfloor \frac{n}{2} \rfloor} E\left[Logf(t_i|\alpha_1,\beta_1,\gamma_1)\right] \times E\left[Logf(t_j|\alpha_1,\beta_1,\gamma_1)\right] \\ + \sum_{i=\lfloor \frac{n}{2} \rfloor+1}^{n} E\left[Log^2 f(t_i|\alpha_2,\beta_2,\gamma_2)\right] \\ + \sum_{i=\lfloor \frac{n}{2} \rfloor+1}^{n} \sum_{j=\lfloor \frac{n}{2} \rfloor+1,j\neq i}^{n} E\left[Logf(t_i|\alpha_2,\beta_2,\gamma_2)\right] \times E\left[Logf(t_j|\alpha_2,\beta_2,\gamma_2)\right] \\ -2 \sum_{i=1}^{\lfloor \frac{n}{2} \rfloor} E\left[Logf(t_i|\alpha_0,\beta_0,\gamma_0) \times Logf(t_i|\alpha_1,\beta_1,\gamma_1)\right] \\ -2 \sum_{i=1}^{n} \sum_{j=1,j\neq i}^{\lfloor \frac{n}{2} \rfloor} E\left[Logf(t_i|\alpha_0,\beta_0,\gamma_0)\right] \times E\left[Logf(t_j|\alpha_1,\beta_1,\gamma_1)\right] \\ -2 \sum_{i=\lfloor \frac{n}{2} \rfloor+1}^{n} E\left[Logf(t_i|\alpha_0,\beta_0,\gamma_0) \times Logf(t_i|\alpha_2,\beta_2,\gamma_2)\right] \\ -2 \sum_{i=1}^{n} \sum_{j=\lfloor \frac{n}{2} \rfloor+1,j\neq i}^{n} E\left[Logf(t_i|\alpha_0,\beta_0,\gamma_0)\right] \times E\left[Logf(t_j|\alpha_2,\beta_2,\gamma_2)\right] \\ +2 \sum_{i=1}^{\lfloor \frac{n}{2} \rfloor} \sum_{j=\lfloor \frac{n}{2} \rfloor+1}^{n} E\left[Logf(t_i|\alpha_1,\beta_1,\gamma_1)\right] \times E\left[Logf(t_j|\alpha_2,\beta_2,\gamma_2)\right] \end{array} \right) \tag{3.20}$$

Since it is assumed that $t_i > \text{Max}(\gamma_1, \gamma_2), \forall i : i \in \{1..n\}$, parts of the right hand side of Equation 3.20 are expanded below.

$$
\begin{aligned}
&E\left[Log^2 f_T(t_i|\alpha_0, \beta_0, \gamma_0)\right] = \\
&\left(\begin{array}{l}
Log^2\Gamma(\alpha_0) + 2Log\Gamma(\alpha_0)\alpha_0 Log(\beta_0) \\
-2(\alpha_0 - 1)Log\Gamma(\alpha_0)E\left[Log(t_i - \gamma_0)\right] + 2Log\Gamma(\alpha_0)E\left[\frac{t_i-\gamma_0}{\beta_0}\right] \\
+\alpha_0^2 Log^2(\beta_0) - 2(\alpha_0 - 1)\alpha_0 Log(\beta_0)E\left[Log(t_i - \gamma_0)\right] \\
+2\alpha_0 Log(\beta_0)E\left[\frac{t_i-\gamma_0}{\beta_0}\right] + (\alpha_0 - 1)^2 E\left[Log^2(t_i - \gamma_0)\right] \\
-2(\alpha_0 - 1)E\left[Log(t_i - \gamma_0)\frac{t_i-\gamma_0}{\beta_0}\right] + E\left[\frac{(t_i-\gamma_0)^2}{\beta_0^2}\right]
\end{array}\right)
\end{aligned}
\tag{3.21}
$$

Expressions for expected values needed to solve this equation further are obtained below. An expression for expected value $E[Log(t_i - \gamma_0)]$ that was derived in Equation 3.14 can be substituted in the right hand side of Equation 3.21 to solve it further.

$$E[Log(t_i - \gamma_0)] = Log(\beta_0) + \psi(\alpha_0)$$

Also, since T is Gamma distributed with parameters α_0, β_0 and γ_0, $E\left[\frac{t_i-\gamma_0}{\beta_0}\right]$ can be expressed as follows.

$$E\left[\frac{t_i - \gamma_0}{\beta_0}\right] = \frac{\gamma_0 + \alpha_0\beta_0 - \gamma_0}{\beta_0} = \alpha_0$$

In the derivation of Equation 3.14, the first derivative of the cumulant generating function was obtained. The second derivative of this same cumulant generating function can be used to find $E[Log^2(t_i - \gamma_0)]$. The cumulant generating function is as follows.

$$K(u) = Log[M(u)] = uLog(\beta_0) + Log[\Gamma(u + \alpha_0)] - Log[\Gamma(\alpha_0)]$$

The second derivative of this function at $u = 0$ is the variance of the random variable $Log(T - \gamma_0)$.

$$\sigma^2 = \frac{d^2}{du^2}K(u)\bigg|_{u=0} = \kappa_2(Log(t_i - \gamma_0)) = E[Log^2(t_i - \gamma_0)] - (E[Log(t_i - \gamma_0)])^2$$

The second moment of the random variable $Log(T-\gamma_0)$ can be obtained from the expected value and variance as follows.

$$E[Log^2(t_i - \gamma_0)] = \frac{d^2}{du^2}K(u)\bigg|_{u=0} - (E[Log(t_i - \gamma_0)])^2$$

$$\begin{aligned} E[Log^2(t_i - \gamma_0)] &= \psi^{(1)}(\alpha_0) + (Log(\beta_0) + \psi(\alpha_0))^2 \\ &= \psi^{(1)}(\alpha_0) + Log^2(\beta_0) + (\psi(\alpha_0))^2 + 2Log(\beta_0)\psi(\alpha_0) \end{aligned}$$

An expression for $E\left[Log(t_i - \gamma_0)\frac{t_i-\gamma_0}{\beta_0}\right]$ can also be derived from Equation 3.14 as follows. Recall that random variable Y is related to the random variable T by $Y = T - \gamma_0$.

$\frac{1}{\Gamma(\alpha_0)\beta_0^{\alpha_0}} \int_0^\infty Log(y) y^{\alpha_0 - 1} e^{-\frac{y}{\beta_0}} dy = Log(\beta_0) + \psi(\alpha_0)$

$\frac{1}{\Gamma(\alpha_0+1)\beta_0^{(\alpha_0+1)}} \int_0^\infty Log(y) y^{(\alpha_0+1)-1} e^{-\frac{y}{\beta_0}} dy = [Log(\beta_0) + \psi(\alpha_0 + 1)]$

$\frac{1}{\Gamma(\alpha_0+1)\beta_0^{(\alpha_0+1)}} \int_0^\infty Log(y) y y^{\alpha_0 - 1} e^{-\frac{y}{\beta_0}} dy = [Log(\beta_0) + \psi(\alpha_0 + 1)]$

$\frac{1}{\Gamma(\alpha_0+1)\beta_0^{(\alpha_0+1)}} \int_{\gamma_0}^\infty Log(t_i - \gamma_0)(t_i - \gamma_0)(t_i - \gamma_0)^{\alpha_0 - 1} e^{-\frac{t_i-\gamma_0}{\beta_0}} dt_i = [Log(\beta_0) + \psi(\alpha_0 + 1)]$

$E\left[Log(t_i - \gamma_0)\frac{t_i-\gamma_0}{\beta_0}\right] = \frac{\Gamma(\alpha_0+1)}{\Gamma(\alpha_0)}[Log(\beta_0) + \psi(\alpha_0 + 1)]$

The final expression needed to be substituted into Equation 3.21 is the one for $E\left[\frac{(t_i-\gamma_0)^2}{\beta_0^2}\right]$. Since T is Gamma distributed with parameters α_0, β_0 and γ_0, it

follows that

$$\begin{aligned} E\left[\frac{(t_i-\gamma_0)^2}{\beta_0^2}\right] &= \frac{1}{\beta_0^2}E\left[(t_i-\gamma_0)^2\right] = \frac{1}{\beta_0^2}E\left[y^2\right] \\ &= \alpha_0(1+\alpha_0) \end{aligned}$$

Equation 3.21 can be rewritten as follows by substituting the expressions derived above.

$$E\left[Log^2 f_T(t_i|\alpha_0,\beta_0,\gamma_0)\right] = A_{H_0} =$$

$$\left(\begin{array}{l} Log^2\Gamma(\alpha_0) + 2Log\Gamma(\alpha_0)\alpha_0 Log(\beta_0) \\ -2(\alpha_0-1)Log\Gamma(\alpha_0)\left(Log(\beta_0)+\psi(\alpha_0)\right) + 2Log\Gamma(\alpha_0)\alpha_0 \\ +\alpha_0^2 Log^2(\beta_0) - 2(\alpha_0-1)\alpha_0 Log(\beta_0)\left(Log(\beta_0)+\psi(\alpha_0)\right) \\ +2\alpha_0 Log(\beta_0)\alpha_0 + (\alpha_0-1)^2(\psi^{(1)}(\alpha_0) + Log^2(\beta_0) + \left(\psi(\alpha_0)\right)^2 \\ +2Log(\beta_0)\psi(\alpha_0)) \\ -2(\alpha_0-1)\frac{\Gamma(\alpha_0+1)}{\Gamma(\alpha_0)}[Log(\beta_0)+\psi(\alpha_0+1)] + \alpha_0(1+\alpha_0) \end{array}\right) \tag{3.22}$$

The expression obtained above in Equation 3.22 can be substituted for the first term in Equation 3.20. The second term in the right hand side of Equation 3.20 is expanded below. Note that $E\left[Logf(t_i|\alpha_0,\beta_0,\gamma_0)\right] \times E\left[Logf(t_j|\alpha_0,\beta_0,\gamma_0)\right]$ is same as $\left(E\left[Logf(t_i|\alpha_0,\beta_0,\gamma_0)\right]\right)^2$ since it is assumed that samples t_i and t_j are independent identically distributed. Expected value $E[Logf(t_i|\alpha_0,\beta_0,\gamma_0)]$ can be expressed as follows.

$$E[Logf(t_i|\alpha_0,\beta_0,\gamma_0)] = \left(\begin{array}{l} -Log\Gamma(\alpha_0) - \alpha_0 Log\beta_0 \\ +(\alpha_0-1)E[Log(t_i-\gamma_0)] - \alpha_0 \end{array}\right)$$

Substituting the expression for $E[Log(t_i - \gamma_0)]$ from Equation 3.14 the above equation can be solved as follows.

$$E[Logf(t_i|\alpha_0, \beta_0, \gamma_0)] = \left(\begin{array}{l} -Log\Gamma(\alpha_0) - Log\beta_0 + (\alpha_0 - 1)\psi(\alpha_0) - \alpha_0 \end{array} \right)$$

$$(E[Logf(t_i|\alpha_0, \beta_0, \gamma_0)])^2 = \begin{array}{l} (-Log\Gamma(\alpha_0) - Log\beta_0 + (\alpha_0 - 1)\psi(\alpha_0) - \alpha_0)\times \\ (-Log\Gamma(\alpha_0) - Log\beta_0 + (\alpha_0 - 1)\psi(\alpha_0) - \alpha_0) \end{array}$$

$$\begin{aligned} &(E[Logf(t_i|\alpha_0, \beta_0, \gamma_0)])^2 = B_{H_0} = \\ &= \left(\begin{array}{l} Log^2\Gamma(\alpha_0) + 2Log\Gamma(\alpha_0)Log\beta_0 \\ -2(\alpha_0 - 1)Log\Gamma(\alpha_0)\psi(\alpha_0) + 2\alpha_0 Log\Gamma(\alpha_0) \\ +Log^2\beta_0 - 2(\alpha_0 - 1)Log\beta_0\psi(\alpha_0) \\ +2\alpha_0 Log\beta_0 + (\alpha_0 - 1)^2(\psi(\alpha_0))^2 \\ -2\alpha_0(\alpha_0 - 1)\psi(\alpha_0) + \alpha_0^2 \end{array} \right) \end{aligned} \tag{3.23}$$

The third term in Equation 3.20 is $E\left[Log^2 f_T(t_i|\alpha_1, \beta_1, \gamma_1)\right]$ and it can be expanded as follows.

$$\begin{aligned} &E\left[Log^2 f_T(t_i|\alpha_1, \beta_1, \gamma_1)\right] = \\ &\left(\begin{array}{l} Log^2\Gamma(\alpha_1) + 2Log\Gamma(\alpha_1)\alpha_1 Log(\beta_1) \\ -2(\alpha_1 - 1)Log\Gamma(\alpha_1)E\left[Log(t_i - \gamma_1)\right] + 2Log\Gamma(\alpha_1)E\left[\frac{t_i - \gamma_1}{\beta_1}\right] \\ +\alpha_1^2 Log^2(\beta_1) - 2(\alpha_1 - 1)\alpha_1 Log(\beta_1)E\left[Log(t_i - \gamma_1)\right] \\ +2\alpha_1 Log(\beta_1)E\left[\frac{t_i - \gamma_1}{\beta_1}\right] + (\alpha_1 - 1)^2 E\left[Log^2(t_i - \gamma_1)\right] \\ -2(\alpha_1 - 1)E\left[Log(t_i - \gamma_1)\frac{t_i - \gamma_1}{\beta_1}\right] + E\left[\frac{(t_i - \gamma_1)^2}{\beta_1^2}\right] \end{array} \right) \end{aligned} \tag{3.24}$$

Expressions for expected values in the right hand side of the above Equation 3.24 are listed below. The numerical solution to $E[Log(t_i - \gamma_1)]$ is denoted by the

following (Equation 3.15).

$$E[Log(t_i - \gamma_1)] = I1(\alpha_0, \beta_0, \gamma_0, \gamma_1)$$

Also, $E\left[\frac{t_i-\gamma_1}{\beta_1}\right]$ can be expanded as follows.

$$E\left[\frac{t_i - \gamma_1}{\beta_1}\right] = \frac{\gamma_0 + \alpha_0\beta_0 - \gamma_1}{\beta_1}$$

To the best of our knowledge, a closed form expression for $E\left[Log^2(t_i - \gamma_1)\right]$ cannot be obtained. Numerical integration is used to find this expected value.

$$\begin{aligned} E\left[Log^2(t_i - \gamma_1)\right] = & \ \frac{1}{\Gamma(\alpha_0)\beta_0^{\alpha_0}} \int_{\gamma_0}^{\infty} Log^2(t - \gamma_1)(t - \gamma_0)^{(\alpha_0 - 1)} e^{-\frac{t-\gamma_0}{\beta_0}} dt \\ & = I2(\alpha_0, \beta_0, \gamma_0, \gamma_1) \end{aligned}$$

An expression for $E\left[Log(t_i - \gamma_1)(t_i - \gamma_1)\right]$ can be obtained as follows.

$$\begin{aligned} E\left[Log(t_i - \gamma_1)(t_i - \gamma_1)\right] & = E\left[Log(t_i - \gamma_1)((t_i - \gamma_0) - (\gamma_1 - \gamma_0))\right] \\ & = E\left[Log(t_i - \gamma_1)(t_i - \gamma_0)\right] - (\gamma_1 - \gamma_0)E\left[Log(t_i - \gamma_1)\right] \\ & = \beta_0 \frac{\Gamma(\alpha_0 + 1)}{\Gamma(\alpha_0)} I1(\alpha_0 + 1, \beta_0, \gamma_0, \gamma_1) \\ & -(\gamma_1 - \gamma_0) I1(\alpha_0, \beta_0, \gamma_0, \gamma_1) \end{aligned}$$

Expected value $E\left[\frac{(t_i-\gamma_1)^2}{\beta_1^2}\right]$ can be expressed as follows.

$$\begin{aligned} E\left[\frac{(t_i-\gamma_1)^2}{\beta_1^2}\right] & = E\left[\frac{((t_i-\gamma_0)-(\gamma_1-\gamma_0))^2}{\beta_1^2}\right] \\ & = \frac{\left(\alpha_0(\alpha_0+1)\beta_0^2 + (\gamma_1-\gamma_0)^2 - 2(\gamma_1-\gamma_0)\alpha_0\beta_0\right)}{\beta_1^2} \end{aligned}$$

Substituting these expressions into Equation 3.24, this equation can be rewritten as follows.

$$E\left[Log^2 f_T(t_i|\alpha_1,\beta_1,\gamma_1)\right] = C_{H_0} =$$
$$\left(\begin{array}{l} Log^2\Gamma(\alpha_1) + 2Log\Gamma(\alpha_1)\alpha_1 Log(\beta_1) \\ -2(\alpha_1-1)Log\Gamma(\alpha_1)I1(\alpha_0,\beta_0,\gamma_0,\gamma_1) + 2Log\Gamma(\alpha_1)\frac{\gamma_0+\alpha_0\beta_0-\gamma_1}{\beta_1} \\ +\alpha_1^2 Log^2(\beta_1) - 2(\alpha_1-1)\alpha_1 Log(\beta_1)I1(\alpha_0,\beta_0,\gamma_0,\gamma_1) \\ +2\alpha_1 Log(\beta_1)\frac{\gamma_0+\alpha_0\beta_0-\gamma_1}{\beta_1} + (\alpha_1-1)^2 I2(\alpha_0,\beta_0,\gamma_0,\gamma_1) \\ -2\frac{(\alpha_1-1)}{\beta_1}\left(\beta_0\frac{\Gamma(\alpha_0+1)}{\Gamma(\alpha_0)}I1(\alpha_0+1,\beta_0,\gamma_0,\gamma_1)\right. \\ \left.-(\gamma_1-\gamma_0)I1(\alpha_0,\beta_0,\gamma_0,\gamma_1)\right) + \frac{\left(\alpha_0(\alpha_0+1)\beta_0^2+(\gamma_1-\gamma_0)^2-2(\gamma_1-\gamma_0)\alpha_0\beta_0\right)}{\beta_1^2} \end{array}\right) \quad (3.25)$$

The expression for $E\left[Log^2 f_T(t_i|\alpha_2,\beta_2,\gamma_2)\right]$ is similar to the one in Equation 3.25 above: -

$$E\left[Log^2 f_T(t_i|\alpha_2,\beta_2,\gamma_2)\right] = D_{H_0}$$
$$\left(\begin{array}{l} Log^2\Gamma(\alpha_2) + 2Log\Gamma(\alpha_2)\alpha_2 Log(\beta_2) \\ -2(\alpha_2-1)Log\Gamma(\alpha_2)I1(\alpha_0,\beta_0,\gamma_0,\gamma_2) + 2Log\Gamma(\alpha_2)\frac{\gamma_0+\alpha_0\beta_0-\gamma_2}{\beta_2} \\ +\alpha_2^2 Log^2(\beta_2) - 2(\alpha_2-1)\alpha_2 Log(\beta_2)I1(\alpha_0,\beta_0,\gamma_0,\gamma_2) \\ +2\alpha_2 Log(\beta_2)\frac{\gamma_0+\alpha_0\beta_0-\gamma_2}{\beta_2} + (\alpha_2-1)^2 I2(\alpha_0,\beta_0,\gamma_0,\gamma_2) \\ -2\frac{(\alpha_2-1)}{\beta_2}\left(\beta_0\frac{\Gamma(\alpha_0+1)}{\Gamma(\alpha_0)}I1(\alpha_0+1,\beta_0,\gamma_0,\gamma_2)\right. \\ \left.-(\gamma_2-\gamma_0)I1(\alpha_0,\beta_0,\gamma_0,\gamma_2)\right) + \frac{\left(\alpha_0(\alpha_0+1)\beta_0^2+(\gamma_2-\gamma_0)^2-2(\gamma_2-\gamma_0)\alpha_0\beta_0\right)}{\beta_2^2} \end{array}\right) \quad (3.26)$$

Since it is assumed that t_i and t_j are independent identically distributed, the expressions $E\left[Logf(t_i|\alpha_1,\beta_1,\gamma_1)\right]\times E\left[Logf(t_j|\alpha_1,\beta_1,\gamma_1)\right]$ and $\left(E\left[Logf(t_i|\alpha_1,\beta_1,\gamma_1)\right]\right)^2$

are equivalent. Expected value $E[Logf(t_i|\alpha_1,\beta_1,\gamma_1)]$ can be expressed as follows.

$$E[Logf(t_i|\alpha_1,\beta_1,\gamma_1)] = \left(\begin{array}{l} -Log\Gamma(\alpha_1) - \alpha_1 Log\beta_1 \\ +(\alpha_1-1)E[Log(t_i-\gamma_1)] - E\left[\frac{t_i-\gamma_1}{\beta_1}\right] \end{array} \right)$$

or,

$$E[Logf(t_i|\alpha_1,\beta_1,\gamma_1)] = \\ \left(-Log\Gamma(\alpha_1) - \alpha_1 Log\beta_1 + (\alpha_1-1)I1(\alpha_0,\beta_0,\gamma_0,\gamma_1) - \frac{\gamma_0+\alpha_0\beta_0-\gamma_1}{\beta_1} \right)$$

The expression $(E[Logf(t_i|\alpha_0,\beta_0,\gamma_0)])^2$ can then be written as follows.

$$(E[Logf(t_i|\alpha_0,\beta_0,\gamma_0)])^2 = \\ (-Log\Gamma(\alpha_1) - \alpha_1 Log\beta_1 + (\alpha_1-1)I1(\alpha_0,\beta_0,\gamma_0,\gamma_1) - \frac{\gamma_0+\alpha_0\beta_0-\gamma_1}{\beta_1})\times \\ (-Log\Gamma(\alpha_1) - \alpha_1 Log\beta_1 + (\alpha_1-1)I1(\alpha_0,\beta_0,\gamma_0,\gamma_1) - \frac{\gamma_0+\alpha_0\beta_0-\gamma_1}{\beta_1})$$

Solving, there is the equality,

$$(E[Logf(t_i|\alpha_1,\beta_1,\gamma_1)])^2 = E_{H_0} = \\ \left(\begin{array}{l} Log^2\Gamma(\alpha_1) + 2\alpha_1 Log\Gamma(\alpha_1)Log\beta_1 \\ -2(\alpha_1-1)Log\Gamma(\alpha_1)I1(\alpha_0,\beta_0,\gamma_0,\gamma_1) + 2Log\Gamma(\alpha_1)\frac{\gamma_0+\alpha_0\beta_0-\gamma_1}{\beta_1} \\ +\alpha_1^2 Log^2\beta_1 - 2\alpha_1(\alpha_1-1)Log\beta_1 I1(\alpha_0,\beta_0,\gamma_0,\gamma_1) \\ +2\alpha_1 Log\beta_1\frac{\gamma_0+\alpha_0\beta_0-\gamma_1}{\beta_1} + (\alpha_1-1)^2(I1(\alpha_0,\beta_0,\gamma_0,\gamma_1))^2 \\ -2(\alpha_1-1)I1(\alpha_0,\beta_0,\gamma_0,\gamma_1)\frac{\gamma_0+\alpha_0\beta_0-\gamma_1}{\beta_1} + \left(\frac{\gamma_0+\alpha_0\beta_0-\gamma_1}{\beta_1}\right)^2 \end{array} \right) \quad (3.27)$$

The expression for $(E[Logf(t_i|\alpha_2,\beta_2,\gamma_2)])^2$ is similar to the expression above in Equation 3.27.

$$
\begin{aligned}
&(E[Logf(t_i|\alpha_2,\beta_2,\gamma_2)])^2 = F_{H_0} = \\
&\left(\begin{array}{l}
Log^2\Gamma(\alpha_2) + 2\alpha_2 Log\Gamma(\alpha_2) Log\beta_2 \\
-2(\alpha_2-1)Log\Gamma(\alpha_2) I1(\alpha_0,\beta_0,\gamma_0,\gamma_2) + 2Log\Gamma(\alpha_2)\frac{\gamma_0+\alpha_0\beta_0-\gamma_2}{\beta_2} \\
+\alpha_2^2 Log^2\beta_2 - 2\alpha_2(\alpha_2-1)Log\beta_2 I1(\alpha_0,\beta_0,\gamma_0,\gamma_2) \\
+2\alpha_2 Log\beta_2\frac{\gamma_0+\alpha_0\beta_0-\gamma_2}{\beta_2} + (\alpha_2-1)^2(I1(\alpha_0,\beta_0,\gamma_0,\gamma_2))^2 \\
-2(\alpha_2-1)I1(\alpha_0,\beta_0,\gamma_0,\gamma_2)\frac{\gamma_0+\alpha_0\beta_0-\gamma_2}{\beta_2} + \left(\frac{\gamma_0+\alpha_0\beta_0-\gamma_2}{\beta_2}\right)^2
\end{array}\right)
\end{aligned}
\tag{3.28}
$$

The expression $E\left[Logf(t_i|\alpha_0,\beta_0,\gamma_0) \times Logf(t_i|\alpha_1,\beta_1,\gamma_1)\right]$ can be expanded as follows.

$$
\begin{aligned}
&E\left[Logf(t_i|\alpha_0,\beta_0,\gamma_0) \times Logf(t_i|\alpha_1,\beta_1,\gamma_1)\right] = \\
&E\left[\begin{array}{l}
Log\Gamma(\alpha_0)Log\Gamma(\alpha_1) + \alpha_1 Log\beta_1 Log\Gamma(\alpha_0) - Log\Gamma(\alpha_0)(\alpha_1-1)Log(t_i-\gamma_1) \\
+Log\Gamma(\alpha_0)\frac{t_i-\gamma_1}{\beta_1} + \alpha_0 Log\beta_0 Log\Gamma(\alpha_1) + \alpha_0\alpha_1 Log\beta_0 Log\beta_1 \\
-\alpha_0 Log\beta_0(\alpha_1-1)Log(t_i-\gamma_1) + \alpha_0 Log\beta_0\frac{t_i-\gamma_1}{\beta_1} \\
-(\alpha_0-1)Log(t_i-\gamma_0)Log\Gamma(\alpha_1) - \alpha_1(\alpha_0-1)Log(t_i-\gamma_0)Log\beta_1 \\
+(\alpha_0-1)(\alpha_1-1)Log(t_i-\gamma_0)Log(t_i-\gamma_1) - (\alpha_0-1)\frac{t_i-\gamma_1}{\beta_1}Log(t_i-\gamma_0) \\
+Log\Gamma(\alpha_1)\frac{t_i-\gamma_0}{\beta_0} + \frac{t_i-\gamma_0}{\beta_0}\alpha_1 Log\beta_1 - \frac{t_i-\gamma_0}{\beta_0}(\alpha_1-1)Log(t_i-\gamma_1) \\
+\left(\frac{t_i-\gamma_0}{\beta_0}\right)\left(\frac{t_i-\gamma_1}{\beta_1}\right)
\end{array}\right]
\end{aligned}
$$

Solving, there is the equality

$$
\begin{aligned}
&E\left[Logf(t_i|\alpha_0,\beta_0,\gamma_0)\times Logf(t_i|\alpha_1,\beta_1,\gamma_1)\right]= \\
&\left(\begin{array}{l}
Log\Gamma(\alpha_0)Log\Gamma(\alpha_1)+\alpha_1 Log\beta_1 Log\Gamma(\alpha_0) \\
-Log\Gamma(\alpha_0)(\alpha_1-1)I1(\alpha_0,\beta_0,\gamma_0,\gamma_1)+Log\Gamma(\alpha_0)\frac{\gamma_0+\alpha_0\beta_0-\gamma_1}{\beta_1} \\
+\alpha_0 Log\beta_0 Log\Gamma(\alpha_1)+\alpha_0\alpha_1 Log\beta_0 Log\beta_1 \\
-\alpha_0 Log\beta_0(\alpha_1-1)I1(\alpha_0,\beta_0,\gamma_0,\gamma_1)+\alpha_0 Log\beta_0\frac{\gamma_0+\alpha_0\beta_0-\gamma_1}{\beta_1} \\
-(\alpha_0-1)\left(Log\beta_0+\psi(\alpha_0)\right)Log\Gamma(\alpha_1)-\alpha_1(\alpha_0-1)\left(Log\beta_0+\psi(\alpha_0)\right)Log\beta_1 \\
+(\alpha_0-1)(\alpha_1-1)E\left[Log(t_i-\gamma_0)Log(t_i-\gamma_1)\right] \\
-(\alpha_0-1)E\left[\frac{t_i-\gamma_1}{\beta_1}Log(t_i-\gamma_0)\right]+Log\Gamma(\alpha_1)\alpha_0+\alpha_0\alpha_1 Log\beta_1 \\
-(\alpha_1-1)E\left[\frac{t_i-\gamma_0}{\beta_0}Log(t_i-\gamma_1)\right]+E\left[\left(\frac{t_i-\gamma_0}{\beta_0}\right)\left(\frac{t_i-\gamma_1}{\beta_1}\right)\right]
\end{array}\right)
\end{aligned}
\tag{3.29}
$$

A closed form expression for $E\left[Log(t_i-\gamma_0)Log(t_i-\gamma_1)\right]$ is not available. A new function is defined to represent the expected value that is obtained using numerical integration.

$$
\begin{aligned}
&E\left[Log(t_i-\gamma_0)Log(t_i-\gamma_1)\right]= \\
&\frac{1}{\Gamma(\alpha_0)\beta_0^{\alpha_0}}\int_{\gamma_0}^{\infty}Log(t_i-\gamma_0)Log(t_i-\gamma_1)(t_i-\gamma_0)^{(\alpha_0-1)}e^{-\frac{t_i-\gamma_0}{\beta_0}}dt_i=I3(\alpha_0,\beta_0,\gamma_0,\gamma_1)
\end{aligned}
$$

Expressions for expected values $E[(t_i-\gamma_1)Log(t_i-\gamma_0)]$, $E[(t_i-\gamma_0)Log(t_i-\gamma_1)]$ and $E[(t_i-\gamma_0)(t_i-\gamma_1)]$ are as follows.

$$
E[(t_i-\gamma_1)Log(t_i-\gamma_0)]=\frac{\beta_0\Gamma(\alpha_0+1)}{\Gamma(\alpha_0)}(Log\beta_0+\psi(\alpha_0+1))-(\gamma_1-\gamma_0)(Log\beta_0+\psi(\alpha_0))
$$

$$
E[(t_i-\gamma_0)Log(t_i-\gamma_1)]=\frac{\beta_0\Gamma(\alpha_0+1)}{\Gamma(\alpha_0)}I1(\alpha_0+1,\beta_0,\gamma_0,\gamma_1)
$$

$$
E[(t_i-\gamma_0)(t_i-\gamma_1)]=\alpha_0\beta_0^2(1+\alpha_0)-\alpha_0\beta_0(\gamma_1-\gamma_0)
$$

Substituting these values, Equation 3.29 can be rewritten as follows.

$$E\left[Logf(t_i|\alpha_0,\beta_0,\gamma_0)\times Logf(t_i|\alpha_1,\beta_1,\gamma_1)\right]=G_{H_0}=$$
$$\left(\begin{array}{l}
Log\Gamma(\alpha_0)Log\Gamma(\alpha_1)+\alpha_1 Log\beta_1 Log\Gamma(\alpha_0)-Log\Gamma(\alpha_0)(\alpha_1-1)I1(\alpha_0,\beta_0,\gamma_0,\gamma_1)\\
+Log\Gamma(\alpha_0)\frac{\gamma_0+\alpha_0\beta_0-\gamma_1}{\beta_1}+\alpha_0 Log\beta_0 Log\Gamma(\alpha_1)+\alpha_0\alpha_1 Log\beta_0 Log\beta_1\\
-\alpha_0 Log\beta_0(\alpha_1-1)I1(\alpha_0,\beta_0,\gamma_0,\gamma_1)+\alpha_0 Log\beta_0\frac{\gamma_0+\alpha_0\beta_0-\gamma_1}{\beta_1}\\
-(\alpha_0-1)\left(Log\beta_0+\psi(\alpha_0)\right)Log\Gamma(\alpha_1)-\alpha_1(\alpha_0-1)\left(Log\beta_0+\psi(\alpha_0)\right)Log\beta_1\\
+(\alpha_0-1)(\alpha_1-1)I3(\alpha_0,\beta_0,\gamma_0,\gamma_1)\\
-(\alpha_0-1)\left(\frac{\frac{\beta_0\Gamma(\alpha_0+1)}{\Gamma(\alpha_0)}(Log\beta_0+\psi(\alpha_0+1))-(\gamma_1-\gamma_0)(Log\beta_0+\psi(\alpha_0))}{\beta_1}\right)+Log\Gamma(\alpha_1)\alpha_0\\
+\alpha_0\alpha_1 Log\beta_1-(\alpha_1-1)\frac{\Gamma(\alpha_0+1)}{\Gamma(\alpha_0)}I1(\alpha_0+1,\beta_0,\gamma_0,\gamma_1)+\frac{\alpha_0\beta_0(1+\alpha_0)-\alpha_0(\gamma_1-\gamma_0)}{\beta_1}
\end{array}\right)\tag{3.30}$$

The expression for $E\left[Logf(t_i|\alpha_0,\beta_0,\gamma_0)\times Logf(t_i|\alpha_2,\beta_2,\gamma_2)\right]$ is similar to the expression in the Equation 3.30 above.

$$E\left[Logf(t_i|\alpha_0,\beta_0,\gamma_0)\times Logf(t_i|\alpha_2,\beta_2,\gamma_2)\right]=H_{H_0}=$$
$$\left(\begin{array}{l}
Log\Gamma(\alpha_0)Log\Gamma(\alpha_2)+\alpha_2 Log\beta_2 Log\Gamma(\alpha_0)-Log\Gamma(\alpha_0)(\alpha_2-1)I1(\alpha_0,\beta_0,\gamma_0,\gamma_2)\\
+Log\Gamma(\alpha_0)\frac{\gamma_0+\alpha_0\beta_0-\gamma_2}{\beta_2}+\alpha_0 Log\beta_0 Log\Gamma(\alpha_2)+\alpha_0\alpha_2 Log\beta_0 Log\beta_2\\
-\alpha_0 Log\beta_0(\alpha_2-1)I1(\alpha_0,\beta_0,\gamma_0,\gamma_2)+\alpha_0 Log\beta_0\frac{\gamma_0+\alpha_0\beta_0-\gamma_2}{\beta_2}\\
-(\alpha_0-1)\left(Log\beta_0+\psi(\alpha_0)\right)Log\Gamma(\alpha_2)-\alpha_2(\alpha_0-1)\left(Log\beta_0+\psi(\alpha_0)\right)Log\beta_2\\
+(\alpha_0-1)(\alpha_2-1)I3(\alpha_0,\beta_0,\gamma_0,\gamma_2)\\
-(\alpha_0-1)\left(\frac{\frac{\beta_0\Gamma(\alpha_0+1)}{\Gamma(\alpha_0)}(Log\beta_0+\psi(\alpha_0+1))-(\gamma_2-\gamma_0)(Log\beta_0+\psi(\alpha_0))}{\beta_2}\right)+Log\Gamma(\alpha_2)\alpha_0\\
+\alpha_0\alpha_2 Log\beta_2-(\alpha_2-1)\frac{\Gamma(\alpha_0+1)}{\Gamma(\alpha_0)}I1(\alpha_0+1,\beta_0,\gamma_0,\gamma_2)+\frac{\alpha_0\beta_0(1+\alpha_0)-\alpha_0(\gamma_2-\gamma_0)}{\beta_2}
\end{array}\right)\tag{3.31}$$

The expression for $E[Logf(t_i|\alpha_0,\beta_0,\gamma_0)]\times E[Logf(t_j|\alpha_1,\beta_1,\gamma_1)]$ is the product

of the expressions for $E[Logf(t_i|\alpha_0,\beta_0,\gamma_0)]$ and $E[Logf(t_j|\alpha_1,\beta_1,\gamma_1)]$.

$$E[Logf(t_i|\alpha_0,\beta_0,\gamma_0)] = \left(\; -Log\Gamma(\alpha_0) - Log\beta_0 + (\alpha_0-1)\psi(\alpha_0) - \alpha_0 \; \right)$$

$$E[Logf(t_j|\alpha_1,\beta_1,\gamma_1)] = \left(\; -Log\Gamma(\alpha_1) - \alpha_1 Log\beta_1 + (\alpha_1-1)I1(\alpha_0,\beta_0,\gamma_0,\gamma_1) - \tfrac{\gamma_0+\alpha_0\beta_0-\gamma_1}{\beta_1} \; \right)$$

$$E[Logf(t_i|\alpha_0,\beta_0,\gamma_0)] \times E[Logf(t_j|\alpha_1,\beta_1,\gamma_1)] = I_{H_0} =$$

$$\left(\begin{array}{l} Log\Gamma(\alpha_0)Log\Gamma(\alpha_1) + \alpha_1 Log\Gamma(\alpha_0)Log\beta_1 - Log\Gamma(\alpha_0)(\alpha_1-1)I1(\alpha_0,\beta_0,\gamma_0,\gamma_1) \\ +Log\Gamma(\alpha_0)\frac{\gamma_0+\alpha_0\beta_0-\gamma_1}{\beta_1} + Log\beta_0 Log\Gamma(\alpha_1) + Log\beta_0\alpha_1 Log\beta_1 \\ -Log\beta_0(\alpha_1-1)I1(\alpha_0,\beta_0,\gamma_0,\gamma_1) + Log\beta_0\frac{\gamma_0+\alpha_0\beta_0-\gamma_1}{\beta_1} \\ -(\alpha_0-1)\psi(\alpha_0)Log\Gamma(\alpha_1) - (\alpha_0-1)\psi(\alpha_0)\alpha_1 Log\beta_1 \\ +(\alpha_0-1)\psi(\alpha_0)(\alpha_1-1)I1(\alpha_0,\beta_0,\gamma_0,\gamma_1) - (\alpha_0-1)\psi(\alpha_0)\frac{\gamma_0+\alpha_0\beta_0-\gamma_1}{\beta_1} \\ +\alpha_0 Log\Gamma(\alpha_1) + \alpha_0\alpha_1 Log\beta_1 - \alpha_0(\alpha_1-1)I1(\alpha_0,\beta_0,\gamma_0,\gamma_1) + \alpha_0\frac{\gamma_0+\alpha_0\beta_0-\gamma_1}{\beta_1} \end{array} \right) \tag{3.32}$$

The expression for $E[Logf(t_i|\alpha_0,\beta_0,\gamma_0)] \times E[Logf(t_j|\alpha_2,\beta_2,\gamma_2)]$ is similar to the one above in Equation 3.32.

$$E[Logf(t_i|\alpha_0,\beta_0,\gamma_0)] \times E[Logf(t_j|\alpha_2,\beta_2,\gamma_2)] = J_{H_0} =$$

$$\left(\begin{array}{l} Log\Gamma(\alpha_0)Log\Gamma(\alpha_2) + \alpha_2 Log\Gamma(\alpha_0)Log\beta_2 - Log\Gamma(\alpha_0)(\alpha_2-1)I1(\alpha_0,\beta_0,\gamma_0,\gamma_2) \\ +Log\Gamma(\alpha_0)\frac{\gamma_0+\alpha_0\beta_0-\gamma_2}{\beta_2} + Log\beta_0 Log\Gamma(\alpha_2) + Log\beta_0\alpha_2 Log\beta_2 \\ -Log\beta_0(\alpha_2-1)I1(\alpha_0,\beta_0,\gamma_0,\gamma_2) + Log\beta_0\frac{\gamma_0+\alpha_0\beta_0-\gamma_2}{\beta_2} \\ -(\alpha_0-1)\psi(\alpha_0)Log\Gamma(\alpha_2) - (\alpha_0-1)\psi(\alpha_0)\alpha_2 Log\beta_2 \\ +(\alpha_0-1)\psi(\alpha_0)(\alpha_2-1)I1(\alpha_0,\beta_0,\gamma_0,\gamma_2) - (\alpha_0-1)\psi(\alpha_0)\frac{\gamma_0+\alpha_0\beta_0-\gamma_2}{\beta_2} \\ +\alpha_0 Log\Gamma(\alpha_2) + \alpha_0\alpha_2 Log\beta_2 - \alpha_0(\alpha_2-1)I1(\alpha_0,\beta_0,\gamma_0,\gamma_2) + \alpha_0\frac{\gamma_0+\alpha_0\beta_0-\gamma_2}{\beta_2} \end{array} \right) \tag{3.33}$$

The final expression needed to be substituted in Equation 3.20 is the one for

$E[Logf(t_i|\alpha_1,\beta_1,\gamma_1)] \times E[Logf(t_j|\alpha_2,\beta_2,\gamma_2)]$ and this expression is simply the product of the expressions for $E[Logf(t_i|\alpha_1,\beta_1,\gamma_1)]$ and $E[Logf(t_i|\alpha_2,\beta_2,\gamma_2)]$.

$$E[Logf(t_i|\alpha_1,\beta_1,\gamma_1)] =$$
$$\left(-Log\Gamma(\alpha_1) - \alpha_1 Log\beta_1 + (\alpha_1-1)I1(\alpha_0,\beta_0,\gamma_0,\gamma_1) - \tfrac{\gamma_0+\alpha_0\beta_0-\gamma_1}{\beta_1}\right)$$

$$E[Logf(t_i|\alpha_2,\beta_2,\gamma_2)] =$$
$$\left(-Log\Gamma(\alpha_2) - \alpha_2 Log\beta_2 + (\alpha_2-1)I1(\alpha_0,\beta_0,\gamma_0,\gamma_2) - \tfrac{\gamma_0+\alpha_0\beta_0-\gamma_2}{\beta_2}\right)$$

$$E[Logf(t_i|\alpha_1,\beta_1,\gamma_1)] \times E[Logf(t_j|\alpha_2,\beta_2,\gamma_2)] = K_{H_0} =$$
$$\left(\begin{array}{l}
Log\Gamma(\alpha_1)Log\Gamma(\alpha_2) + Log\Gamma(\alpha_1)\alpha_2 Log\beta_2 - Log\Gamma(\alpha_1)(\alpha_2-1)I1(\alpha_0,\beta_0,\gamma_0,\gamma_2) \\
+Log\Gamma(\alpha_1)\frac{\gamma_0+\alpha_0\beta_0-\gamma_2}{\beta_2} + \alpha_1 Log\beta_1 Log\Gamma(\alpha_2) + \alpha_1 Log\beta_1\alpha_2 Log\beta_2 \\
-\alpha_1 Log\beta_1(\alpha_2-1)I1(\alpha_0,\beta_0,\gamma_0,\gamma_2) + \alpha_1 Log\beta_1\frac{\gamma_0+\alpha_0\beta_0-\gamma_2}{\beta_2} \\
-(\alpha_1-1)I1(\alpha_0,\beta_0,\gamma_0,\gamma_1)Log\Gamma(\alpha_2) - (\alpha_1-1)I1(\alpha_0,\beta_0,\gamma_0,\gamma_1)\alpha_2 Log\beta_2 \\
+(\alpha_1-1)I1(\alpha_0,\beta_0,\gamma_0,\gamma_1)(\alpha_2-1)I1(\alpha_0,\beta_0,\gamma_0,\gamma_2) \\
-(\alpha_1-1)I1(\alpha_0,\beta_0,\gamma_0,\gamma_1)\frac{\gamma_0+\alpha_0\beta_0-\gamma_2}{\beta_2} + \frac{\gamma_0+\alpha_0\beta_0-\gamma_1}{\beta_1}Log\Gamma(\alpha_2) \\
+\frac{\gamma_0+\alpha_0\beta_0-\gamma_1}{\beta_1}\alpha_2 Log\beta_2 - \frac{\gamma_0+\alpha_0\beta_0-\gamma_1}{\beta_1}(\alpha_2-1)I1(\alpha_0,\beta_0,\gamma_0,\gamma_2) \\
+\frac{\gamma_0+\alpha_0\beta_0-\gamma_1}{\beta_1}\frac{\gamma_0+\alpha_0\beta_0-\gamma_2}{\beta_2}
\end{array}\right) \tag{3.34}$$

The right hand side of Equation 3.20 can be rewritten as follows by using the expressions obtained in Equations 3.22, 3.23, 3.25, 3.26, 3.27, 3.28, 3.30, 3.31, 3.32, 3.33 and 3.34.

$$E[L^2] = \left(\begin{array}{l}
nA_{H_0} + n(n-1)B_{H_0} + \lfloor\tfrac{n}{2}\rfloor C_{H_0} + \lfloor\tfrac{n}{2}\rfloor(\lfloor\tfrac{n}{2}\rfloor - 1)E_{H_0} \\
+\lceil\tfrac{n}{2}\rceil D_{H_0} + \lceil\tfrac{n}{2}\rceil(\lceil\tfrac{n}{2}\rceil - 1)F_{H_0} - 2\lfloor\tfrac{n}{2}\rfloor G_{H_0} - 2\lfloor\tfrac{n}{2}\rfloor(n-1)I_{H_0} \\
-2\lceil\tfrac{n}{2}\rceil H_{H_0} - 2\lceil\tfrac{n}{2}\rceil(n-1)J_{H_0} + 2\lfloor\tfrac{n}{2}\rfloor\lceil\tfrac{n}{2}\rceil K_{H_0}
\end{array}\right) \tag{3.35}$$

This final expression for second moment of L when H_0 is true and parameters are in the *L-finite* subspace was validated using simulations and it accurately predicts the second moment. Formal validation results are presented in Chapter 4 where the expression obtained above in Equation 3.35 is used to obtain the receiver operating characteristics.

3.4.4 Expected value: *L-infinite*

Recall that when parameters are in the *L-infinite* subspace, $\gamma_0 < \text{Max}(\gamma_1, \gamma_2)$, and in this subspace L is finite with probability that given by Equation 3.7, and is infinite with probability that is given by Equation 3.6. When parameters are in *L-infinite* subspace, $E[L] = \infty$ because the probability of L being infinite is nonzero. However, if the samples of L for which L is infinite are excluded and only the samples for which L is finite are considered then the expected value of L is finite. In this section, an expression for this expected value of L will be derived given the conditions that the parameters are in the *L-infinite* subspace and L is finite. Likelihood ratio L is finite when $t_i > \text{Max}(\gamma_1, \gamma_2), \forall i : i \in \{1..n\}$. Samples t_i are drawn from the Gamma distribution with parameters α_0, β_0 and γ_0. If the samples t_i that have a value less than $\text{Max}(\gamma_1, \gamma_2)$ are to be ignored and all other samples are to be considered, then these samples have a truncated Gamma probability density function. Define a new random variable Z that has a truncated Gamma probability density function and all values less than some constant ξ are truncated. The the PDF of Z is as follows

$$f_Z(z) = \begin{cases} \frac{1}{K}\frac{1}{\Gamma(\alpha)\beta^\alpha}(z-\gamma)^{\alpha-1}e^{-\frac{z-\gamma}{\beta}} & z \geq \xi \\ 0 & \text{otherwise} \end{cases} \tag{3.36}$$

Where,

$$K = \frac{1}{\Gamma(\alpha)\beta^{\alpha}} \int_{\xi}^{\infty} (x-\gamma)^{\alpha-1} e^{-\frac{x-\gamma}{\beta}} dx \tag{3.37}$$

Numerical integration will be used to find all the expected values that involve this PDF. When H_0 is true and only the RTT samples that have a value greater than ξ ($\xi \geq \gamma_0$) are selected, then the functions defined below represent the expected values can be obtained using numerical integration.

$$Ez(\alpha_0, \beta_0, \gamma_0, \xi) = E[z] = \frac{1}{K} \frac{1}{\Gamma(\alpha_0)\beta_0^{\alpha_0}} \int_{\xi}^{\infty} z(z-\gamma_0)^{\alpha_0-1} e^{-\frac{z-\gamma_0}{\beta_0}} dz$$

Define

$$ELzMG(\alpha_0, \beta_0, \gamma_0, \xi, \gamma_1) = E[Log(z-\gamma_1)]$$
$$= \frac{1}{K} \frac{1}{\Gamma(\alpha_0)\beta_0^{\alpha_0}} \int_{\xi}^{\infty} Log(z-\gamma_1)(z-\gamma_0)^{\alpha_0-1} e^{-\frac{z-\gamma_0}{\beta_0}} dz$$

The expression for likelihood ratio can be rewritten as follows.

$$L = Log \frac{\prod_{j=1}^{\lfloor \frac{n}{2} \rfloor} f_Z(z_j|\alpha_0, \beta_0, \gamma_0) \prod_{k=\lfloor \frac{n}{2} \rfloor + 1}^{n} f_Z(z_k|\alpha_0, \beta_0, \gamma_0)}{\prod_{j=1}^{\lfloor \frac{n}{2} \rfloor} f_Z(z_j|\alpha_1, \beta_1, \gamma_1) \prod_{k=\lfloor \frac{n}{2} \rfloor + 1}^{n} f_Z(z_k|\alpha_2, \beta_2, \gamma_2)} \tag{3.38}$$

The expression for $E[L|H_0]$ similar to the one in Section 3.4.2.

$$\begin{aligned} E[L|H_0] = \; & -nLog[\Gamma(\alpha_0)] - n\alpha_0 Log[\beta_0] + \lfloor \tfrac{n}{2} \rfloor (\alpha_0 - 1) E[Log(z_j - \gamma_0)] \\ & - \lfloor \tfrac{n}{2} \rfloor \tfrac{(E[z_j] - \gamma_0)}{\beta_0} + \lceil \tfrac{n}{2} \rceil (\alpha_0 - 1) E[Log(z_k - \gamma_0)] \\ & - \lceil \tfrac{n}{2} \rceil \tfrac{(E[z_k] - \gamma_0)}{\beta_0} + \lfloor \tfrac{n}{2} \rfloor Log[\Gamma(\alpha_1)] + \lfloor \tfrac{n}{2} \rfloor \alpha_1 Log[\beta_1] \\ & - \lfloor \tfrac{n}{2} \rfloor (\alpha_1 - 1) E[Log(z_j - \gamma_1)] + \lfloor \tfrac{n}{2} \rfloor \tfrac{(E[z_j] - \gamma_1)}{\beta_1} + \lceil \tfrac{n}{2} \rceil Log[\Gamma(\alpha_2)] \\ & + \lceil \tfrac{n}{2} \rceil \alpha_2 Log[\beta_2] - \lceil \tfrac{n}{2} \rceil (\alpha_2 - 1) E[Log(z_j - \gamma_2)] + \lceil \tfrac{n}{2} \rceil \tfrac{(E[z_j] - \gamma_2)}{\beta_2} \end{aligned} \tag{3.39}$$

Since closed form solutions to the various expressions in the right hand side of the above equation are not known, numerical integration is used to obtain a value of

the above expression. Let $\xi_1 = \text{Max}(\gamma_0, \gamma_1)$ and $\xi_2 = \text{Max}(\gamma_0, \gamma_2)$. For L to be finite, the samples $z_j, j \in \{1..\lfloor \frac{n}{2} \rfloor\}$ should all have a value that is greater than ξ_1 and samples $z_k, k \in \{\lfloor \frac{n}{2} \rfloor + 1..n\}$ should all be greater than ξ_2. Hence, it is assumed that z_j's are samples from a truncated Gamma distribution with parameters α_0, β_0, γ_0, truncated at ξ_1 and z_k's are samples from truncated Gamma distribution with the same parameters but truncated at ξ_2.

$$\begin{aligned} E[L|H_0] = \; & -nLog[\Gamma(\alpha_0)] - n\alpha_0 Log[\beta_0] \\ & + \lfloor \tfrac{n}{2} \rfloor (\alpha_0 - 1) ELzMG(\alpha_0, \beta_0, \gamma_0, \xi_1, \gamma_0) \\ & - \lfloor \tfrac{n}{2} \rfloor \tfrac{(Ez(\alpha_0, \beta_0, \gamma_0, \xi_1) - \gamma_0)}{\beta_0} + \lceil \tfrac{n}{2} \rceil (\alpha_0 - 1) ELzMG(\alpha_0, \beta_0, \gamma_0, \xi_2, \gamma_0) \\ & - \lceil \tfrac{n}{2} \rceil \tfrac{(Ez(\alpha_0, \beta_0, \gamma_0, \xi_2) - \gamma_0)}{\beta_0} + \lfloor \tfrac{n}{2} \rfloor Log[\Gamma(\alpha_1)] + \lfloor \tfrac{n}{2} \rfloor \alpha_1 Log[\beta_1] \\ & - \lfloor \tfrac{n}{2} \rfloor (\alpha_1 - 1) ELzMG(\alpha_0, \beta_0, \gamma_0, \xi_1, \gamma_1) + \lfloor \tfrac{n}{2} \rfloor \tfrac{(Ez(\alpha_0, \beta_0, \gamma_0, \xi_1) - \gamma_1)}{\beta_1} \\ & + \lceil \tfrac{n}{2} \rceil Log[\Gamma(\alpha_2)] + \lceil \tfrac{n}{2} \rceil \alpha_2 Log[\beta_2] \\ & - \lceil \tfrac{n}{2} \rceil (\alpha_2 - 1) ELzMG(\alpha_0, \beta_0, \gamma_0, \xi_2, \gamma_2) + \lceil \tfrac{n}{2} \rceil \tfrac{(Ez(\alpha_0, \beta_0, \gamma_0, \xi_2) - \gamma_2)}{\beta_2} \end{aligned} \tag{3.40}$$

The expression for expected value derived above in Equation 3.40 was validated using simulations and it accurately predicts the expected value of L when parameters are in *L-infinite* subspace and only samples of L that have a finite value are considered. Formal validation results are presented in chapter 4 where the expression obtained above in Equation 3.40 is used to predict the receiver operating characteristics.

3.4.5 Second Moment: *L-infinite*

An expression for second moment of L when H_0 is true and the parameters are in the *L-infinite* subspace will be found in this section. The expression for

second moment can be written as follows.

$$E[L^2] = E\left[\left(\begin{array}{l} \sum_{j=1}^{\lfloor \frac{n}{2} \rfloor} Logf_Z(z_j|\alpha_0,\beta_0,\gamma_0) + \sum_{k=\lfloor \frac{n}{2} \rfloor+1}^{n} Logf_Z(z_k|\alpha_0,\beta_0,\gamma_0) \\ -\sum_{j=1}^{\lfloor \frac{n}{2} \rfloor} Logf_Z(z_j|\alpha_1,\beta_1,\gamma_1) - \sum_{k=\lfloor \frac{n}{2} \rfloor+1}^{n} Logf_Z(z_k|\alpha_2,\beta_2,\gamma_2) \end{array}\right)^2\right]$$

This expression can be expanded as follows.

$$E[L^2] = E\left[\begin{array}{l} \sum_{j1=1}^{\lfloor \frac{n}{2} \rfloor}\sum_{j2=1}^{\lfloor \frac{n}{2} \rfloor}(Logf_Z(z_{j1}|\alpha_0,\beta_0,\gamma_0)) \times (Logf_Z(z_{j2}|\alpha_0,\beta_0,\gamma_0)) \\ +\sum_{k1=\lfloor \frac{n}{2} \rfloor+1}^{n}\sum_{k2=\lfloor \frac{n}{2} \rfloor+1}^{n}(Logf_Z(z_{k1}|\alpha_0,\beta_0,\gamma_0)) \times (Logf_Z(z_{k2}|\alpha_0,\beta_0,\gamma_0)) \\ +\sum_{j1=1}^{\lfloor \frac{n}{2} \rfloor}\sum_{j2=1}^{\lfloor \frac{n}{2} \rfloor}(Logf_Z(z_{j1}|\alpha_1,\beta_1,\gamma_1)) \times (Logf_Z(z_{j2}|\alpha_1,\beta_1,\gamma_1)) \\ +\sum_{k1=\lfloor \frac{n}{2} \rfloor+1}^{n}\sum_{k2=\lfloor \frac{n}{2} \rfloor+1}^{n}(Logf_Z(z_{k1}|\alpha_2,\beta_2,\gamma_2)) \times (Logf_Z(z_{k2}|\alpha_2,\beta_2,\gamma_2)) \\ +2 \times \sum_{j=1}^{\lfloor \frac{n}{2} \rfloor}\sum_{k=\lfloor \frac{n}{2} \rfloor+1}^{n}(Logf_Z(z_j|\alpha_0,\beta_0,\gamma_0)) \times (Logf_Z(z_k|\alpha_0,\beta_0,\gamma_0)) \\ -2 \times \sum_{j1=1}^{\lfloor \frac{n}{2} \rfloor}\sum_{j2=1}^{\lfloor \frac{n}{2} \rfloor}(Logf_Z(z_{j1}|\alpha_0,\beta_0,\gamma_0)) \times (Logf_Z(z_{j2}|\alpha_1,\beta_1,\gamma_1)) \\ -2 \times \sum_{j=1}^{\lfloor \frac{n}{2} \rfloor}\sum_{k=\lfloor \frac{n}{2} \rfloor+1}^{n}(Logf_Z(z_j|\alpha_0,\beta_0,\gamma_0)) \times (Logf_Z(z_k|\alpha_2,\beta_2,\gamma_2)) \\ -2 \times \sum_{j=1}^{\lfloor \frac{n}{2} \rfloor}\sum_{k=\lfloor \frac{n}{2} \rfloor+1}^{n}(Logf_Z(z_j|\alpha_1,\beta_1,\gamma_1)) \times (Logf_Z(z_k|\alpha_0,\beta_0,\gamma_0)) \\ -2 \times \sum_{k1=\lfloor \frac{n}{2} \rfloor+1}^{n}\sum_{k2=\lfloor \frac{n}{2} \rfloor+1}^{n}(Logf_Z(z_{k1}|\alpha_0,\beta_0,\gamma_0)) \times \\ (Logf_Z(z_{k2}|\alpha_2,\beta_2,\gamma_2)) \\ +2 \times \sum_{j=1}^{\lfloor \frac{n}{2} \rfloor}\sum_{k=\lfloor \frac{n}{2} \rfloor+1}^{n}(Logf_Z(z_j|\alpha_1,\beta_1,\gamma_1)) \times (Logf_Z(z_k|\alpha_2,\beta_2,\gamma_2)) \end{array}\right]$$

This equation can be expanded further by separating the terms for which $z_{j1} = z_{j2}$(or $z_{k1} = z_{k2}$). Also, since it is assumed that z_{j1} (or z_{k1}) and z_{j2} (or z_{k2}) are samples from independent identically distributed random variables, expressions of the form $E[u(z_{j1})v(z_{j2})]$ can be simplified as $E[u(z_{j1})v(z_{j2})] = E[u(z_{j1})]E[v(z_{j2})]$, where u and v are some functions. Here, z_j's and z_k's are samples from truncated Gamma distribution with parameters α_0, β_0, γ_0, truncated at ξ_1 and ξ_2

respectively.

$$
\begin{aligned}
&E[L^2] = \\
&\Bigg(\\
&\sum_{j=1}^{\lfloor \frac{n}{2} \rfloor} E\left[Log^2 f_Z(z_j|\alpha_0,\beta_0,\gamma_0)\right] \\
&+\sum_{j1=1}^{\lfloor \frac{n}{2} \rfloor}\sum_{j2=1,j2\neq j1}^{\lfloor \frac{n}{2} \rfloor} E\left[Log f_Z(z_{j1}|\alpha_0,\beta_0,\gamma_0)\right] \times E\left[Log f_Z(z_{j2}|\alpha_0,\beta_0,\gamma_0)\right] \\
&+\sum_{k=\lfloor \frac{n}{2} \rfloor+1}^{n} E\left[Log^2 f_Z(z_k|\alpha_0,\beta_0,\gamma_0)\right] \\
&+\sum_{k1=\lfloor \frac{n}{2} \rfloor+1}^{n}\sum_{k2=\lfloor \frac{n}{2} \rfloor+1,k2\neq k1}^{n} E\left[Log f_Z(z_{k1}|\alpha_0,\beta_0,\gamma_0)\right] \times \\
&E\left[Log f_Z(z_{k2}|\alpha_0,\beta_0,\gamma_0)\right] \\
&+\sum_{j=1}^{\lfloor \frac{n}{2} \rfloor} E\left[Log^2 f_Z(z_j|\alpha_1,\beta_1,\gamma_1)\right] \\
&+\sum_{j1=1}^{\lfloor \frac{n}{2} \rfloor}\sum_{j2=1,j2\neq j1}^{\lfloor \frac{n}{2} \rfloor} E\left[Log f_Z(z_{j1}|\alpha_1,\beta_1,\gamma_1)\right] \times E\left[Log f_Z(z_{j2}|\alpha_1,\beta_1,\gamma_1)\right] \\
&+\sum_{k=\lfloor \frac{n}{2} \rfloor+1}^{n} E\left[Log^2 f_Z(z_k|\alpha_2,\beta_2,\gamma_2)\right] \\
&+\sum_{k1=\lfloor \frac{n}{2} \rfloor+1}^{n}\sum_{k2=\lfloor \frac{n}{2} \rfloor+1,k2\neq k1}^{n} E\left[Log f_Z(z_{k1}|\alpha_2,\beta_2,\gamma_2)\right] \times \\
&E\left[Log f_Z(z_{k2}|\alpha_2,\beta_2,\gamma_2)\right] \\
&+2 \times \sum_{j=1}^{\lfloor \frac{n}{2} \rfloor}\sum_{k=\lfloor \frac{n}{2} \rfloor+1}^{n} E\left[Log f_Z(z_j|\alpha_0,\beta_0,\gamma_0)\right] \times E\left[Log f_Z(z_k|\alpha_0,\beta_0,\gamma_0)\right] \\
&-2 \times \sum_{j=1}^{\lfloor \frac{n}{2} \rfloor} E\left[(Log f_Z(z_j|\alpha_0,\beta_0,\gamma_0)) \times (Log f_Z(z_j|\alpha_1,\beta_1,\gamma_1))\right] \\
&-2 \times \sum_{j1=1}^{\lfloor \frac{n}{2} \rfloor}\sum_{j2=1,j2\neq j1}^{\lfloor \frac{n}{2} \rfloor} E\left[Log f_Z(z_{j1}|\alpha_0,\beta_0,\gamma_0)\right] \times E\left[Log f_Z(z_{j2}|\alpha_1,\beta_1,\gamma_1)\right] \\
&-2 \times \sum_{j=1}^{\lfloor \frac{n}{2} \rfloor}\sum_{k=\lfloor \frac{n}{2} \rfloor+1}^{n} E\left[Log f_Z(z_j|\alpha_0,\beta_0,\gamma_0)\right] \times E\left[Log f_Z(z_k|\alpha_2,\beta_2,\gamma_2)\right] \\
&-2 \times \sum_{j=1}^{\lfloor \frac{n}{2} \rfloor}\sum_{k=\lfloor \frac{n}{2} \rfloor+1}^{n} E\left[Log f_Z(z_j|\alpha_1,\beta_1,\gamma_1)\right] \times E\left[Log f_Z(z_k|\alpha_0,\beta_0,\gamma_0)\right] \\
&-2 \times \sum_{k=\lfloor \frac{n}{2} \rfloor+1}^{n} E\left[(Log f_Z(z_k|\alpha_0,\beta_0,\gamma_0)) \times (Log f_Z(z_k|\alpha_2,\beta_2,\gamma_2))\right] \\
&-2 \times \sum_{k1=\lfloor \frac{n}{2} \rfloor+1}^{n}\sum_{k2=\lfloor \frac{n}{2} \rfloor+1,k2\neq k1}^{n} E\left[Log f_Z(z_{k1}|\alpha_0,\beta_0,\gamma_0)\right] \times \\
&E\left[Log f_Z(z_{k2}|\alpha_2,\beta_2,\gamma_2)\right] \\
&+2 \times \sum_{j=1}^{\lfloor \frac{n}{2} \rfloor}\sum_{k=\lfloor \frac{n}{2} \rfloor+1}^{n} E\left[Log f_Z(z_j|\alpha_1,\beta_1,\gamma_1)\right] \times E\left[Log f_Z(z_k|\alpha_2,\beta_2,\gamma_2)\right] \\
&\Bigg)
\end{aligned}
\tag{3.41}
$$

Equation 3.41 above can be rewritten as follows: -

$$
\begin{aligned}
&E[L^2] = \\
&\Bigg(\\
&\lfloor \tfrac{n}{2} \rfloor E\left[Log^2 f_Z(z_j|\alpha_0,\beta_0,\gamma_0)\right] \\
&+\lfloor \tfrac{n}{2} \rfloor (\lfloor \tfrac{n}{2} \rfloor - 1) E\left[Log f_Z(z_{j1}|\alpha_0,\beta_0,\gamma_0)\right] \times E\left[Log f_Z(z_{j2}|\alpha_0,\beta_0,\gamma_0)\right] \\
&+\lceil \tfrac{n}{2} \rceil E\left[Log^2 f_Z(z_k|\alpha_0,\beta_0,\gamma_0)\right] \\
&+\lceil \tfrac{n}{2} \rceil (\lceil \tfrac{n}{2} \rceil - 1) E\left[Log f_Z(z_{k1}|\alpha_0,\beta_0,\gamma_0)\right] \times E\left[Log f_Z(z_{k2}|\alpha_0,\beta_0,\gamma_0)\right] \\
&+\lfloor \tfrac{n}{2} \rfloor E\left[Log^2 f_Z(z_j|\alpha_1,\beta_1,\gamma_1)\right] \\
&+\lfloor \tfrac{n}{2} \rfloor (\lfloor \tfrac{n}{2} \rfloor - 1) E\left[Log f_Z(z_{j1}|\alpha_1,\beta_1,\gamma_1)\right] \times E\left[Log f_Z(z_{j2}|\alpha_1,\beta_1,\gamma_1)\right] \\
&+\lceil \tfrac{n}{2} \rceil E\left[Log^2 f_Z(z_k|\alpha_2,\beta_2,\gamma_2)\right] \\
&+\lceil \tfrac{n}{2} \rceil (\lceil \tfrac{n}{2} \rceil - 1) E\left[Log f_Z(z_{k1}|\alpha_2,\beta_2,\gamma_2)\right] \times E\left[Log f_Z(z_{k2}|\alpha_2,\beta_2,\gamma_2)\right] \\
&+2\lfloor \tfrac{n}{2} \rfloor \lceil \tfrac{n}{2} \rceil E\left[Log f_Z(z_j|\alpha_0,\beta_0,\gamma_0)\right] \times E\left[Log f_Z(z_k|\alpha_0,\beta_0,\gamma_0)\right] \\
&-2\lfloor \tfrac{n}{2} \rfloor E\left[(Log f_Z(z_j|\alpha_0,\beta_0,\gamma_0)) \times (Log f_Z(z_j|\alpha_1,\beta_1,\gamma_1))\right] \\
&-2\lfloor \tfrac{n}{2} \rfloor (\lfloor \tfrac{n}{2} \rfloor - 1) E\left[Log f_Z(z_{j1}|\alpha_0,\beta_0,\gamma_0)\right] \times E\left[Log f_Z(z_{j2}|\alpha_1,\beta_1,\gamma_1)\right] \\
&-2\lfloor \tfrac{n}{2} \rfloor \lceil \tfrac{n}{2} \rceil E\left[Log f_Z(z_j|\alpha_0,\beta_0,\gamma_0)\right] \times E\left[Log f_Z(z_k|\alpha_2,\beta_2,\gamma_2)\right] \\
&-2\lfloor \tfrac{n}{2} \rfloor \lceil \tfrac{n}{2} \rceil E\left[Log f_Z(z_j|\alpha_1,\beta_1,\gamma_1)\right] \times E\left[Log f_Z(z_k|\alpha_0,\beta_0,\gamma_0)\right] \\
&-2\lceil \tfrac{n}{2} \rceil E\left[(Log f_Z(z_k|\alpha_0,\beta_0,\gamma_0)) \times (Log f_Z(z_k|\alpha_2,\beta_2,\gamma_2))\right] \\
&-2\lceil \tfrac{n}{2} \rceil (\lceil \tfrac{n}{2} \rceil - 1) E\left[Log f_Z(z_{k1}|\alpha_0,\beta_0,\gamma_0)\right] \times E\left[Log f_Z(z_{k2}|\alpha_2,\beta_2,\gamma_2)\right] \\
&+2\lfloor \tfrac{n}{2} \rfloor \lceil \tfrac{n}{2} \rceil E\left[Log f_Z(z_j|\alpha_1,\beta_1,\gamma_1)\right] \times E\left[Log f_Z(z_k|\alpha_2,\beta_2,\gamma_2)\right] \\
&\Bigg)
\end{aligned}
\tag{3.42}
$$

Numerical methods are used to obtain a value for the above expression in Equation 3.42 because the samples z are from a truncated Gamma distribution and closed form expressions for the expected values with this distribution are not known. Although the summations have been removed in Equation 3.42, the subscripts j and k in z_j and z_k have been retained because they represent samples from two different distributions. The subscript j represents a sample from trun-

cated Gamma distribution truncated at ξ_1 and subscript k represents the same distribution truncated at ξ_2. The values for the second moment from above equation obtained using numerical integration were validated using simulation and the above method accurately predicts the second moment of L. Formal validation results are presented in chapter 4 where the expression obtained above in Equation 3.42 is used to predict the receiver operating characteristics.

3.5 Moments of L: H_1 true

In this section, expressions for the first two moments of L when H_1 is true are derived. Just like in the case when H_0 was true, here the base parameter space is partitioned into two subspaces (*L-finite*, *L-infinte*) and the moments of L can be found using different methods for each of the two subspaces. Section 3.5.1 discusses how parameter space is partitioned. The probability of L being finite when parameters are in *L-infinite* subspace is also derived in Section 3.5.1. When H_1 is true, first $\lfloor \frac{n}{2} \rfloor$ samples have Gamma density with parameters α_1, β_1 and γ_1 and the remaining $\lceil \frac{n}{2} \rceil$ samples have Gamma density with parameters α_2, β_2 and γ_2. The likelihood ratio function can be expressed as follows.

$$L = Log \frac{\prod_{j=1}^{\lfloor \frac{n}{2} \rfloor} f_T(t_j|\alpha_0, \beta_0, \gamma_0) \prod_{k=\lfloor \frac{n}{2} \rfloor + 1}^{n} f_T(t_k|\alpha_0, \beta_0, \gamma_0)}{\prod_{j=1}^{\lfloor \frac{n}{2} \rfloor} f_T(t_j|\alpha_1, \beta_1, \gamma_1) \prod_{k=\lfloor \frac{n}{2} \rfloor + 1}^{n} f_T(t_k|\alpha_2, \beta_2, \gamma_2)} \tag{3.43}$$

Equation 3.43 will be used to derive expressions for expected value of L and variance of L. Expected value and variance of L when parameters are in the *L-finite* subspace are derived in Sections 3.5.2 and 3.5.3 respectively. Expected value and variance of L when parameters are in *L-infinite* subspace are derived in Sections 3.5.4 and 3.5.5 respectively.

3.5.1 Parameter subspaces: $\gamma_0 > \mathbf{Min}(\gamma_1, \gamma_2)$ and $\gamma_0 \leq \mathbf{Min}(\gamma_1, \gamma_2)$

When $\gamma_0 \leq \text{Min}(\gamma_1, \gamma_2)$, both L and its first two moments are finite and the parameters are in *L-finite* subspace. When $\gamma_0 > \text{Min}(\gamma_1, \gamma_2)$, it is possible for L to be $-\infty$ and the parameters are in *L-infinite* subspace. When $\gamma_0 > \text{Min}(\gamma_1, \gamma_2)$ and H_1 is true, it may happen that one or more of the samples t_i have a value such that $t_i < \gamma_0$ and therefore $L = -\infty$ (see Equation 3.43). For L to be finite when $\gamma_0 > \text{Min}(\gamma_1, \gamma_2)$, all n samples should have a value that is greater than or equal to γ_0, i.e., $t_i \geq \gamma_0, \forall i : i \in \{1..n\}$. The probability of this happening ($P\left(t_i > \gamma_0, \forall i : i \in \{1..n\}\right)$) can be evaluated as follows (assuming i.i.d.)

$$
\begin{aligned}
&P\left(t_i > \gamma_0, \forall i : i \in \{1..n\}\right) = \\
&P\left(t_j > \gamma_0, \forall j : j \in \left\{1..\left\lfloor \tfrac{n}{2} \right\rfloor\right\}\right) \times P\left(t_k > \gamma_0, \forall k : k \in \left\{\left(\left\lfloor \tfrac{n}{2} \right\rfloor + 1\right)..n\right\}\right)
\end{aligned}
$$

Where

$$
P\left(t_j > \gamma_0, \forall j : j \in \left\{1..\left\lfloor \frac{n}{2} \right\rfloor\right\}\right) = P\left(Min\left[t_j, j \in \left\{1..\lfloor \frac{n}{2} \rfloor\right\}\right] > \gamma_0\right)
$$

and

$$
P\left(t_k > \gamma_0, \forall k : k \in \left\{\left(\left\lfloor \frac{n}{2} \right\rfloor + 1\right)..n\right\}\right) = P\left(Min\left[t_k, k \in \left\{\lfloor \frac{n}{2} \rfloor + 1..n\right\}\right] > \gamma_0\right)
$$

Therefore,

$$
\begin{aligned}
P\left(t_i > \gamma_0, \forall i : i \in \{1..n\}\right) &= \left(P\left(Min\left[t_j, j \in \left\{1..\lfloor \tfrac{n}{2} \rfloor\right\}\right] > \gamma_0\right)\right) \\
&\times \left(P\left(Min\left[t_k, k \in \left\{\lfloor \tfrac{n}{2} \rfloor + 1..n\right\}\right] > \gamma_0\right)\right)
\end{aligned} \tag{3.44}
$$

When $Min(\gamma_1, \gamma_2) < \gamma_0$, then one of the following cases is true

- $(\gamma_1 < \gamma_0)$ and $(\gamma_2 < \gamma_0)$
- $(\gamma_1 < \gamma_0)$ and $(\gamma_2 \geq \gamma_0)$
- $(\gamma_1 \geq \gamma_0)$ and $(\gamma_2 < \gamma_0)$

Using the PDF of the first order statistic (see section 3.4.1), the probability $P\left(t_i > \gamma_0, \forall i : i \in \{1..n\}\right)$ can be evaluated as follows for each of the three cases.

- $(\gamma_1 < \gamma_0)$ and $(\gamma_2 < \gamma_0)$

$$P\left(t_i > \gamma_0, \forall i : i \in \{1..n\}\right) = \left(\begin{array}{l} \left(\frac{\lfloor n/2 \rfloor}{[\Gamma(\alpha_1)]^{\lfloor n/2 \rfloor} \beta_1^{\alpha_1}} \int_{\gamma_0 - \gamma_1}^{\infty} q^{\alpha_1 - 1} e^{-\frac{q}{\beta_1}} \left[\Gamma\left(\alpha_1, \frac{q}{\beta_1}\right) \right]^{\lfloor \frac{n}{2} \rfloor - 1} dq \right) \times \\ \left(\frac{\lceil n/2 \rceil}{[\Gamma(\alpha_2)]^{\lceil n/2 \rceil} \beta_2^{\alpha_2}} \int_{\gamma_0 - \gamma_2}^{\infty} q^{\alpha_2 - 1} e^{-\frac{q}{\beta_2}} \left[\Gamma\left(\alpha_2, \frac{q}{\beta_2}\right) \right]^{\lceil \frac{n}{2} \rceil - 1} dq \right) \end{array} \right) \tag{3.45}$$

- $(\gamma_1 < \gamma_0)$ and $(\gamma_2 \geq \gamma_0)$

$$P\left(t_i > \gamma_0, \forall i : i \in \{1..n\}\right) = \left(\frac{\lfloor n/2 \rfloor}{[\Gamma(\alpha_1)]^{\lfloor n/2 \rfloor} \beta_1^{\alpha_1}} \int_{\gamma_0 - \gamma_1}^{\infty} q^{\alpha_1 - 1} e^{-\frac{q}{\beta_1}} \left[\Gamma\left(\alpha_1, \frac{q}{\beta_1}\right) \right]^{\lfloor \frac{n}{2} \rfloor - 1} dq \right) \tag{3.46}$$

- $(\gamma_1 \geq \gamma_0)$ and $(\gamma_2 < \gamma_0)$

$$P\left(t_i > \gamma_0, \forall i : i \in \{1..n\}\right) = \left(\frac{\lceil n/2 \rceil}{[\Gamma(\alpha_2)]^{\lceil n/2 \rceil} \beta_2^{\alpha_2}} \int_{\gamma_0 - \gamma_2}^{\infty} q^{\alpha_2 - 1} e^{-\frac{q}{\beta_2}} \left[\Gamma\left(\alpha_2, \frac{q}{\beta_2}\right) \right]^{\lceil \frac{n}{2} \rceil - 1} dq \right) \tag{3.47}$$

Hence, when $Min(\gamma_1, \gamma_2) < \gamma_0$ and H_1 is true, then probability that L is finite is given by Equations 3.45, 3.46 and 3.47. These expressions will be used later in Chapter 4 where expressions for probability of detection and false alarms are derived. When $\gamma_0 \leq \text{Min}(\gamma_1, \gamma_2)$, then L is finite and so are the first two moments.

An expression for the expected value of L when parameters are in *L-finite* subspace will be obtained in the following section.

3.5.2 Expected Value: *L-finite*

In this section an expression for the expected value of L will be derived given that H_1 is true and $\gamma_0 \leq \text{Min}(\gamma_1, \gamma_2)$ (*L-finite*). Solving Equation 3.43 can be expressed as follows

$$L = \begin{pmatrix} \sum_{j=1}^{\lfloor \frac{n}{2} \rfloor} Log f_T(t_j|\alpha_0, \beta_0, \gamma_0) + \sum_{k=\lfloor \frac{n}{2} \rfloor + 1}^{n} Log f_T(t_k|\alpha_0, \beta_0, \gamma_0) \\ -\sum_{j=1}^{\lfloor \frac{n}{2} \rfloor} Log f_T(t_j|\alpha_1, \beta_1, \gamma_1) - \sum_{k=\lfloor \frac{n}{2} \rfloor + 1}^{n} Log f_T(t_k|\alpha_2, \beta_2, \gamma_2) \end{pmatrix}$$

Since $t_i > \gamma_0, \forall i : i \in \{1..n\}$, from Equation 3.1 it follows that

$$L = \begin{pmatrix} -\lfloor \frac{n}{2} \rfloor Log(\Gamma(\alpha_0)) - \lfloor \frac{n}{2} \rfloor \alpha_0 Log\beta_0 + (\alpha_0 - 1) \sum_{j=1}^{\lfloor \frac{n}{2} \rfloor} Log(t_j - \gamma_0) \\ -\sum_{j=1}^{\lfloor \frac{n}{2} \rfloor} \frac{t_j - \gamma_0}{\beta_0} - \lceil \frac{n}{2} \rceil Log(\Gamma(\alpha_0)) - \lceil \frac{n}{2} \rceil \alpha_0 Log\beta_0 \\ +(\alpha_0 - 1) \sum_{k=\lfloor \frac{n}{2} \rfloor + 1}^{n} Log(t_k - \gamma_0) - \sum_{k=\lfloor \frac{n}{2} \rfloor + 1}^{n} \frac{t_k - \gamma_0}{\beta_0} + \lfloor \frac{n}{2} \rfloor Log(\Gamma(\alpha_1)) \\ +\lfloor \frac{n}{2} \rfloor \alpha_1 Log\beta_1 - (\alpha_1 - 1) \sum_{j=1}^{\lfloor \frac{n}{2} \rfloor} Log(t_j - \gamma_1) + \sum_{j=1}^{\lfloor \frac{n}{2} \rfloor} \frac{t_j - \gamma_1}{\beta_1} \\ +\lceil \frac{n}{2} \rceil Log(\Gamma(\alpha_2)) + \lceil \frac{n}{2} \rceil \alpha_2 Log\beta_2 - (\alpha_2 - 1) \sum_{k=\lfloor \frac{n}{2} \rfloor + 1}^{n} Log(t_k - \gamma_2) \\ +\sum_{k=\lfloor \frac{n}{2} \rfloor + 1}^{n} \frac{t_k - \gamma_2}{\beta_2} \end{pmatrix}$$

Expected value of L can then be expressed as follows.

$$E[L] = \begin{pmatrix} -\lfloor \frac{n}{2} \rfloor Log(\Gamma(\alpha_0)) - \lfloor \frac{n}{2} \rfloor \alpha_0 Log\beta_0 + (\alpha_0 - 1)\sum_{j=1}^{\lfloor \frac{n}{2} \rfloor} E\left[Log(t_j - \gamma_0)\right] \\ -\sum_{j=1}^{\lfloor \frac{n}{2} \rfloor} \frac{E[t_j]-\gamma_0}{\beta_0} - \lceil \frac{n}{2} \rceil Log(\Gamma(\alpha_0)) - \lceil \frac{n}{2} \rceil \alpha_0 Log\beta_0 \\ +(\alpha_0 - 1)\sum_{k=\lfloor \frac{n}{2} \rfloor + 1}^{n} E\left[Log(t_k - \gamma_0)\right] - \sum_{k=\lfloor \frac{n}{2} \rfloor + 1}^{n} \frac{E[t_k]-\gamma_0}{\beta_0} \\ +\lfloor \frac{n}{2} \rfloor Log(\Gamma(\alpha_1)) + \lfloor \frac{n}{2} \rfloor \alpha_1 Log\beta_1 - (\alpha_1 - 1)\sum_{j=1}^{\lfloor \frac{n}{2} \rfloor} E\left[Log(t_j - \gamma_1)\right] \\ +\sum_{j=1}^{\lfloor \frac{n}{2} \rfloor} \frac{E[t_j]-\gamma_1}{\beta_1} + \lceil \frac{n}{2} \rceil Log(\Gamma(\alpha_2)) + \lceil \frac{n}{2} \rceil \alpha_2 Log\beta_2 \\ -(\alpha_2 - 1)\sum_{k=\lfloor \frac{n}{2} \rfloor + 1}^{n} E\left[Log(t_k - \gamma_2)\right] + \sum_{k=\lfloor \frac{n}{2} \rfloor + 1}^{n} \frac{E[t_k]-\gamma_2}{\beta_2} \end{pmatrix} \tag{3.48}$$

Since it is assumed that H_1 is true, the first $\lfloor \frac{n}{2} \rfloor$ samples t_j are from a Gamma distribution with parameters $\alpha_1, \beta_1, \gamma_1$ and the last $\lceil \frac{n}{2} \rceil$ samples t_k are from a Gamma distribution with parameters $\alpha_2, \beta_2, \gamma_2$. Closed form expressions for $E\left[Log(t_j - \gamma_0)\right]$ and $E\left[Log(t_k - \gamma_0)\right]$ are not known and for this reason, numerical integration is used.

$$\begin{aligned} E\left[Log(t_j - \gamma_0)\right] &= \frac{1}{\Gamma(\alpha_1)\beta_1^{\alpha_1}} \int_{\gamma_1}^{\infty} Log(t_j - \gamma_0)(t_j - \gamma_1)^{(\alpha_1 - 1)} e^{-\frac{t_j - \gamma_1}{\beta_1}} dt_j \\ &= I1(\alpha_1, \beta_1, \gamma_1, \gamma_0) \end{aligned}$$

Similarly,

$$E\left[Log(t_k - \gamma_0)\right] = I1(\alpha_2, \beta_2, \gamma_2, \gamma_0)$$

Expected values $E[t_j]$ and $E[t_k]$ can be expressed as $E[t_j] = \gamma_1 + \alpha_1\beta_1$ and $E[t_k] = \gamma_2 + \alpha_2\beta_2$. From Equation 3.14, it follows that

$$E\left[Log(t_j - \gamma_1)\right] = Log(\beta_1) + \psi(\alpha_1)$$

and

$$E\left[Log(t_k - \gamma_2)\right] = Log(\beta_2) + \psi(\alpha_2)$$

The expressions obtained above can be substituted into Equation 3.48 to obtain the following.

$$E[L] = \left(\begin{array}{l} -\lfloor \frac{n}{2} \rfloor Log(\Gamma(\alpha_0)) - \lfloor \frac{n}{2} \rfloor \alpha_0 Log\beta_0 + \lfloor \frac{n}{2} \rfloor (\alpha_0 - 1) I1(\alpha_1, \beta_1, \gamma_1, \gamma_0) \\ -\lfloor \frac{n}{2} \rfloor \frac{\gamma_1 + \alpha_1\beta_1 - \gamma_0}{\beta_0} - \lceil \frac{n}{2} \rceil Log(\Gamma(\alpha_0)) - \lceil \frac{n}{2} \rceil \alpha_0 Log\beta_0 \\ +\lceil \frac{n}{2} \rceil (\alpha_0 - 1) I1(\alpha_2, \beta_2, \gamma_2, \gamma_0) - \lceil \frac{n}{2} \rceil \frac{\gamma_2 + \alpha_2\beta_2 - \gamma_0}{\beta_0} + \lfloor \frac{n}{2} \rfloor Log(\Gamma(\alpha_1)) \\ +\lfloor \frac{n}{2} \rfloor \alpha_1 Log\beta_1 - \lfloor \frac{n}{2} \rfloor (\alpha_1 - 1)(Log(\beta_1) + \psi(\alpha_1)) + \lfloor \frac{n}{2} \rfloor \alpha_1 \\ +\lceil \frac{n}{2} \rceil Log(\Gamma(\alpha_2)) + \lceil \frac{n}{2} \rceil \alpha_2 Log\beta_2 - \lceil \frac{n}{2} \rceil (\alpha_2 - 1)(Log(\beta_2) + \psi(\alpha_2))] \\ +\lceil \frac{n}{2} \rceil \alpha_2 \end{array} \right) \tag{3.49}$$

The equation 3.49 above was validated using simulation and it accurately predicts the expected value of L when H_1 is true. Formal validation results are presented in Chapter 4 where the expression obtained above in Equation 3.49 is used to predict the receiver operating characteristics.

3.5.3 Second Moment: *L-finite*

An expression for second moment of L when H_1 is true and parameters are in *L-finite* subspace will be obtained in this section. The second moment can be derived from Equation 3.43 as follows.

$$E[L^2] = E\left[\left(Log \frac{\prod_{j=1}^{\lfloor \frac{n}{2} \rfloor} f_T(t_j|\alpha_0, \beta_0, \gamma_0) \prod_{k=\lfloor \frac{n}{2} \rfloor + 1}^{n} f_T(t_k|\alpha_0, \beta_0, \gamma_0)}{\prod_{j=1}^{\lfloor \frac{n}{2} \rfloor} f_T(t_j|\alpha_1, \beta_1, \gamma_1) \prod_{k=\lfloor \frac{n}{2} \rfloor + 1}^{n} f_T(t_k|\alpha_2, \beta_2, \gamma_2)} \right)^2 \right]$$

This equation can be expanded as follows

$$E[L^2] = E\left[\left(\begin{array}{l} \sum_{j=1}^{\lfloor \frac{n}{2} \rfloor} Log f_T(t_j|\alpha_0, \beta_0, \gamma_0) + \sum_{k=\lfloor \frac{n}{2} \rfloor + 1}^{n} Log f_T(t_k|\alpha_0, \beta_0, \gamma_0) \\ -\sum_{j=1}^{\lfloor \frac{n}{2} \rfloor} Log f_T(t_j|\alpha_1, \beta_1, \gamma_1) - \sum_{k=\lfloor \frac{n}{2} \rfloor + 1}^{n} Log f_T(t_k|\alpha_2, \beta_2, \gamma_2) \end{array} \right)^2 \right]$$

$$E[L^2] =$$
$$E\left[\begin{array}{l}\left(\begin{array}{l}\sum_{j=1}^{\lfloor\frac{n}{2}\rfloor} Logf_T(t_j|\alpha_0,\beta_0,\gamma_0) + \sum_{k=\lfloor\frac{n}{2}\rfloor+1}^{n} Logf_T(t_k|\alpha_0,\beta_0,\gamma_0) \\ -\sum_{j=1}^{\lfloor\frac{n}{2}\rfloor} Logf_T(t_j|\alpha_1,\beta_1,\gamma_1) - \sum_{k=\lfloor\frac{n}{2}\rfloor+1}^{n} Logf_T(t_k|\alpha_2,\beta_2,\gamma_2)\end{array}\right) \times \\ \left(\begin{array}{l}\sum_{j=1}^{\lfloor\frac{n}{2}\rfloor} Logf_T(t_j|\alpha_0,\beta_0,\gamma_0) + \sum_{k=\lfloor\frac{n}{2}\rfloor+1}^{n} Logf_T(t_k|\alpha_0,\beta_0,\gamma_0) \\ -\sum_{j=1}^{\lfloor\frac{n}{2}\rfloor} Logf_T(t_j|\alpha_1,\beta_1,\gamma_1) - \sum_{k=\lfloor\frac{n}{2}\rfloor+1}^{n} Logf_T(t_k|\alpha_2,\beta_2,\gamma_2)\end{array}\right)\end{array}\right]$$

$$E[L^2] =$$
$$E\left[\begin{array}{l}\sum_{j1=1}^{\lfloor\frac{n}{2}\rfloor}\sum_{j2=1}^{\lfloor\frac{n}{2}\rfloor}(Logf_T(t_{j1}|\alpha_0,\beta_0,\gamma_0)) \times (Logf_T(t_{j2}|\alpha_0,\beta_0,\gamma_0)) \\ +\sum_{k1=\lfloor\frac{n}{2}\rfloor+1}^{n}\sum_{k2=\lfloor\frac{n}{2}\rfloor+1}^{n}(Logf_T(t_{k1}|\alpha_0,\beta_0,\gamma_0)) \times (Logf_T(t_{k2}|\alpha_0,\beta_0,\gamma_0)) \\ +\sum_{j1=1}^{\lfloor\frac{n}{2}\rfloor}\sum_{j2=1}^{\lfloor\frac{n}{2}\rfloor}(Logf_T(t_{j1}|\alpha_1,\beta_1,\gamma_1)) \times (Logf_T(t_{j2}|\alpha_1,\beta_1,\gamma_1)) \\ +\sum_{k1=\lfloor\frac{n}{2}\rfloor+1}^{n}\sum_{k2=\lfloor\frac{n}{2}\rfloor+1}^{n}(Logf_T(t_{k1}|\alpha_2,\beta_2,\gamma_2)) \times (Logf_T(t_{k2}|\alpha_2,\beta_2,\gamma_2)) \\ +2 \times \sum_{j=1}^{\lfloor\frac{n}{2}\rfloor}\sum_{k=\lfloor\frac{n}{2}\rfloor+1}^{n}(Logf_T(t_j|\alpha_0,\beta_0,\gamma_0)) \times (Logf_T(t_k|\alpha_0,\beta_0,\gamma_0)) \\ -2 \times \sum_{j1=1}^{\lfloor\frac{n}{2}\rfloor}\sum_{j2=1}^{\lfloor\frac{n}{2}\rfloor}(Logf_T(t_{j1}|\alpha_0,\beta_0,\gamma_0)) \times (Logf_T(t_{j2}|\alpha_1,\beta_1,\gamma_1)) \\ -2 \times \sum_{j=1}^{\lfloor\frac{n}{2}\rfloor}\sum_{k=\lfloor\frac{n}{2}\rfloor+1}^{n}(Logf_T(t_j|\alpha_0,\beta_0,\gamma_0)) \times (Logf_T(t_k|\alpha_2,\beta_2,\gamma_2)) \\ -2 \times \sum_{j=1}^{\lfloor\frac{n}{2}\rfloor}\sum_{k=\lfloor\frac{n}{2}\rfloor+1}^{n}(Logf_T(t_j|\alpha_1,\beta_1,\gamma_1)) \times (Logf_T(t_k|\alpha_0,\beta_0,\gamma_0)) \\ -2 \times \sum_{k1=\lfloor\frac{n}{2}\rfloor+1}^{n}\sum_{k2=\lfloor\frac{n}{2}\rfloor+1}^{n}(Logf_T(t_{k1}|\alpha_0,\beta_0,\gamma_0))\times \\ (Logf_T(t_{k2}|\alpha_2,\beta_2,\gamma_2)) \\ +2 \times \sum_{j=1}^{\lfloor\frac{n}{2}\rfloor}\sum_{k=\lfloor\frac{n}{2}\rfloor+1}^{n}(Logf_T(t_j|\alpha_1,\beta_1,\gamma_1)) \times (Logf_T(t_k|\alpha_2,\beta_2,\gamma_2))\end{array}\right]$$

This equation can be expanded further by separating the terms for which $t_{j1} = t_{j2}$(or $t_{k1} = t_{k2}$). Also, since it is assumed that t_{j1} (or t_{k1}) and t_{j2} (or t_{k2}) are samples from independent distributions, expressions of the form $E[u(t_{j1})v(t_{j2})]$ can be simplified as $E[u(t_{j1})v(t_{j2})] = E[u(t_{j1})]E[v(t_{j2})]$, where u and v are some

functions.

$$
E[L^2] =
\left(
\begin{array}{l}
\sum_{j=1}^{\lfloor \frac{n}{2} \rfloor} E\left[Log^2 f_T(t_j|\alpha_0,\beta_0,\gamma_0)\right] \\
+\sum_{j1=1}^{\lfloor \frac{n}{2} \rfloor} \sum_{j2=1,j2\neq j1}^{\lfloor \frac{n}{2} \rfloor} E\left[Log f_T(t_{j1}|\alpha_0,\beta_0,\gamma_0)\right] \times E\left[Log f_T(t_{j2}|\alpha_0,\beta_0,\gamma_0)\right] \\
+\sum_{k=\lfloor \frac{n}{2} \rfloor+1}^{n} E\left[Log^2 f_T(t_k|\alpha_0,\beta_0,\gamma_0)\right] \\
+\sum_{k1=\lfloor \frac{n}{2} \rfloor+1}^{n} \sum_{k2=\lfloor \frac{n}{2} \rfloor+1,k2\neq k1}^{n} E\left[Log f_T(t_{k1}|\alpha_0,\beta_0,\gamma_0)\right] \times \\
E\left[Log f_T(t_{k2}|\alpha_0,\beta_0,\gamma_0)\right] \\
+\sum_{j=1}^{\lfloor \frac{n}{2} \rfloor} E\left[Log^2 f_T(t_j|\alpha_1,\beta_1,\gamma_1)\right] \\
+\sum_{j1=1}^{\lfloor \frac{n}{2} \rfloor} \sum_{j2=1,j2\neq j1}^{\lfloor \frac{n}{2} \rfloor} E\left[Log f_T(t_{j1}|\alpha_1,\beta_1,\gamma_1)\right] \times E\left[Log f_T(t_{j2}|\alpha_1,\beta_1,\gamma_1)\right] \\
+\sum_{k=\lfloor \frac{n}{2} \rfloor+1}^{n} E\left[Log^2 f_T(t_k|\alpha_2,\beta_2,\gamma_2)\right] \\
+\sum_{k1=\lfloor \frac{n}{2} \rfloor+1}^{n} \sum_{k2=\lfloor \frac{n}{2} \rfloor+1,k2\neq k1}^{n} E\left[Log f_T(t_{k1}|\alpha_2,\beta_2,\gamma_2)\right] \times \\
E\left[Log f_T(t_{k2}|\alpha_2,\beta_2,\gamma_2)\right] \\
+2 \times \sum_{j=1}^{\lfloor \frac{n}{2} \rfloor} \sum_{k=\lfloor \frac{n}{2} \rfloor+1}^{n} E\left[Log f_T(t_j|\alpha_0,\beta_0,\gamma_0)\right] \times E\left[Log f_T(t_k|\alpha_0,\beta_0,\gamma_0)\right] \\
-2 \times \sum_{j=1}^{\lfloor \frac{n}{2} \rfloor} E\left[\left(Log f_T(t_j|\alpha_0,\beta_0,\gamma_0)\right) \times \left(Log f_T(t_j|\alpha_1,\beta_1,\gamma_1)\right)\right] \\
-2 \times \sum_{j1=1}^{\lfloor \frac{n}{2} \rfloor} \sum_{j2=1,j2\neq j1}^{\lfloor \frac{n}{2} \rfloor} E\left[Log f_T(t_{j1}|\alpha_0,\beta_0,\gamma_0)\right] \times E\left[Log f_T(t_{j2}|\alpha_1,\beta_1,\gamma_1)\right] \\
-2 \times \sum_{j=1}^{\lfloor \frac{n}{2} \rfloor} \sum_{k=\lfloor \frac{n}{2} \rfloor+1}^{n} E\left[Log f_T(t_j|\alpha_0,\beta_0,\gamma_0)\right] \times E\left[Log f_T(t_k|\alpha_2,\beta_2,\gamma_2)\right] \\
-2 \times \sum_{j=1}^{\lfloor \frac{n}{2} \rfloor} \sum_{k=\lfloor \frac{n}{2} \rfloor+1}^{n} E\left[Log f_T(t_j|\alpha_1,\beta_1,\gamma_1)\right] \times E\left[Log f_T(t_k|\alpha_0,\beta_0,\gamma_0)\right] \\
-2 \times \sum_{k=\lfloor \frac{n}{2} \rfloor+1}^{n} E\left[\left(Log f_T(t_k|\alpha_0,\beta_0,\gamma_0)\right) \times \left(Log f_T(t_k|\alpha_2,\beta_2,\gamma_2)\right)\right] \\
-2 \times \sum_{k1=\lfloor \frac{n}{2} \rfloor+1}^{n} \sum_{k2=\lfloor \frac{n}{2} \rfloor+1,k2\neq k1}^{n} E\left[Log f_T(t_{k1}|\alpha_0,\beta_0,\gamma_0)\right] \times \\
\left[Log f_T(t_{k2}|\alpha_2,\beta_2,\gamma_2)\right] \\
+2 \times \sum_{j=1}^{\lfloor \frac{n}{2} \rfloor} \sum_{k=\lfloor \frac{n}{2} \rfloor+1}^{n} E\left[Log f_T(t_j|\alpha_1,\beta_1,\gamma_1)\right] \times E\left[Log f_T(t_k|\alpha_2,\beta_2,\gamma_2)\right]
\end{array}
\right)
\tag{3.50}
$$

Expressions of each of the terms on right hand side of equation 3.50 will now be obtained. Expected value $E[Log^2 f_T(t_j|\alpha_0, \beta_0, \gamma_0)]$ can be expressed as follows.

$$
\begin{aligned}
&E[Log^2 f_T(t_j|\alpha_0, \beta_0, \gamma_0)] = \\
&E\left[\begin{array}{l}
Log^2\Gamma(\alpha_0) + \alpha_0 Log\Gamma(\alpha_0) Log\beta_0 \\
-Log\Gamma(\alpha_0)(\alpha_0 - 1)Log(t_j - \gamma_0) + Log\Gamma(\alpha_0)\frac{t_j-\gamma_0}{\beta_0} \\
+\alpha_0 Log\beta_0 Log\Gamma(\alpha_0) + \alpha_0^2 Log^2\beta_0 \\
-\alpha_0 Log\beta_0(\alpha_0 - 1)Log(t_j - \gamma_0) + \alpha_0 Log\beta_0\frac{t_j-\gamma_0}{\beta_0} \\
-(\alpha_0 - 1)Log(t_j - \gamma_0)Log\Gamma(\alpha_0) \\
-(\alpha_0 - 1)Log(t_j - \gamma_0)\alpha_0 Log\beta_0 \\
+(\alpha_0 - 1)^2 Log^2(t_j - \gamma_0) - (\alpha_0 - 1)Log(t_j - \gamma_0)\frac{t_j-\gamma_0}{\beta_0} \\
+\frac{t_j-\gamma_0}{\beta_0} Log\Gamma(\alpha_0) + \frac{t_j-\gamma_0}{\beta_0}\alpha_0 Log\beta_0 \\
-\frac{t_j-\gamma_0}{\beta_0}(\alpha_0 - 1)Log(t_j - \gamma_0) + \frac{(t_j-\gamma_0)^2}{\beta_0^2}
\end{array}\right]
\end{aligned}
$$

Which is the same as

$$
\begin{aligned}
&E[Log^2 f_T(t_j|\alpha_0, \beta_0, \gamma_0)] \\
&= \left(\begin{array}{l}
Log^2\Gamma(\alpha_0) + 2\alpha_0 Log\Gamma(\alpha_0) Log\beta_0 \\
-2Log\Gamma(\alpha_0)(\alpha_0 - 1)E[Log(t_j - \gamma_0)] + 2Log\Gamma(\alpha_0)E\left[\frac{t_j-\gamma_0}{\beta_0}\right] \\
+\alpha_0^2 Log^2\beta_0 - 2\alpha_0 Log\beta_0(\alpha_0 - 1)E[Log(t_j - \gamma_0)] \\
+2\alpha_0 Log\beta_0 E\left[\frac{t_j-\gamma_0}{\beta_0}\right] + (\alpha_0 - 1)^2 E[Log^2(t_j - \gamma_0)] \\
-2(\alpha_0 - 1)E\left[Log(t_j - \gamma_0)\frac{t_j-\gamma_0}{\beta_0}\right] + E\left[\frac{(t_j-\gamma_0)^2}{\beta_0^2}\right]
\end{array}\right)
\end{aligned}
\tag{3.51}
$$

Since t_j has Gamma density with parameters α_1, β_1 and γ_1, it follows that

$$E[t_j] = \gamma_1 + \alpha_1\beta_1$$

Closed form solutions to $E[Log(t_j-\gamma_0)]$ and $E[Log^2(t_j-\gamma_0)]$ are not known and these are solved numerically.

$$\begin{aligned} E[Log(t_j-\gamma_0)] &= \tfrac{1}{\Gamma(\alpha_1)\beta_1{}^{\alpha_1}} \int_{\gamma_1}^{\infty} Log(t_j-\gamma_0)(t_j-\gamma_1)^{(\alpha_1-1)} e^{-\frac{t_j-\gamma_1}{\beta_1}} dt_j \\ &= I1(\alpha_1,\beta_1,\gamma_1,\gamma_0) \end{aligned}$$

$$\begin{aligned} E[Log^2(t_j-\gamma_0)] &= \tfrac{1}{\Gamma(\alpha_1)\beta_1{}^{\alpha_1}} \int_{\gamma_1}^{\infty} Log^2(t_j-\gamma_0)(t_j-\gamma_1)^{(\alpha_1-1)} e^{-\frac{t_j-\gamma_1}{\beta_1}} dt_j \\ &= I2(\alpha_1,\beta_1,\gamma_1,\gamma_0) \end{aligned}$$

Expression for $E[(t_j-\gamma_0)Log(t_j-\gamma_0)]$ and $E[(t_j-\gamma_0)^2]$ can be obtained by simple algebraic manipulation as follows.

$$\begin{aligned} E[(t_j-\gamma_0)Log(t_j-\gamma_0)] &= E\left[(t_j-\gamma_1)Log(t_j-\gamma_0) - (\gamma_0-\gamma_1)Log(t_j-\gamma_0)\right] \\ &= \tfrac{\Gamma(\alpha_1+1)}{\Gamma(\alpha_1)}\beta_1 I1(\alpha_1+1,\beta_1,\gamma_1,\gamma_0) \\ &\quad -(\gamma_0-\gamma_1)I1(\alpha_1,\beta_1,\gamma_1,\gamma_0) \end{aligned}$$

$$\begin{aligned} E[(t_j-\gamma_0)^2] &= E[((t_j-\gamma_1)-(\gamma_0-\gamma_1))^2] \\ &= E[(t_j-\gamma_1)^2] + (\gamma_0-\gamma_1)^2 - 2(\gamma_0-\gamma_1)E[t_j-\gamma_1] \\ &= \beta_1^2\alpha_1(\alpha_1+1) + (\gamma_0-\gamma_1)^2 - 2(\gamma_0-\gamma_1)\alpha_1\beta_1 \end{aligned}$$

Substituting the expressions above into right hand side of Equation 3.51, this equation can be rewritten as follows.

$$E[Log^2 f_T(t_j|\alpha_0,\beta_0,\gamma_0)] = A_{H_1} =$$
$$\left(\begin{array}{l} Log^2\Gamma(\alpha_0) + 2\alpha_0 Log\Gamma(\alpha_0)Log\beta_0 \\ -2Log\Gamma(\alpha_0)(\alpha_0-1)I1(\alpha_1,\beta_1,\gamma_1,\gamma_0) + 2Log\Gamma(\alpha_0)\frac{\gamma_1+\alpha_1\beta_1-\gamma_0}{\beta_0} \\ +\alpha_0^2 Log^2\beta_0 - 2\alpha_0 Log\beta_0(\alpha_0-1)I1(\alpha_1,\beta_1,\gamma_1,\gamma_0) \\ +2\alpha_0 Log\beta_0\frac{\gamma_1+\alpha_1\beta_1-\gamma_0}{\beta_0} + (\alpha_0-1)^2 I2(\alpha_1,\beta_1,\gamma_1,\gamma_0) \\ -2(\alpha_0-1)\left(\frac{\Gamma(\alpha_1+1)\beta_1}{\Gamma(\alpha_1)\beta_0}I1(\alpha_1+1,\beta_1,\gamma_1,\gamma_0)\right. \\ \left.-\frac{(\gamma_0-\gamma_1)}{\beta_0}I1(\alpha_1,\beta_1,\gamma_1,\gamma_0)\right) + \frac{\beta_1^2\alpha_1(\alpha_1+1)+(\gamma_0-\gamma_1)^2-2(\gamma_0-\gamma_1)\alpha_1\beta_1}{\beta_0^2} \end{array}\right) \quad (3.52)$$

Since t_{j1} and t_{j2} are samples from independent identically distributed random variables, second term in the right hand side of Equation 3.50 can be expanded as follows.

$$E[Logf_T(t_{j1}|\alpha_0,\beta_0,\gamma_0)] \times E[Logf_T(t_{j2}|\alpha_0,\beta_0,\gamma_0)] \quad = \{E[Logf_T(t_j|\alpha_0,\beta_0,\gamma_0)]\}^2$$

$$\{E[Logf_T(t_j|\alpha_0,\beta_0,\gamma_0)]\}^2 = B_{H_1} =$$
$$\left(\begin{array}{l} Log^2\Gamma(\alpha_0) + 2Log\Gamma(\alpha_0)\alpha_0 Log\beta_0 \\ -2Log\Gamma(\alpha_0)(\alpha_0-1)I1(\alpha_1,\beta_1,\gamma_1,\gamma_0) \\ +2Log\Gamma(\alpha_0)\left(\frac{\gamma_1+\alpha_1\beta_1-\gamma_0}{\beta_0}\right) + \alpha_0^2 Log^2\beta_0 \\ -2\alpha_0 Log\beta_0(\alpha_0-1)I1(\alpha_1,\beta_1,\gamma_1,\gamma_0) \\ +2\alpha_0 Log\beta_0\left(\frac{\gamma_1+\alpha_1\beta_1-\gamma_0}{\beta_0}\right) + (\alpha_0-1)^2\left(I1(\alpha_1,\beta_1,\gamma_1,\gamma_0)\right)^2 \\ -2(\alpha_0-1)I1(\alpha_1,\beta_1,\gamma_1,\gamma_0)\left(\frac{\gamma_1+\alpha_1\beta_1-\gamma_0}{\beta_0}\right) + \left(\frac{(\gamma_1+\alpha_1\beta_1-\gamma_0)}{\beta_0}\right)^2 \end{array}\right) \quad (3.53)$$

Samples t_k are drawn from a Gamma distribution with parameters α_2, β_2 and γ_2 and if t_j is replaced by t_k in the left hand sides of the Equations 3.52 and 3.53

above, the right hand sides of these equations are similar.

$$E[Log^2 f_T(t_k|\alpha_0,\beta_0,\gamma_0)] = C_{H_1} =$$
$$\left(\begin{array}{l} Log^2\Gamma(\alpha_0) + 2\alpha_0 Log\Gamma(\alpha_0) Log\beta_0 \\ -2Log\Gamma(\alpha_0)(\alpha_0-1)I1(\alpha_2,\beta_2,\gamma_2,\gamma_0) + 2Log\Gamma(\alpha_0)\frac{\gamma_2+\alpha_2\beta_2-\gamma_0}{\beta_0} \\ +\alpha_0^2 Log^2\beta_0 - 2\alpha_0 Log\beta_0(\alpha_0-1)I1(\alpha_2,\beta_2,\gamma_2,\gamma_0) \\ +2\alpha_0 Log\beta_0\frac{\gamma_2+\alpha_2\beta_2-\gamma_0}{\beta_0} + (\alpha_0-1)^2 I2(\alpha_2,\beta_2,\gamma_2,\gamma_0) \\ -2(\alpha_0-1)\left(\frac{\Gamma(\alpha_2+1)\beta_2}{\Gamma(\alpha_2)\beta_0}I1(\alpha_2+1,\beta_2,\gamma_2,\gamma_0)\right. \\ \left.-\frac{(\gamma_0-\gamma_2)}{\beta_0}I1(\alpha_2,\beta_2,\gamma_2,\gamma_0)\right) + \frac{\beta_2^2\alpha_2(\alpha_2+1)+(\gamma_0-\gamma_2)^2-2(\gamma_0-\gamma_2)\alpha_2\beta_2}{\beta_0^2} \end{array}\right) \tag{3.54}$$

$$E[Log f_T(t_{k1}|\alpha_0,\beta_0,\gamma_0)] \times E[Log f_T(t_{k2}|\alpha_0,\beta_0,\gamma_0)] \;\; = \{E[Log f_T(t_k|\alpha_0,\beta_0,\gamma_0)]\}^2$$

$$\{E[Log f_T(t_k|\alpha_0,\beta_0,\gamma_0)]\}^2 = D_{H_1} =$$
$$\left(\begin{array}{l} Log^2\Gamma(\alpha_0) + 2Log\Gamma(\alpha_0)\alpha_0 Log\beta_0 \\ -2Log\Gamma(\alpha_0)(\alpha_0-1)I1(\alpha_2,\beta_2,\gamma_2,\gamma_0) \\ +2Log\Gamma(\alpha_0)\left(\frac{\gamma_2+\alpha_2\beta_2-\gamma_0}{\beta_0}\right) + \alpha_0^2 Log^2\beta_0 \\ -2\alpha_0 Log\beta_0(\alpha_0-1)I1(\alpha_2,\beta_2,\gamma_2,\gamma_0) \\ +2\alpha_0 Log\beta_0\left(\frac{\gamma_2+\alpha_2\beta_2-\gamma_0}{\beta_0}\right) + (\alpha_0-1)^2\left(I1(\alpha_2,\beta_2,\gamma_2,\gamma_0)\right)^2 \\ -2(\alpha_0-1)I1(\alpha_2,\beta_2,\gamma_2,\gamma_0)\left(\frac{\gamma_2+\alpha_2\beta_2-\gamma_0}{\beta_0}\right) + \left(\frac{(\gamma_2+\alpha_2\beta_2-\gamma_0)}{\beta_0}\right)^2 \end{array}\right) \tag{3.55}$$

An expression for $E[Log^2 f_T(t_j|\alpha_1,\beta_1,\gamma_1)]$ can be expanded as follows.

$$E[Log^2 f_T(t_j|\alpha_1,\beta_1,\gamma_1)] = \left(\begin{array}{l} Log^2\Gamma(\alpha_1) + 2\alpha_1 Log\Gamma(\alpha_1) Log\beta_1 \\ -2Log\Gamma(\alpha_1)(\alpha_1-1)E[Log(t_j-\gamma_1)] + 2Log\Gamma(\alpha_1)E\left[\frac{t_j-\gamma_1}{\beta_1}\right] \\ +\alpha_1^2 Log^2\beta_1 - 2\alpha_1 Log\beta_1(\alpha_1-1)E[Log(t_j-\gamma_1)] \\ +2\alpha_1 Log\beta_1 E\left[\frac{t_j-\gamma_1}{\beta_1}\right] + (\alpha_1-1)^2 E[Log^2(t_j-\gamma_1)] \\ -2(\alpha_1-1)E\left[Log(t_j-\gamma_1)\frac{t_j-\gamma_1}{\beta_1}\right] + E\left[\frac{(t_j-\gamma_1)^2}{\beta_1^2}\right] \end{array} \right) \tag{3.56}$$

The following expected values can be obtained from the expressions that have already been obtained previously in this chapter.

$$E[Log(t_j-\gamma_1)] = Log\beta_1 + \psi(\alpha_1)$$

$$E\left[\frac{t_j-\gamma_1}{\beta_1}\right] = \alpha_1$$

$$E[Log^2(t_j-\gamma_1)] = \psi^{(1)}(\alpha_1) + Log^2(\beta_1) + (\psi(\alpha_1))^2 + 2Log(\beta_1)\psi(\alpha_1)$$

$$E\left[Log(t_j-\gamma_1)\frac{t_j-\gamma_1}{\beta_1}\right] = \frac{\Gamma(\alpha_1+1)}{\Gamma(\alpha_1)}[Log\beta_1 + \psi(\alpha_1+1)]$$

$$E\left[\frac{(t_j-\gamma_1)^2}{\beta_1^2}\right] = \alpha_1(1+\alpha_1)$$

Equation 3.56 can be rewritten as follows by substituting the expressions obtained above.

$$E[Log^2 f_T(t_j|\alpha_1,\beta_1,\gamma_1)] = E_{H_1} = \begin{pmatrix} Log^2\Gamma(\alpha_1) + 2\alpha_1 Log\Gamma(\alpha_1) Log\beta_1 \\ -2Log\Gamma(\alpha_1)(\alpha_1-1)(Log\beta_1+\psi(\alpha_1)) + 2Log\Gamma(\alpha_1)\alpha_1 \\ +\alpha_1^2 Log^2\beta_1 - 2\alpha_1 Log\beta_1(\alpha_1-1)(Log\beta_1+\psi(\alpha_1)) \\ +2\alpha_1 Log\beta_1\alpha_1 + (\alpha_1-1)^2\Big(\psi^{(1)}(\alpha_1) + Log^2(\beta_1) \\ +(\psi(\alpha_1))^2 + 2Log(\beta_1)\psi(\alpha_1)\Big) \\ -2(\alpha_1-1)\frac{\Gamma(\alpha_1+1)}{\Gamma(\alpha_1)}[Log\beta_1+\psi(\alpha_1+1)] + \alpha_1(1+\alpha_1) \end{pmatrix} \tag{3.57}$$

Since t_{j1} and t_{j2} are samples from independent identically distributed random variables, it follows that.

$$E[Logf_T(t_{j1}|\alpha_1,\beta_1,\gamma_1)] \times E[Logf_T(t_{j2}|\alpha_1,\beta_1,\gamma_1)] \;\; = \{E[Logf_T(t_j|\alpha_1,\beta_1,\gamma_1)]\}^2$$

Expression for $\{E[Logf_T(t_j|\alpha_1,\beta_1,\gamma_1)]\}^2$ is as follows.

$$\{E[Logf_T(t_j|\alpha_1,\beta_1,\gamma_1)]\}^2 = F_{H_1} = \begin{pmatrix} Log^2\Gamma(\alpha_1) + 2Log\Gamma(\alpha_1)\alpha_1 Log\beta_1 \\ -2Log\Gamma(\alpha_1)(\alpha_1-1)(Log\beta_1+\psi(\alpha_1)) \\ +2Log\Gamma(\alpha_1)\alpha_1 + \alpha_1^2 Log^2\beta_1 \\ -2\alpha_1 Log\beta_1(\alpha_1-1)(Log\beta_1+\psi(\alpha_1)) \\ +2\alpha_1^2 Log\beta_1 + (\alpha_1-1)^2(Log\beta_1+\psi(\alpha_1))^2 \\ -2(\alpha_1-1)(Log\beta_1+\psi(\alpha_1))\alpha_1 + \alpha_1^2 \end{pmatrix} \tag{3.58}$$

Expression for $E[Log^2 f_T(t_k|\alpha_2,\beta_2,\gamma_2)]$ and $\{E[Log f_T(t_k|\alpha_2,\beta_2,\gamma_2)]\}^2$ are similar to the ones obtained in Equations 3.57 and 3.58.

$$E[Log^2 f_T(t_k|\alpha_2,\beta_2,\gamma_2)] = G_{H_1} = \begin{pmatrix} Log^2\Gamma(\alpha_2) + 2\alpha_2 Log\Gamma(\alpha_2) Log\beta_2 \\ -2Log\Gamma(\alpha_2)(\alpha_2-1)(Log\beta_2+\psi(\alpha_2)) + 2Log\Gamma(\alpha_2)\alpha_2 \\ +\alpha_2^2 Log^2\beta_2 - 2\alpha_2 Log\beta_2(\alpha_2-1)(Log\beta_2+\psi(\alpha_2)) \\ +2\alpha_2 Log\beta_2\alpha_2 + (\alpha_2-1)^2\Big(\psi^{(1)}(\alpha_2) + Log^2(\beta_2) \\ +(\psi(\alpha_2))^2 + 2Log(\beta_2)\psi(\alpha_2)\Big) \\ -2(\alpha_2-1)\frac{\Gamma(\alpha_2+1)}{\Gamma(\alpha_2)}[Log\beta_2+\psi(\alpha_2+1)] + \alpha_2(1+\alpha_2) \end{pmatrix} \tag{3.59}$$

Also,

$$E[Log f_T(t_{k1}|\alpha_2,\beta_2,\gamma_2)] \times E[Log f_T(t_{k2}|\alpha_2,\beta_2,\gamma_2)] \;\; = \{E[Log f_T(t_k|\alpha_2,\beta_2,\gamma_2)]\}^2$$

$$\{E[Log f_T(t_k|\alpha_2,\beta_2,\gamma_2)]\}^2 = H_{H_1} = \begin{pmatrix} Log^2\Gamma(\alpha_2) + 2Log\Gamma(\alpha_2)\alpha_2 Log\beta_2 \\ -2Log\Gamma(\alpha_2)(\alpha_2-1)(Log\beta_2+\psi(\alpha_2)) \\ +2Log\Gamma(\alpha_2)\alpha_2 + \alpha_2^2 Log^2\beta_2 \\ -2\alpha_2 Log\beta_2(\alpha_2-1)(Log\beta_2+\psi(\alpha_2)) \\ +2\alpha_2^2 Log\beta_2 + (\alpha_2-1)^2(Log\beta_2+\psi(\alpha_2))^2 \\ -2(\alpha_2-1)(Log\beta_2+\psi(\alpha_2))\alpha_2 + \alpha_2^2 \end{pmatrix} \tag{3.60}$$

The expression for $E[Logf_T(t_j|\alpha_0,\beta_0,\gamma_0)]\times E[Logf_T(t_k|\alpha_0,\beta_0,\gamma_0)]$ can be obtained as follows.

$$E[Logf_T(t_j|\alpha_0,\beta_0,\gamma_0)] \times E[Logf_T(t_k|\alpha_0,\beta_0,\gamma_0)] =$$
$$E\left[\begin{array}{l} Log^2\Gamma(\alpha_0) + 2Log\Gamma(\alpha_0)\alpha_0 Log\beta_0 - Log\Gamma(\alpha_0)(\alpha_0-1)Log(t_k-\gamma_0) \\ +Log\Gamma(\alpha_0)\left(\frac{t_k-\gamma_0}{\beta_0}\right) + \alpha_0^2 Log^2\beta_0 - \alpha_0 Log\beta_0(\alpha_0-1)Log(t_k-\gamma_0) \\ +\alpha_0 Log\beta_0\left(\frac{t_k-\gamma_0}{\beta_0}\right) - Log\Gamma(\alpha_0)(\alpha_0-1)Log(t_j-\gamma_0) \\ -\alpha_0 Log\beta_0(\alpha_0-1)Log(t_j-\gamma_0) + (\alpha_0-1)^2 Log(t_j-\gamma_0)Log(t_k-\gamma_0) \\ -(\alpha_0-1)Log(t_j-\gamma_0)\left(\frac{t_k-\gamma_0}{\beta_0}\right) + Log\Gamma(\alpha_0)\left(\frac{t_j-\gamma_0}{\beta_0}\right) + \alpha_0 Log\beta_0\left(\frac{t_j-\gamma_0}{\beta_0}\right) \\ -\left(\frac{t_j-\gamma_0}{\beta_0}\right)(\alpha_0-1)Log(t_k-\gamma_0) + \left(\frac{t_j-\gamma_0}{\beta_0}\right)\left(\frac{t_k-\gamma_0}{\beta_0}\right) \end{array}\right]$$

$$E[Logf_T(t_j|\alpha_0,\beta_0,\gamma_0)] \times E[Logf_T(t_k|\alpha_0,\beta_0,\gamma_0)] =$$
$$\left(\begin{array}{l} Log^2\Gamma(\alpha_0) + 2Log\Gamma(\alpha_0)\alpha_0 Log\beta_0 - Log\Gamma(\alpha_0)(\alpha_0-1)E[Log(t_k-\gamma_0)] \\ +Log\Gamma(\alpha_0)E\left[\frac{t_k-\gamma_0}{\beta_0}\right] + \alpha_0^2 Log^2\beta_0 - \alpha_0 Log\beta_0(\alpha_0-1)E[Log(t_k-\gamma_0)] \\ +\alpha_0 Log\beta_0 E\left[\frac{t_k-\gamma_0}{\beta_0}\right] - Log\Gamma(\alpha_0)(\alpha_0-1)E[Log(t_j-\gamma_0)] \\ -\alpha_0 Log\beta_0(\alpha_0-1)E[Log(t_j-\gamma_0)] + (\alpha_0-1)^2 E[Log(t_j-\gamma_0)Log(t_k-\gamma_0)] \\ -(\alpha_0-1)E\left[Log(t_j-\gamma_0)\left(\frac{t_k-\gamma_0}{\beta_0}\right)\right] + Log\Gamma(\alpha_0)E\left[\frac{t_j-\gamma_0}{\beta_0}\right] + \alpha_0 Log\beta_0 E\left[\frac{t_j-\gamma_0}{\beta_0}\right] \\ -(\alpha_0-1)E\left[\left(\frac{t_j-\gamma_0}{\beta_0}\right)Log(t_k-\gamma_0)\right] + E\left[\left(\frac{t_j-\gamma_0}{\beta_0}\right)\left(\frac{t_k-\gamma_0}{\beta_0}\right)\right] \end{array}\right) \tag{3.61}$$

The terms in the right hand side of Equation 3.61 can be expressed as follows.

$$E[Log(t_j-\gamma_0)] = I1(\alpha_1,\beta_1,\gamma_1,\gamma_0)$$

$$E[Log(t_k-\gamma_0)] = I1(\alpha_2,\beta_2,\gamma_2,\gamma_0)$$

$$E\left[\frac{t_j-\gamma_0}{\beta_0}\right] = \frac{\gamma_1+\alpha_1\beta_1-\gamma_0}{\beta_0}$$

$$E\left[\frac{t_k-\gamma_0}{\beta_0}\right]=\frac{\gamma_2+\alpha_2\beta_2-\gamma_0}{\beta_0}$$

Equation 3.61 can be rewritten as follows by substituting the expressions above.

$$\begin{aligned}
&E[Logf_T(t_j|\alpha_0,\beta_0,\gamma_0)]\times E[Logf_T(t_k|\alpha_0,\beta_0,\gamma_0)]=I_{H_1}= \\
&\left(\begin{array}{l}
Log^2\Gamma(\alpha_0)+2Log\Gamma(\alpha_0)\alpha_0Log\beta_0-Log\Gamma(\alpha_0)(\alpha_0-1)I1(\alpha_2,\beta_2,\gamma_2,\gamma_0) \\
+Log\Gamma(\alpha_0)\left(\frac{\gamma_2+\alpha_2\beta_2-\gamma_0}{\beta_0}\right)+\alpha_0^2Log^2\beta_0-\alpha_0Log\beta_0(\alpha_0-1)I1(\alpha_2,\beta_2,\gamma_2,\gamma_0) \\
+\alpha_0Log\beta_0\left(\frac{\gamma_2+\alpha_2\beta_2-\gamma_0}{\beta_0}\right)-Log\Gamma(\alpha_0)(\alpha_0-1)I1(\alpha_1,\beta_1,\gamma_1,\gamma_0) \\
-\alpha_0Log\beta_0(\alpha_0-1)I1(\alpha_1,\beta_1,\gamma_1,\gamma_0) \\
+(\alpha_0-1)^2I1(\alpha_1,\beta_1,\gamma_1,\gamma_0)I1(\alpha_2,\beta_2,\gamma_2,\gamma_0) \\
-(\alpha_0-1)I1(\alpha_1,\beta_1,\gamma_1,\gamma_0)\left(\frac{\gamma_2+\alpha_2\beta_2-\gamma_0}{\beta_0}\right)+Log\Gamma(\alpha_0)\left(\frac{\gamma_1+\alpha_1\beta_1-\gamma_0}{\beta_0}\right) \\
+\alpha_0Log\beta_0\left(\frac{\gamma_1+\alpha_1\beta_1-\gamma_0}{\beta_0}\right)-(\alpha_0-1)\left(\frac{\gamma_1+\alpha_1\beta_1-\gamma_0}{\beta_0}\right)I1(\alpha_2,\beta_2,\gamma_2,\gamma_0) \\
+\left(\frac{\gamma_1+\alpha_1\beta_1-\gamma_0}{\beta_0}\right)\left(\frac{\gamma_2+\alpha_2\beta_2-\gamma_0}{\beta_0}\right)
\end{array}\right)
\end{aligned} \tag{3.62}$$

The expression for $E[Logf_T(t_j|\alpha_0,\beta_0,\gamma_0)\times Logf_T(t_j|\alpha_1,\beta_1,\gamma_1)]$ can be obtained as follows.

$$\begin{aligned}
&E[Logf_T(t_j|\alpha_0,\beta_0,\gamma_0)\times Logf_T(t_j|\alpha_1,\beta_1,\gamma_1)]= \\
&E\left[\begin{array}{l}
Log\Gamma(\alpha_0)Log\Gamma(\alpha_1)+Log\Gamma(\alpha_0)\alpha_1Log\beta_1-Log\Gamma(\alpha_0)(\alpha_1-1)Log(t_j-\gamma_1) \\
+Log\Gamma(\alpha_0)\left(\frac{t_j-\gamma_1}{\beta_1}\right)+\alpha_0Log\beta_0Log\Gamma(\alpha_1)+\alpha_0Log\beta_0\alpha_1Log\beta_1 \\
-\alpha_0Log\beta_0(\alpha_1-1)Log(t_j-\gamma_1)+\alpha_0Log\beta_0\left(\frac{t_j-\gamma_1}{\beta_1}\right) \\
-(\alpha_0-1)Log(t_j-\gamma_0)Log\Gamma(\alpha_1)-(\alpha_0-1)Log(t_j-\gamma_0)\alpha_1Log\beta_1 \\
+(\alpha_0-1)Log(t_j-\gamma_0)(\alpha_1-1)Log(t_j-\gamma_1) \\
-(\alpha_0-1)Log(t_j-\gamma_0)\left(\frac{t_j-\gamma_1}{\beta_1}\right)+\left(\frac{t_j-\gamma_0}{\beta_0}\right)Log\Gamma(\alpha_1)+\left(\frac{t_j-\gamma_0}{\beta_0}\right)\alpha_1Log\beta_1 \\
-\left(\frac{t_j-\gamma_0}{\beta_0}\right)(\alpha_1-1)Log(t_j-\gamma_1)+\left(\frac{t_j-\gamma_0}{\beta_0}\right)\left(\frac{t_j-\gamma_1}{\beta_1}\right)
\end{array}\right]
\end{aligned}$$

$$E[Logf_T(t_j|\alpha_0,\beta_0,\gamma_0) \times Logf_T(t_j|\alpha_1,\beta_1,\gamma_1)] =$$

$$\left(\begin{array}{l} Log\Gamma(\alpha_0)Log\Gamma(\alpha_1) + Log\Gamma(\alpha_0)\alpha_1 Log\beta_1 - Log\Gamma(\alpha_0)(\alpha_1-1)E[Log(t_j-\gamma_1)] \\ +Log\Gamma(\alpha_0)E\left[\frac{t_j-\gamma_1}{\beta_1}\right] + \alpha_0 Log\beta_0 Log\Gamma(\alpha_1) + \alpha_0 Log\beta_0\alpha_1 Log\beta_1 \\ -\alpha_0 Log\beta_0(\alpha_1-1)E[Log(t_j-\gamma_1)] + \alpha_0 Log\beta_0 E\left[\frac{t_j-\gamma_1}{\beta_1}\right] \\ -(\alpha_0-1)E[Log(t_j-\gamma_0)]Log\Gamma(\alpha_1) - (\alpha_0-1)E[Log(t_j-\gamma_0)]\alpha_1 Log\beta_1 \\ +(\alpha_0-1)(\alpha_1-1)E[Log(t_j-\gamma_0)Log(t_j-\gamma_1)] \\ -(\alpha_0-1)E\left[Log(t_j-\gamma_0)\left(\frac{t_j-\gamma_1}{\beta_1}\right)\right] + E\left[\frac{t_j-\gamma_0}{\beta_0}\right]Log\Gamma(\alpha_1) \\ +E\left[\frac{t_j-\gamma_0}{\beta_0}\right]\alpha_1 Log\beta_1 - (\alpha_1-1)E\left[\left(\frac{t_j-\gamma_0}{\beta_0}\right)Log(t_j-\gamma_1)\right] \\ +E\left[\left(\frac{t_j-\gamma_0}{\beta_0}\right)\left(\frac{t_j-\gamma_1}{\beta_1}\right)\right] \end{array} \right) \tag{3.63}$$

The following expressions can be substituted into the right hand side of Equation 3.63.

$$E[log(t_j-\gamma_1)] = Log\beta_1 + \psi(\alpha_1)$$

$$E\left[\frac{t_j-\gamma_1}{\beta_1}\right] = \alpha_1$$

$$E\left[\frac{t_j-\gamma_0}{\beta_0}\right] = \left(\frac{\gamma_1+\alpha_1\beta_1-\gamma_0}{\beta_1}\right)$$

$$E[Log(t_j-\gamma_0)] = I1(\alpha_1,\beta_1,\gamma_1,\gamma_0)$$

$$E[Log(t_j-\gamma_0)Log(t_j-\gamma_1)] =$$
$$\frac{1}{\Gamma(\alpha_1)\beta_1^{\alpha_1}}\int_{\gamma_1}^{\infty} Log(t_j-\gamma_0)Log(t_j-\gamma_1)(t_j-\gamma_1)^{(\alpha_1-1)}e^{-\frac{t_j-\gamma_1}{\beta_1}}dt_j$$
$$= I3(\alpha_1,\beta_1,\gamma_1,\gamma_0)$$

$$E[(t_j-\gamma_1)Log(t_j-\gamma_0)] = \frac{\Gamma(\alpha_1+1)\beta_1}{\Gamma(\alpha_1)}I1(\alpha_1+1,\beta_1,\gamma_1,\gamma_0)$$

$$E[(t_j-\gamma_0)Log(t_j-\gamma_1)] = \frac{\beta_1\Gamma(\alpha_1+1)}{\Gamma(\alpha_1)}(Log\beta_1+\psi(\alpha_1+1))-(\gamma_0-\gamma_1)(Log\beta_1+\psi(\alpha_1))$$

$$E[(t_j-\gamma_0)(t_j-\gamma_1)] = \alpha_1\beta_1^2(1+\alpha_1)-(\gamma_0-\gamma_1)\alpha_1\beta_1$$

Equation 3.63 can be rewritten as follows using the above expressions.

$$E[Logf_T(t_j|\alpha_0,\beta_0,\gamma_0)\times Logf_T(t_j|\alpha_1,\beta_1,\gamma_1)] = J_{H_1} =$$
$$\left(\begin{array}{l} Log\Gamma(\alpha_0)Log\Gamma(\alpha_1) + Log\Gamma(\alpha_0)\alpha_1 Log\beta_1 - Log\Gamma(\alpha_0)(\alpha_1-1)(Log\beta_1+\psi(\alpha_1)) \\ +Log\Gamma(\alpha_0)\alpha_1 + \alpha_0 Log\beta_0 Log\Gamma(\alpha_1) + \alpha_0 Log\beta_0\alpha_1 Log\beta_1 \\ -\alpha_0 Log\beta_0(\alpha_1-1)(Log\beta_1+\psi(\alpha_1)) + \alpha_0 Log\beta_0\alpha_1 \\ -(\alpha_0-1)I1(\alpha_1,\beta_1,\gamma_1,\gamma_0)Log\Gamma(\alpha_1) - (\alpha_0-1)I1(\alpha_1,\beta_1,\gamma_1,\gamma_0)\alpha_1 Log\beta_1 \\ +(\alpha_0-1)(\alpha_1-1)I3(\alpha_1,\beta_1,\gamma_1,\gamma_0) - (\alpha_0-1)\frac{\Gamma(\alpha_1+1)}{\Gamma(\alpha_1)}I1(\alpha_1+1,\beta_1,\gamma_1,\gamma_0) \\ +\left(\frac{\gamma_1+\alpha_1\beta_1-\gamma_0}{\beta_1}\right)Log\Gamma(\alpha_1) + \left(\frac{\gamma_1+\alpha_1\beta_1-\gamma_0}{\beta_1}\right)\alpha_1 Log\beta_1 \\ -\frac{(\alpha_1-1)}{\beta_0}\left(\frac{\beta_1\Gamma(\alpha_1+1)}{\Gamma(\alpha_1)}(Log\beta_1+\psi(\alpha_1+1)) - (\gamma_0-\gamma_1)(Log\beta_1+\psi(\alpha_1))\right) \\ +\left(\frac{\alpha_1\beta_1(1+\alpha_1)-(\gamma_0-\gamma_1)\alpha_1}{\beta_0}\right) \end{array}\right) \tag{3.64}$$

The expression for $E[Logf_T(t_k|\alpha_0,\beta_0,\gamma_0)\times Logf_T(t_k|\alpha_2,\beta_2,\gamma_2)]$ is similar to the one in Equation 3.64.

$$E[Logf_T(t_k|\alpha_0,\beta_0,\gamma_0)\times Logf_T(t_k|\alpha_2,\beta_2,\gamma_2)] = K_{H_1} =$$
$$\left(\begin{array}{l} Log\Gamma(\alpha_0)Log\Gamma(\alpha_2) + Log\Gamma(\alpha_0)\alpha_2 Log\beta_2 - Log\Gamma(\alpha_0)(\alpha_2-1)(Log\beta_2+\psi(\alpha_2)) \\ +Log\Gamma(\alpha_0)\alpha_2 + \alpha_0 Log\beta_0 Log\Gamma(\alpha_2) + \alpha_0 Log\beta_0\alpha_2 Log\beta_2 \\ -\alpha_0 Log\beta_0(\alpha_2-1)(Log\beta_2+\psi(\alpha_2)) + \alpha_0 Log\beta_0\alpha_2 \\ -(\alpha_0-1)I1(\alpha_2,\beta_2,\gamma_2,\gamma_0)Log\Gamma(\alpha_2) - (\alpha_0-1)I1(\alpha_2,\beta_2,\gamma_2,\gamma_0)\alpha_2 Log\beta_2 \\ +(\alpha_0-1)(\alpha_2-1)I3(\alpha_2,\beta_2,\gamma_2,\gamma_0) - (\alpha_0-1)\frac{\Gamma(\alpha_2+1)}{\Gamma(\alpha_2)}I1(\alpha_2+1,\beta_2,\gamma_2,\gamma_0) \\ +\left(\frac{\gamma_2+\alpha_2\beta_2-\gamma_0}{\beta_2}\right)Log\Gamma(\alpha_2) + \left(\frac{\gamma_2+\alpha_2\beta_2-\gamma_0}{\beta_2}\right)\alpha_2 Log\beta_2 \\ -\frac{(\alpha_2-1)}{\beta_0}\left(\frac{\beta_2\Gamma(\alpha_2+1)}{\Gamma(\alpha_2)}(Log\beta_2+\psi(\alpha_2+1)) - (\gamma_0-\gamma_2)(Log\beta_2+\psi(\alpha_2))\right) \\ +\left(\frac{\alpha_2\beta_2(1+\alpha_2)-(\gamma_0-\gamma_2)\alpha_2}{\beta_0}\right) \end{array}\right) \tag{3.65}$$

The expression for $E[Logf_T(t_{j1}|\alpha_0,\beta_0,\gamma_0)] \times E[Logf_T(t_{j2}|\alpha_1,\beta_1,\gamma_1)]$ can be obtained from the expressions for $E[Logf_T(t_{j1}|\alpha_0,\beta_0,\gamma_0)]$ and $E[Logf_T(t_{j2}|\alpha_1,\beta_1,\gamma_1)]$ as follows.

$$E[Logf_T(t_{j1}|\alpha_0,\beta_0,\gamma_0)] = \begin{pmatrix} -Log\Gamma(\alpha_0) - \alpha_0 Log\beta_0 + (\alpha_0 - 1)I1(\alpha_1,\beta_1,\gamma_1) \\ -\left(\frac{\gamma_1+\alpha_1\beta_1-\gamma_0}{\beta_0}\right) \end{pmatrix}$$

$$E[Logf_T(t_{j2}|\alpha_1,\beta_1,\gamma_1)] =$$
$$\begin{pmatrix} -Log\Gamma(\alpha_1) - \alpha_1 Log\beta_1 + (\alpha_1 - 1)(Log\beta_1 + \psi(\alpha_1)) - \alpha_1 \end{pmatrix}$$

$$E[Logf_T(t_{j1}|\alpha_0,\beta_0,\gamma_0) \times Logf_T(t_{j2}|\alpha_1,\beta_1,\gamma_1)] = L_{H_1} =$$
$$\begin{pmatrix} Log\Gamma(\alpha_0)Log\Gamma(\alpha_1) + Log\Gamma(\alpha_0)\alpha_1 Log\beta_1 - Log\Gamma(\alpha_0)(\alpha_1 - 1)(Log\beta_1 + \psi(\alpha_1)) \\ +\alpha_1 Log\Gamma(\alpha_0) + \alpha_0 Log\beta_0 Log\Gamma(\alpha_1) + \alpha_0 Log\beta_0\alpha_1 Log\beta_1 \\ -\alpha_0 Log\beta_0(\alpha_1 - 1)(Log\beta_1 + \psi(\alpha_1)) + \alpha_0 Log\beta_0\alpha_1 \\ -(\alpha_0 - 1)I1(\alpha_1,\beta_1,\gamma_1,\gamma_0)Log\Gamma(\alpha_1) - (\alpha_0 - 1)I1(\alpha_1,\beta_1,\gamma_1,\gamma_0)\alpha_1 Log\beta_1 \\ +(\alpha_0 - 1)I1(\alpha_1,\beta_1,\gamma_1,\gamma_0)(\alpha_1 - 1)(Log\beta_1 + \psi(\alpha_1)) \\ -(\alpha_0 - 1)I1(\alpha_1,\beta_1,\gamma_1,\gamma_0)\alpha_1 + \left(\frac{\gamma_1+\alpha_1\beta_1-\gamma_0}{\beta_0}\right) Log\Gamma(\alpha_1) \\ +\left(\frac{\gamma_1+\alpha_1\beta_1-\gamma_0}{\beta_0}\right)\alpha_1 Log\beta_1 - \left(\frac{\gamma_1+\alpha_1\beta_1-\gamma_0}{\beta_0}\right)(\alpha_1 - 1)(Log\beta_1 + \psi(\alpha_1)) \\ +\left(\frac{\gamma_1+\alpha_1\beta_1-\gamma_0}{\beta_0}\right)\alpha_1 \end{pmatrix} \tag{3.66}$$

The expression for $E[Logf_T(t_{k1}|\alpha_0,\beta_0,\gamma_0)\times Logf_T(t_{k2}|\alpha_2,\beta_2,\gamma_2)]$ is similar to the one in Equation 3.66 above.

$$E[Logf_T(t_{k1}|\alpha_0,\beta_0,\gamma_0)\times Logf_T(t_{k2}|\alpha_2,\beta_2,\gamma_2)] = M_{H_1} =$$
$$\left(\begin{array}{l} Log\Gamma(\alpha_0)Log\Gamma(\alpha_2)+Log\Gamma(\alpha_0)\alpha_2 Log\beta_2 - Log\Gamma(\alpha_0)(\alpha_2-1)(Log\beta_2+\psi(\alpha_2)) \\ +\alpha_2 Log\Gamma(\alpha_0)+\alpha_0 Log\beta_0 Log\Gamma(\alpha_2)+\alpha_0 Log\beta_0\alpha_2 Log\beta_2 \\ -\alpha_0 Log\beta_0(\alpha_2-1)(Log\beta_2+\psi(\alpha_2))+\alpha_0 Log\beta_0\alpha_2 \\ -(\alpha_0-1)I1(\alpha_2,\beta_2,\gamma_2,\gamma_0)Log\Gamma(\alpha_2)-(\alpha_0-1)I1(\alpha_2,\beta_2,\gamma_2,\gamma_0)\alpha_2 Log\beta_2 \\ +(\alpha_0-1)I1(\alpha_2,\beta_2,\gamma_2,\gamma_0)(\alpha_2-1)(Log\beta_2+\psi(\alpha_2)) \\ -(\alpha_0-1)I1(\alpha_2,\beta_2,\gamma_2,\gamma_0)\alpha_2+\left(\frac{\gamma_2+\alpha_2\beta_2-\gamma_0}{\beta_0}\right)Log\Gamma(\alpha_2) \\ +\left(\frac{\gamma_2+\alpha_2\beta_2-\gamma_0}{\beta_0}\right)\alpha_2 Log\beta_2-\left(\frac{\gamma_2+\alpha_2\beta_2-\gamma_0}{\beta_0}\right)(\alpha_2-1)(Log\beta_2+\psi(\alpha_2)) \\ +\left(\frac{\gamma_2+\alpha_2\beta_2-\gamma_0}{\beta_0}\right)\alpha_2 \end{array}\right) \tag{3.67}$$

The expression for $E[Logf_T(t_j|\alpha_0,\beta_0,\gamma_0)\times Logf_T(t_k|\alpha_2,\beta_2,\gamma_2)]$ can be obtained similarly and is as follows.

$$E[Logf_T(t_j|\alpha_0,\beta_0,\gamma_0)\times Logf_T(t_k|\alpha_2,\beta_2,\gamma_2)] = N_{H_1} =$$
$$\left(\begin{array}{l} Log\Gamma(\alpha_0)Log\Gamma(\alpha_2)+Log\Gamma(\alpha_0)\alpha_2 Log\beta_2 - Log\Gamma(\alpha_0)(\alpha_2-1)(Log\beta_2+\psi(\alpha_2)) \\ +\alpha_2 Log\Gamma(\alpha_0)+\alpha_0 Log\beta_0 Log\Gamma(\alpha_2)+\alpha_0 Log\beta_0\alpha_2 Log\beta_2 \\ -\alpha_0 Log\beta_0(\alpha_2-1)(Log\beta_2+\psi(\alpha_2))+\alpha_0 Log\beta_0\alpha_2 \\ -(\alpha_0-1)I1(\alpha_1,\beta_1,\gamma_1,\gamma_0)Log\Gamma(\alpha_2)-(\alpha_0-1)I1(\alpha_1,\beta_1,\gamma_1,\gamma_0)\alpha_2 Log\beta_2 \\ +(\alpha_0-1)I1(\alpha_1,\beta_1,\gamma_1,\gamma_0)(\alpha_2-1)(Log\beta_2+\psi(\alpha_2)) \\ -(\alpha_0-1)I1(\alpha_1,\beta_1,\gamma_1,\gamma_0)\alpha_2 \\ +\left(\frac{\gamma_1+\alpha_1\beta_1-\gamma_0}{\beta_0}\right)Log\Gamma(\alpha_2)+\left(\frac{\gamma_1+\alpha_1\beta_1-\gamma_0}{\beta_0}\right)\alpha_2 Log\beta_2 \\ -\left(\frac{\gamma_1+\alpha_1\beta_1-\gamma_0}{\beta_0}\right)(\alpha_2-1)(Log\beta_2+\psi(\alpha_2))+\left(\frac{\gamma_1+\alpha_1\beta_1-\gamma_0}{\beta_0}\right)\alpha_2 \end{array}\right) \tag{3.68}$$

The expressions for $E[Logf_T(t_j|\alpha_1,\beta_1,\gamma_1) \times Logf_T(t_k|\alpha_0,\beta_0,\gamma_0)]$ can be obtained similarly and is as follows.

$$E[Logf_T(t_j|\alpha_1,\beta_1,\gamma_1) \times Logf_T(t_k|\alpha_0,\beta_0,\gamma_0)] = O_{H_1} =$$
$$\left(\begin{array}{l} Log\Gamma(\alpha_0)Log\Gamma(\alpha_1) + Log\Gamma(\alpha_0)\alpha_1 Log\beta_1 - Log\Gamma(\alpha_0)(\alpha_1-1)(Log\beta_1+\psi(\alpha_1)) \\ +\alpha_1 Log\Gamma(\alpha_0) + \alpha_0 Log\beta_0 Log\Gamma(\alpha_1) + \alpha_0 Log\beta_0\alpha_1 Log\beta_1 \\ -\alpha_0 Log\beta_0(\alpha_1-1)(Log\beta_1+\psi(\alpha_1)) + \alpha_0 Log\beta_0\alpha_1 \\ -(\alpha_0-1)I1(\alpha_2,\beta_2,\gamma_2,\gamma_0)Log\Gamma(\alpha_1) - (\alpha_0-1)I1(\alpha_2,\beta_2,\gamma_2,\gamma_0)\alpha_1 Log\beta_1 \\ +(\alpha_0-1)I1(\alpha_2,\beta_2,\gamma_2,\gamma_0)(\alpha_1-1)(Log\beta_1+\psi(\alpha_1)) \\ -(\alpha_0-1)I1(\alpha_2,\beta_2,\gamma_2,\gamma_0)\alpha_1 + \left(\frac{\gamma_2+\alpha_2\beta_2-\gamma_0}{\beta_0}\right) Log\Gamma(\alpha_1) \\ +\left(\frac{\gamma_2+\alpha_2\beta_2-\gamma_0}{\beta_0}\right)\alpha_1 Log\beta_1 - \left(\frac{\gamma_2+\alpha_2\beta_2-\gamma_0}{\beta_0}\right)(\alpha_1-1)(Log\beta_1+\psi(\alpha_1)) \\ +\left(\frac{\gamma_2+\alpha_2\beta_2-\gamma_0}{\beta_0}\right)\alpha_1 \end{array}\right) \tag{3.69}$$

The expression for $E[Logf_T(t_j|\alpha_1,\beta_1,\gamma_1) \times Logf_T(t_k|\alpha_2,\beta_2,\gamma_2)]$ is similarly as follows.

$$E[Logf_T(t_j|\alpha_1,\beta_1,\gamma_1) \times Logf_T(t_k|\alpha_2,\beta_2,\gamma_2)] = P_{H_1} =$$
$$\left(\begin{array}{l} Log\Gamma(\alpha_1)Log\Gamma(\alpha_2) + Log\Gamma(\alpha_1)\alpha_2 Log\beta_2 - Log\Gamma(\alpha_1)(\alpha_2-1)(Log\beta_2+\psi(\alpha_2)) \\ +\alpha_2 Log\Gamma(\alpha_1) + \alpha_1 Log\beta_1 Log\Gamma(\alpha_2) + \alpha_1 Log\beta_1\alpha_2 Log\beta_2 \\ -\alpha_1 Log\beta_1(\alpha_2-1)(Log\beta_2+\psi(\alpha_2)) + \alpha_1 Log\beta_1\alpha_2 \\ -(\alpha_1-1)(Log\beta_1+\psi(\alpha_1))Log\Gamma(\alpha_2) - (\alpha_1-1)(Log\beta_1+\psi(\alpha_1))\alpha_2 Log\beta_2 \\ +(\alpha_1-1)(Log\beta_1+\psi(\alpha_1))(\alpha_2-1)(Log\beta_2+\psi(\alpha_2)) \\ -(\alpha_1-1)(Log\beta_1+\psi(\alpha_1))\alpha_2 + \alpha_1 Log\Gamma(\alpha_2) + \alpha_1\alpha_2 Log\beta_2 \\ -\alpha_1(\alpha_2-1)(Log\beta_2+\psi(\alpha_2)) + \alpha_1\alpha_2 \end{array}\right) \tag{3.70}$$

Right hand side of Equation 3.50 can be rewritten as follows by substituting the Expressions obtained in Equations 3.52, 3.53, 3.54, 3.55, 3.57, 3.58, 3.59, 3.60,

3.62, 3.64, 3.65, 3.66, 3.67, 3.68, 3.69 and 3.70.

$$E[L^2] = \left(\begin{array}{l} \lfloor \frac{n}{2} \rfloor A_{H_1} + \lfloor \frac{n}{2} \rfloor (\lfloor \frac{n}{2} \rfloor - 1) B_{H_1} + \lceil \frac{n}{2} \rceil C_{H_1} + \lceil \frac{n}{2} \rceil (\lceil \frac{n}{2} \rceil - 1) D_{H_1} \\ + \lfloor \frac{n}{2} \rfloor E_{H_1} + \lfloor \frac{n}{2} \rfloor (\lfloor \frac{n}{2} \rfloor - 1) F_{H_1} + \lceil \frac{n}{2} \rceil G_{H_1} + \lceil \frac{n}{2} \rceil (\lceil \frac{n}{2} \rceil - 1) H_{H_1} \\ + 2 \lfloor \frac{n}{2} \rfloor \lceil \frac{n}{2} \rceil I_{H_1} - 2 \lfloor \frac{n}{2} \rfloor J_{H_1} - 2 \lfloor \frac{n}{2} \rfloor (\lfloor \frac{n}{2} \rfloor - 1) L_{H_1} - 2 \lfloor \frac{n}{2} \rfloor \lceil \frac{n}{2} \rceil N_{H_1} \\ - 2 \lfloor \frac{n}{2} \rfloor \lceil \frac{n}{2} \rceil O_{H_1} - 2 \lfloor \frac{n}{2} \rfloor K_{H_1} - 2 \lceil \frac{n}{2} \rceil (\lceil \frac{n}{2} \rceil - 1) M_{H_1} + 2 \lfloor \frac{n}{2} \rfloor \lceil \frac{n}{2} \rceil P_{H_1} \end{array} \right) \tag{3.71}$$

This equation for the second moment of L when H_1 is true was validated using simulations and it accurately predicts the second moment. Formal validation results are presented in chapter 4 where the expression obtained above in Equation 3.71 is used to predict the receiver operating characteristics.

3.5.4 Expected value: *L-infinite*

When H_1 is true and parameters are in *L-infinite* subspace, L may equal $-\infty$. An expression for the expected value of L given that only finite samples of L are considered will be derived in this section. Likelihood ratio L is finite only when $t_j > \gamma_1, \forall j : j \in \{1..\lfloor \frac{n}{2} \rfloor\}$ and $t_k > \gamma_2, \forall k : k \in \{\lfloor \frac{n}{2} \rfloor + 1..n\}$. Samples that allow L to be finite have a truncated Gamma distribution represented by the random variable Z. Let z_j represent samples from a Gamma distribution with parameters α_1, β_1, γ_1 truncated from the left at ξ_1 ($\xi_1 = \text{Max}(\gamma_0, \gamma_1)$). Also, let z_k represent samples from a Gamma distribution with parameters α_2, β_2, γ_2 truncated at ξ_2 ($\xi_2 = \text{Max}(\gamma_0, \gamma_2)$). The expression for expected value of L when parameters are

in *L-infinite* subspace and L is finite can be written as follows.

$$E[L] = \begin{pmatrix} \sum_{j=1}^{\lfloor \frac{n}{2} \rfloor} E[Logf_Z(z_j|\alpha_0, \beta_0, \gamma_0)] + \sum_{k=\lfloor \frac{n}{2} \rfloor + 1}^{n} E[Logf_Z(z_k|\alpha_0, \beta_0, \gamma_0)] \\ -\sum_{j=1}^{\lfloor \frac{n}{2} \rfloor} E[Logf_Z(z_j|\alpha_1, \beta_1, \gamma_1)] - \sum_{k=\lfloor \frac{n}{2} \rfloor + 1}^{n} E[Logf_Z(z_k|\alpha_2, \beta_2, \gamma_2)] \end{pmatrix} \tag{3.72}$$

This expression can be rewritten as follows.

$$E[L] = \begin{pmatrix} \lfloor \frac{n}{2} \rfloor E[Logf_Z(z_j|\alpha_0, \beta_0, \gamma_0)] + \lceil \frac{n}{2} \rceil E[Logf_Z(z_k|\alpha_0, \beta_0, \gamma_0)] \\ -\lfloor \frac{n}{2} \rfloor E[Logf_Z(z_j|\alpha_1, \beta_1, \gamma_1)] - \lceil \frac{n}{2} \rceil E[Logf_Z(z_k|\alpha_2, \beta_2, \gamma_2)] \end{pmatrix} \tag{3.73}$$

Since z_j's and z_k's are samples from a truncated Gamma distribution, it is very difficult to obtain closed form solution for $E[L]$. Equation 3.73 is numerically evaluated to obtain a value for $E[L]$. The values obtained using numerical methods were validated using simulation and this method accurately predicts $E[L]$ when parameters are in *L-infinite* subspace and L is finite. Formal validation results are presented in chapter 4 where the expression obtained above in Equation 3.73 is used to predict the receiver operating characteristics.

3.5.5 Second moment *L-infinite*

The expression for second moment of L when H_1 is true, parameters are in *L-infinite* subspace and L is finite is the same as the expression in Equation 3.42. This equation is rewritten here for convenience. In the following equation, z_k's represent samples from Gamma distribution with parameters α_1, β_1, γ_1, truncated at ξ_1 and z_k's represent samples from Gamma distribution with parameters α_2,

β_2, γ_2, truncated at ξ_2.

$$
\begin{aligned}
E[L^2] = & \\
\Bigg(& \\
& \lfloor \tfrac{n}{2} \rfloor E\left[Log^2 f_Z(z_j|\alpha_0,\beta_0,\gamma_0)\right] \\
& + \lfloor \tfrac{n}{2} \rfloor (\lfloor \tfrac{n}{2} \rfloor - 1) E\left[Log f_Z(z_{j1}|\alpha_0,\beta_0,\gamma_0)\right] \times E\left[Log f_Z(z_{j2}|\alpha_0,\beta_0,\gamma_0)\right] \\
& + \lceil \tfrac{n}{2} \rceil E\left[Log^2 f_Z(z_k|\alpha_0,\beta_0,\gamma_0)\right] \\
& + \lceil \tfrac{n}{2} \rceil (\lceil \tfrac{n}{2} \rceil - 1) E\left[Log f_Z(z_{k1}|\alpha_0,\beta_0,\gamma_0)\right] \times E\left[Log f_Z(z_{k2}|\alpha_0,\beta_0,\gamma_0)\right] \\
& + \lfloor \tfrac{n}{2} \rfloor E\left[Log^2 f_Z(z_j|\alpha_1,\beta_1,\gamma_1)\right] \\
& + \lfloor \tfrac{n}{2} \rfloor (\lfloor \tfrac{n}{2} \rfloor - 1) E\left[Log f_Z(z_{j1}|\alpha_1,\beta_1,\gamma_1)\right] \times E\left[Log f_Z(z_{j2}|\alpha_1,\beta_1,\gamma_1)\right] \\
& + \lceil \tfrac{n}{2} \rceil E\left[Log^2 f_Z(z_k|\alpha_2,\beta_2,\gamma_2)\right] \\
& + \lceil \tfrac{n}{2} \rceil (\lceil \tfrac{n}{2} \rceil - 1) E\left[Log f_Z(z_{k1}|\alpha_2,\beta_2,\gamma_2)\right] \times E\left[Log f_Z(z_{k2}|\alpha_2,\beta_2,\gamma_2)\right] \\
& + 2\lfloor \tfrac{n}{2} \rfloor \lceil \tfrac{n}{2} \rceil E\left[Log f_Z(z_j|\alpha_0,\beta_0,\gamma_0)\right] \times E\left[Log f_Z(z_k|\alpha_0,\beta_0,\gamma_0)\right] \\
& - 2\lfloor \tfrac{n}{2} \rfloor E\left[(Log f_Z(z_j|\alpha_0,\beta_0,\gamma_0)) \times (Log f_Z(z_j|\alpha_1,\beta_1,\gamma_1))\right] \\
& - 2\lfloor \tfrac{n}{2} \rfloor (\lfloor \tfrac{n}{2} \rfloor - 1) E\left[Log f_Z(z_{j1}|\alpha_0,\beta_0,\gamma_0)\right] \times E\left[Log f_Z(z_{j2}|\alpha_1,\beta_1,\gamma_1)\right] \\
& - 2\lfloor \tfrac{n}{2} \rfloor \lceil \tfrac{n}{2} \rceil E\left[Log f_Z(z_j|\alpha_0,\beta_0,\gamma_0)\right] \times E\left[Log f_Z(z_k|\alpha_2,\beta_2,\gamma_2)\right] \\
& - 2\lfloor \tfrac{n}{2} \rfloor \lceil \tfrac{n}{2} \rceil E\left[Log f_Z(z_j|\alpha_1,\beta_1,\gamma_1)\right] \times E\left[Log f_Z(z_k|\alpha_0,\beta_0,\gamma_0)\right] \\
& - 2\lceil \tfrac{n}{2} \rceil E\left[(Log f_Z(z_k|\alpha_0,\beta_0,\gamma_0)) \times (Log f_Z(z_k|\alpha_2,\beta_2,\gamma_2))\right] \\
& - 2\lceil \tfrac{n}{2} \rceil (\lceil \tfrac{n}{2} \rceil - 1) E\left[Log f_Z(z_{k1}|\alpha_0,\beta_0,\gamma_0)\right] \times E\left[Log f_Z(z_{k2}|\alpha_2,\beta_2,\gamma_2)\right] \\
& + 2\lfloor \tfrac{n}{2} \rfloor \lceil \tfrac{n}{2} \rceil E\left[Log f_Z(z_j|\alpha_1,\beta_1,\gamma_1)\right] \times E\left[Log f_Z(z_k|\alpha_2,\beta_2,\gamma_2)\right] \\
\Bigg) &
\end{aligned}
\tag{3.74}
$$

It is difficult to obtain closed form expressions with truncated Gamma distribution. Numerical methods were used to determine $E[L^2]$ from Equation 3.74. The values predicted using numerical methods match the values obtained using simulation. Formal validation results are presented in chapter 4 where the expression obtained above in Equation 3.74 is used to predict the receiver operating characteristics.

3.6 Summary

Parameter unaware detector, that can be used to detect route changes was proposed in this chapter in section 3.2. Since PUD is unaware of the Gamma distribution parameters, it estimates these parameters from the RTT samples. These parameter estimates are then used together with the RTT samples to find the value of the likelihood ratio. Since parameter estimates (and not the actual parameters) are used in the likelihood ratio function, it is currently not possible to obtain expressions for moments of likelihood ratio for each of the two hypothesis. Expressions for the PDF of the likelihood ratio for each of the two hypothesis are needed to map the system parameters to probabilities of detection and false alarms. Parameter aware detector was discussed in section 3.3. The PAD is the optimal detector and it provides the theoretical upper bound on the best performance that can be achieved by any detector. Since PAD uses known parameter values in the likelihood ratio test (and not parameter estimates), expressions for the first two moments of likelihood ratio can be obtained for PAD as discussed in sections 3.4 and 3.5. These expressions for the first two moments of the likelihood ratio will be used in chapter 4 to obtain receiver operating characteristics of PAD.

To derive the expressions for the first two moments of L for the PAD, the base parameter space was divided into *L-finite* and *L-infinite* subspaces in both cases (i.e., H_0 true and H_1 true). When parameters are in *L-finite* subspace, L is always finite and expressions for the first two moments for this case were obtained in Sections 3.4.2, 3.4.3, 3.5.2 and 3.5.3. When parameters are in *L-infinite* subspace, likelihood ratio L may be either finite or infinite. The probability that likelihood ratio is finite when parameters are in *L-infinite* subspace was derived in sections 3.4.1 and 3.5.1. Given the conditions that the parameters are in *L-infinite*

subspace and L is finite, expressions for the first two moments of L were obtained in sections 3.4.4, 3.4.5, 3.5.4 and 3.5.5. All of these expressions derived in this chapter combined with the assumption that the conditional PDFs are Gaussian will be used in Chapter 4 which validates this analysis and used to obtain receiver operating characteristics of PAD.

Chapter 4

Model-Based Approach: Validation

4.1 Introduction

The parameter aware detector or the ideal detector was introduced in the previous chapter. The first two moments of L for PAD, when hypothesis H_0 is true and hypothesis H_1 is true were derived in sections 3.4 and 3.5 respectively. In this chapter, these expressions for the first two moments of L combined with a distribution assumption will be used to predict the probabilities of detection and false alarm. Receiver operating characteristics (ROCs) will also be plotted for various values of the parameters to illustrate PADs performance over the entire range of thresholds. ROCs predicted using the analytical expressions will also be compared to ROCs obtained using simulation. This will validate the expressions for first two moments of L obtained in the previous chapter and also the expressions for probabilities of detection and false alarm that will be obtained in this chapter. Expressions for probability of false alarm and detection are obtained in

section 4.2. ROC curves are used to compare probabilities of detection and false alarm obtained using analysis with the ones from simulation in section 4.3. The expressions for probabilities of detection and false alarms are also used in section 4.3 to find the parameter space over which PAD has acceptable performance. A detector is defined to have acceptable performance when the probability of detection is greater than 0.999 and probability of false alarms is less than 0.001.

4.2 Probability of detection and false alarms

Expressions for probability of false alarm and probability of detection are obtained in this section. It is assumed that the random variables $L|H_0$ and $L|H_1$ have a Gaussian distribution for finite values of L. The Gaussian assumption will be validated using simulation in this chapter. Since the Gaussian distribution function is completely defined by the first two moments, the expressions for the first two moments of $L|H_0$ and $L|H_1$ are sufficient to completely define the density of $L|H_0$ and $L|H_1$. Let $P_{LF|H_0}$ be the probability that L is finite when H_0 is true and $P_{LF|H_1}$ be the probability that L is finite when H_1 is true. When $\gamma_0 \geq \text{Max}(\gamma_1, \gamma_2)$, then $P_{LF|H_0} = 1$ and when $\gamma_0 < \text{Max}(\gamma_1, \gamma_2)$ then $P_{LF|H_0}$ is given by one of the three equations 3.8, 3.9 or 3.10. Similarly, when $\gamma_0 \leq \text{Min}(\gamma_1, \gamma_2)$, then $P_{LF|H_1} = 1$ and when $\gamma_0 > \text{Min}(\gamma_1, \gamma_2)$ then $P_{LF|H_1}$ can be found using one of the three equations 3.45, 3.46 or 3.47. Let $\mu_{L|H_0}$ be the expected value of L when H_0 is true that is found using one of the two equations 3.15 or 3.40 depending on whether the parameters are in *L-finite* or *L-infinite* subspace. Also, let $\sigma^2_{L|H_0}$ be the variance of L when H_0 is true. Variance of L can be found from the first two moments of L using the equality $\sigma^2_{L|H_0} = E[L^2] - (\mu_{L|H_0})^2$. Second moment of L when H_0 is true can be found using one of the two equations 3.35 or 3.42 depend-

ing on whether the parameters are in *L-finite* or *L-infinite* subspace. Similarly, let $\mu_{L|H_1}$ and $\sigma^2_{L|H_1}$ represent the first moment and the variance of L when H_1 is true. Let λ be the threshold used to decide which one of the two hypothesis is true. When $L \geq \lambda$ the decision is in favor of H_0 and when $L < \lambda$, the decision is in favor of H_1. Let D_0 denote the event that the decision is in favor of H_0 and let D_1 denote the event that the decision is in favor of H_1. Then probability of detection and probability of false alarm are denoted as $P(D_1|H_1)$ and $P(D_1|H_0)$ respectively. Expressions for these probabilities can be obtained as follows.

Let $\Phi(x)$ be the CDF of standard normal distribution, i.e.,

$$\Phi(x) = \frac{1}{\sqrt{2\pi}} \int_{-\infty}^{x} e^{-\frac{w^2}{2}} dw$$

Also, let $erf(x)$ be the error function defined as follows.

$$erf(x) = \frac{2}{\sqrt{\pi}} \int_{0}^{x} e^{-t^2} dt$$

It is well known that the two functions $\Phi(x)$ and $erf(x)$ are related by the following equality.

$$\Phi(x) = \frac{1 + erf\left(\frac{x}{\sqrt{2}}\right)}{2}$$

The probability of false alarm can be expressed as follows.

$$\begin{aligned} P(D_1|H_0) &= P(L < \lambda|H_0) = P_{LF|H_0} \Phi\left(\frac{\lambda - \mu_{L|H0}}{\sigma_{L|H0}}\right) \\ &= P_{LF|H_0} \frac{1 + erf\left(\frac{\lambda - \mu_{L|H0}}{\sigma_{L|H0}\sqrt{2}}\right)}{2} \end{aligned} \tag{4.1}$$

Similarly, the probability of detection can be expressed as follows.

$$\begin{aligned} P(D_1|H_1) &= P(L < \lambda|H_1) = P_{LF|H_1}\Phi\left(\frac{\lambda-\mu_{L|H_1}}{\sigma_{L|H_1}}\right) + (1 - P_{LF|H_1}) \\ &= P_{LF|H_1}\frac{1+erf\left(\frac{\lambda-\mu_{L|H_1}}{\sigma_{L|H_1}\sqrt{2}}\right)}{2} + (1 - P_{LF|H_1}) \end{aligned} \tag{4.2}$$

Given the set of parameters α_0, β_0, γ_0, α_1, β_1, γ_1, α_2, β_2, γ_2, n and λ, Equations 4.1 and 4.2 can be used to predict the probability of false alarm and detection for the PAD. Expressions for $P_{LF|H_0}$, $P_{LF|H_1}$, $\mu_{L|H_0}$, $\mu_{L|H_1}$, $\sigma_{L|H_0}$ and $\sigma_{L|H_1}$ that were derived in the previous chapter can be substituted in the right hand side of Equations 4.1 and 4.2 so that $P(D_1|H_0)$ and $P(D_1|H_1)$ are a function of only the parameters above. These equations will be validated in the next section by comparing the predicted probabilities of false alarm and detection with the ones obtained using simulation. If probabilities of detection and false alarm found using simulation match the probabilities predicted from analysis, then the expressions for $P_{LF|H_0}$, $P_{LF|H_1}$, $\mu_{L|H_0}$, $\mu_{L|H_1}$, $\sigma_{L|H_0}$ and $\sigma_{L|H_1}$ obtained in the previous chapter will also be validated in addition to the expressions for $P(D_1|H_0)$ and $P(D_1|H_1)$ in Equations 4.1 and 4.2 and the Gaussian assumption.

4.3 Validation

In this section, predicted probabilities of false alarm and detection (from Equations 4.1 and 4.2) are validated using simulation. In the simulation, two sets of n Gamma distributed RTT samples are generated 10,000 times. The first set of n RTT samples are drawn from Gamma distribution with parameters α_0, β_0 and γ_0 (hypothesis H_0 is true). For the second set, the first $\lfloor\frac{n}{2}\rfloor$ samples are from Gamma distribution with parameters α_1, β_1, γ_1 and the last $\lceil\frac{n}{2}\rceil$ samples are

from Gamma distribution with parameters α_2, β_2 and γ_2 (hypothesis H_1 is true). Likelihood ratio L is evaluated using equation 3.4 and the set of n RTT samples. This produces 10,000 samples of $L|H_0$ and 10,000 samples of $L|H_1$. For any given value of λ, the fraction of the samples of $L|H_0$ that have a value less than λ is the simulated probability of false alarm and fraction of samples of $L|H_1$ that have a value less than λ is the simulated probability of detection. Receiver operating characteristics are generated by varying λ from $-\infty$ to ∞ and noting probabilities of false alarm and detection for each value of λ. Simulated and predicted receiver operating characteristics are illustrated in the figures below.

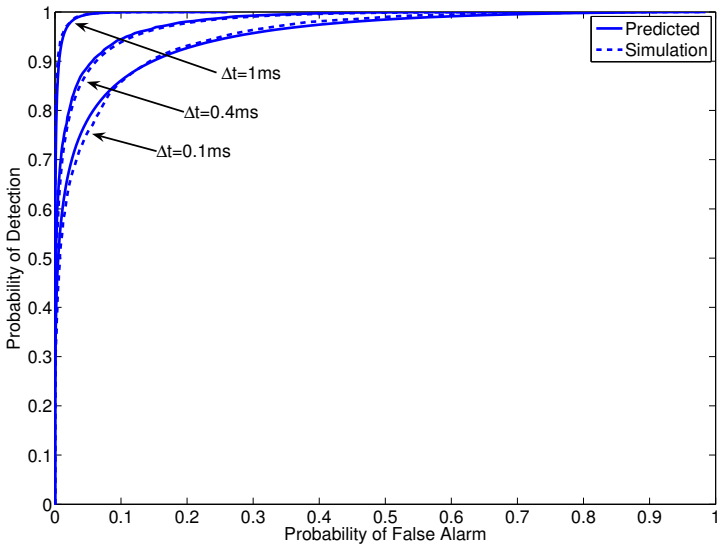

Figure 4.1. Simulation and predicted ROC for three different values of Δt (where $\Delta t = \gamma_2 - \gamma_1$) and fixed values of other parameters ($\alpha_0 = 2$, $\beta_0 = 4$, $\alpha_1 = 2$, $\beta_1 = 4$, $\alpha_2 = 2$, $\beta_2 = 5$, $\gamma_0 = \gamma_1$, $n = 100$). All three Δt values are positive.

Figure 4.1 shows the ROC obtained using both simulation and analysis for three different values of Δt ($\Delta t = 0.1ms$, $\Delta t = 0.4ms$ and $\Delta t = 1ms$). The value of the threshold λ is varied from $-\infty$ to ∞ to generate the ROC curves. The

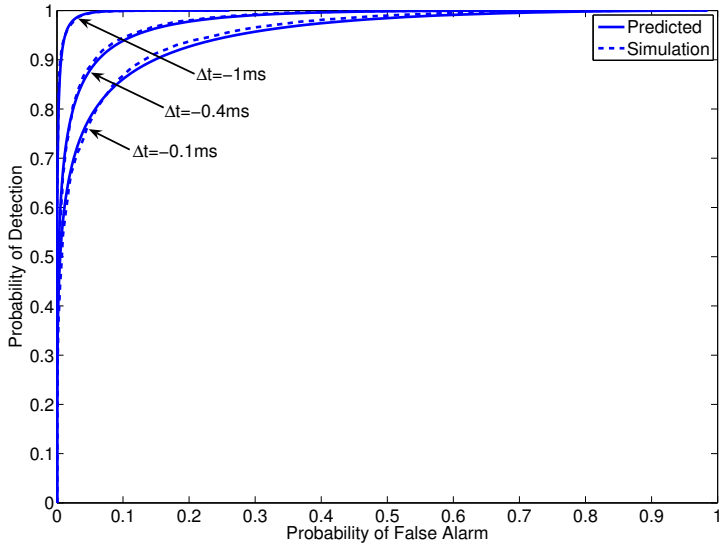

Figure 4.2. Simulation and predicted ROC for three different values of Δt (where $\Delta t = \gamma_2 - \gamma_1$) and fixed values of other parameters ($\alpha_0 = 2$, $\beta_0 = 4$, $\alpha_1 = 2$, $\beta_1 = 4$, $\alpha_2 = 2$, $\beta_2 = 5$, $\gamma_0 = \gamma_1$, $n = 100$). All three Δt values are negative.

values of the remaining parameters were fixed for the three different simulation runs. It is clear from this figure that the predicted ROC is very close to the ROC obtained using simulation. As the minimum RTT change decreases from 1ms to 0.1ms, it becomes harder to detect route changes and for any given value of the probability of detection, the probability of false alarm is higher when $\Delta t = 0.1ms$ than it is when $\Delta t = 1ms$. ROC curves in Figure 4.2 were generated using the same parameters as the ones that were used to generate the ROC curves in Figure 4.1, except the Δt values were negative for the curves in Figure 4.2. The curves in these two figures are identical and this shows that the shape of the ROC curve is a function of only the magnitude of minimum RTT change and not the direction of the change as expected. For the ROC curves that follow, only positive values of Δt will be used since it is assumed that the equivalent ROC curve for negative

value of Δt of the same magnitude is identical as expected.

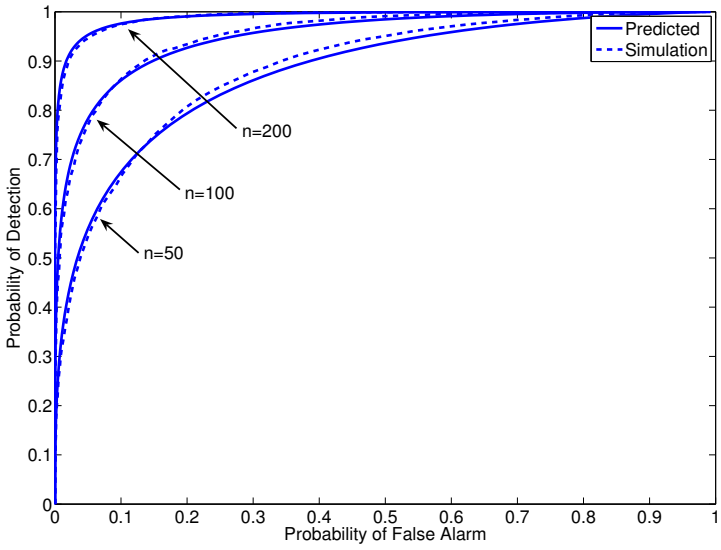

Figure 4.3. Simulation and predicted ROC for three different values of n and fixed values of other parameters ($\alpha_0 = 2$, $\beta_0 = 4$, $\alpha_1 = 2$, $\beta_1 = 4$, $\alpha_2 = 2$, $\beta_2 = 5$, $\gamma_0 = \gamma_1$, $\Delta t = 0.1ms$)

Figure 4.3 illustrates the ROC curves for three different values of the window size n. All other parameters are fixed including Δt which is fixed at 0.1ms. For each of the three different values of n, the predicted ROC curve is very close to the ROC curve from simulation. The ROC curve for a window size of 200 samples is to the top and left of the ROC curves for window sizes 100 and 50. For any fixed value of probability of detection, a window size of 200 allows PAD to achieve a lower probability of false alarm than a window size of 100 or 50 as expected.

	$n = 50$	$n = 30$	$n = 20$
P_F	8.4e-28	6.2e-18	3.0e-12

Table 4.1. Value of P_F for PAD with P_D fixed at 0.99999 for different values of n and fixed values of other parameters ($\alpha_0 = 0.12$, $\beta_0 = 1.99$, $\alpha_1 = 0.12$, $\beta_1 = 1.99$, $\alpha_2 = 0.5$, $\beta_2 = 3$, $\gamma_0 = \gamma_1$, $\Delta t = 1ms$)

For the ROC curves shown in figures 4.1, 4.2 and 4.3, RTT samples were

drawn from Gamma distribution with $\alpha = 2$ and $\beta = 4$. RTTs have very high variance for this set of parameter values and this models the RTTs of a path with a highly loaded (congested) router output port somewhere in the path. A majority of the Internet paths on which measurements were conducted did not have a heavily loaded router and RTTs had a lower delay variation. Parameter values of $\alpha = 0.12$ and $\beta = 1.99$ were used to obtain the P_F results shown in Table 4.1. These parameters were estimated from Internet RTT measurements between planck227.test.ibbt.be (Ghent University, Belgium) and planetlab1.larc.usp.br (University of Sao Paulo, Brazil) on October 21, 2006. Probability of false alarm with probability of detection fixed at 0.999 are shown in Table 4.1 for three window sizes of 20, 30 and 50. Minimum RTT change was fixed at $\Delta t = 1$ms for all three simulations. It is clear from the results in Table 4.1 that with a suitable value of the threshold λ and with a window size as small as 20 samples, PAD can detect minimum RTT change of 1ms with a probability of detection approximately 1 and probability of false alarm approximately zero. ROC curves are a function of the parameters of Gamma distribution from which RTT samples are drawn. This is illustrated further in Figure 4.4 where three different ROC curves are plotted for three different values of α.

A rigorous simulation study was conducted to find the region of acceptable performance for the parameter aware detector (PAD). If for any given threshold, the probability of detection ≥ 0.999 and probability of false alarm ≤ 0.001, then PAD is defined here to have acceptable performance for those parameter values. Parameters α and β were varied from 0.5 to 5 in steps of 0.1, the parameter n was varied from 100 to 300 in steps of 100 and the parameter ΔT was varied from 1ms to 4ms in steps of 1ms. For each combination of the parameter values, the analysis

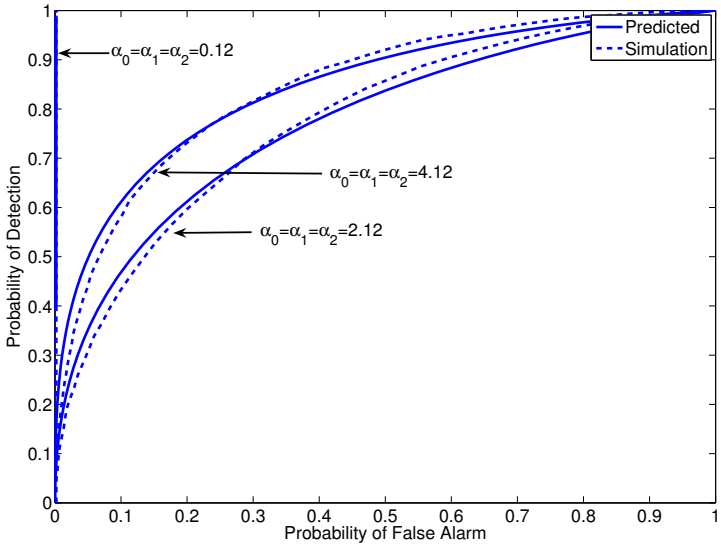

Figure 4.4. Simulation and predicted ROC for three different values of α_0, α_1, α_2 and fixed values of other parameters ($\beta_0 = 4$, $\beta_1 = 4$, $\beta_2 = 5$, $\gamma_0 = \gamma_1$, $\Delta t = 0.1ms$, $n = 20$)

discussed above was used to find the probabilities of false alarm and detection for the entire range of values of the threshold. If the probability conditions are met for any value of the threshold then the PAD has acceptable performance. However, if the probability conditions are not met for any of the threshold values, then PAD does not have acceptable performance. Regions of acceptable performance for PAD are shown in Figures 4.5, 4.6 and 4.7. The analysis developed for predicting performance of PAD was used to generate these plots. The region to the bottom and left of each curve is the region over which PAD has acceptable performance. As expected, the region over which PAD has acceptable performance increases with ΔT and with window size n. In the following chapter, similar acceptable performance regions will be plotted for PUD and heuristic detection algorithm and it will be shown that the PAD, as this is the optimum algorithm has the largest region of acceptable performance amongst all detectors proposed in this

dissertation as expected. Note that for the plots in Figures 4.5, 4.6 and 4.7, $\beta_2 = \beta + 0.5$. Figure 4.8 shows how the acceptable performance region curves change as a function of the parameter β_2.

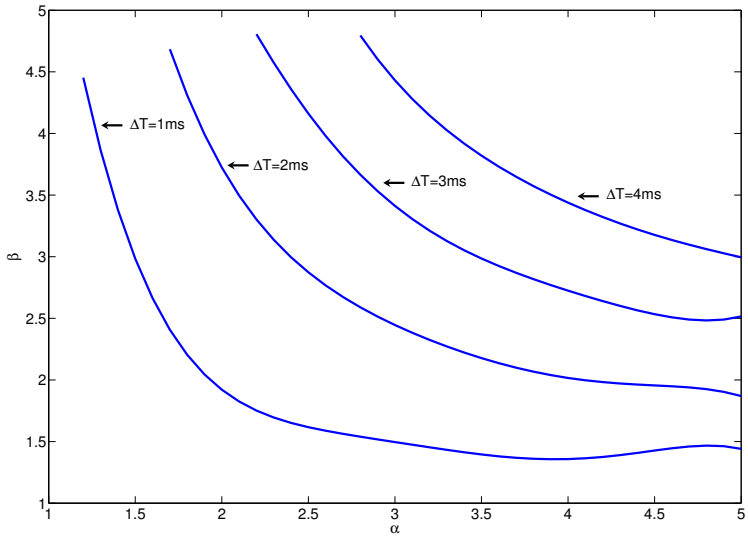

Figure 4.5. Region of acceptable performance for parameter aware detector with window size of 100 and $\alpha_0 = \alpha_1 = \alpha_2 = \alpha$ and $\beta_0 = \beta_1 = \beta$ and $\beta_2 = \beta + 0.5$

4.4 Summary

Given the set of parameters α_0, β_0, γ_0, α_1, β_1, γ_1, α_2, β_2, γ_2, n and λ, expressions for probability of detection and false alarms (Equations 4.1 and 4.2) that were derived in this chapter, can be used to predict these probabilities for the ideal detector. Predicted values of the probabilities of false alarm and detection were validated using simulation in section 4.3. ROCs were plotted for sevaral different values of the parameters Δt, n, α and β. The ROC curve obtained using analysis was close to the ROC curve obtained from simulation for each of the various different combinations of the parameter values. This validates not only

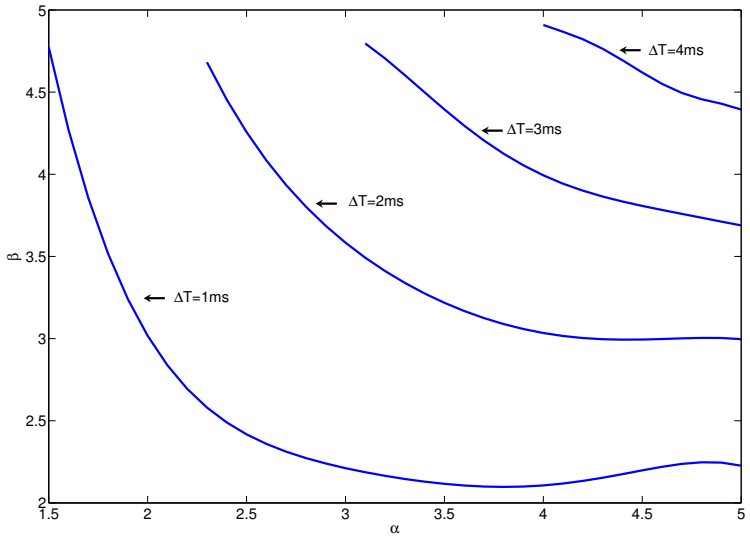

Figure 4.6. Region of acceptable performance for parameter aware detector with window size of 100 and $\alpha_0 = \alpha_1 = \alpha_2 = \alpha$ and $\beta_0 = \beta_1 = \beta$ and $\beta_2 = \beta + 0.5$

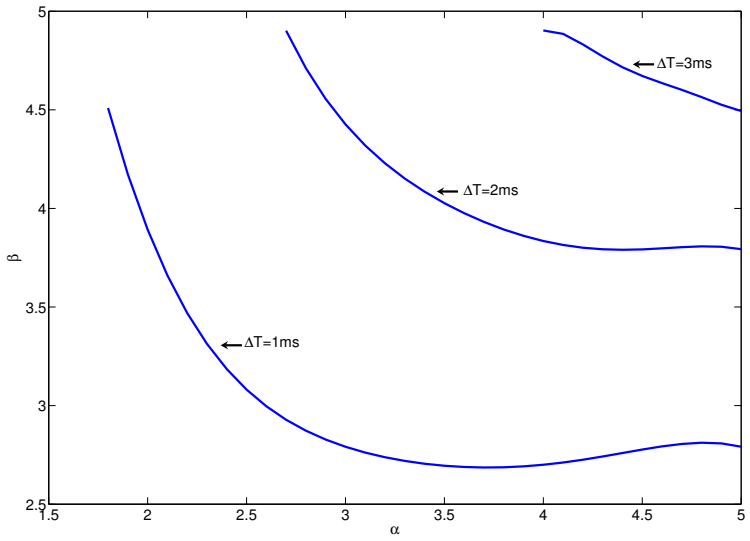

Figure 4.7. Region of acceptable performance for parameter aware detector with window size of 100 and $\alpha_0 = \alpha_1 = \alpha_2 = \alpha$ and $\beta_0 = \beta_1 = \beta$ and $\beta_2 = \beta + 0.5$

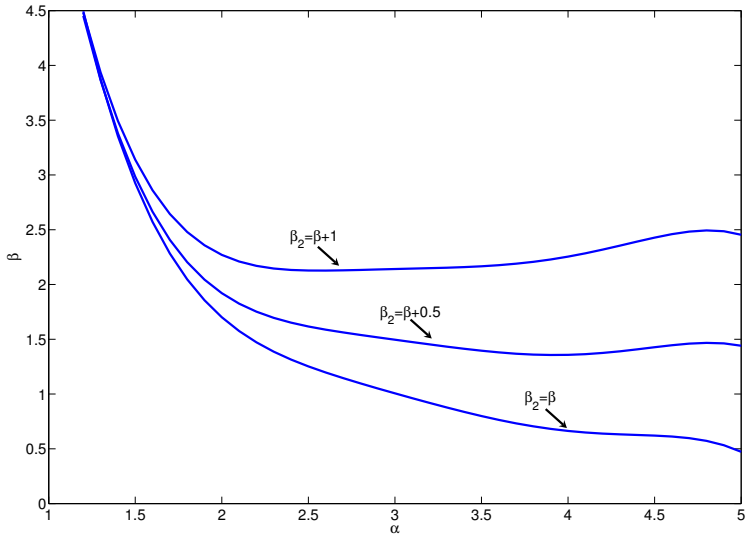

Figure 4.8. Region of acceptable performance for parameter aware detector with window size of 100 and $\Delta T = 1$ ms and and $\alpha_0 = \alpha_1 = \alpha_2 = \alpha$ and $\beta_0 = \beta_1 = \beta$

the expressions to predict probability of false alarm and detection that were derived in Equations 4.1 and 4.2, but also the expressions for $P_{LF|H_0}$, $P_{LF|H_1}$, $\mu_{L|H0}$, $\mu_{L|H1}$, $\sigma_{L|H0}$ and $\sigma_{L|H1}$ that were derived in the previous chapter as well as the Gaussian distribution assumption, because these expressions must also be correct to correctly predict probabilities of detection and false alarm. The region of the parameter space over which PAD has acceptable performance was also obtained in this chapter. Since the PAD is the optimum detector, PADs parameter space region of acceptable performance is larger than that of any other detector.

Chapter 5

Parameter Unaware Detector

5.1 Introduction

Expressions for the first two moments of $L|H_0$ and $L|H_1$ for the PAD were derived in Chapter 3. These expressions were used in Chapter 4 together with a distribution assumption to find expression for probabilities of detection and false alarms for PAD. The predicted probabilities were then compared to the ones obtained from simulation and it was found that the analysis correctly predicts these probabilities. In the current chapter, simulation will be used to generate ROC curves for the PUD. The performance of PUD will be compared with the performance of the ideal detector (PAD). Simulations were also conducted to find the region of the parameter space over which PUD and the heuristic detectors have acceptable performance. It is shown in this chapter that PAD has the largest region of acceptable performance followed by PUD and then by the heuristics-based algorithm. PUD is also applied to the measured data to evaluate its performance.

5.2 Performance

In this section, performance of PUD will be compared to the performance of the ideal detector. Performance curves for the ideal detector were obtained using the analysis in Section 4.2. ROC curves for PUD were generated using simulation. In the simulation, two sets of n Gamma distributed RTT samples are generated 10,000 times. The first set of n RTT samples are drawn from Gamma distribution with parameters α_0, β_0 and γ_0 (hypothesis H_0 is true). For the second set, the first $\lfloor \frac{n}{2} \rfloor$ samples are from Gamma distribution with parameters α_1, β_1, γ_1 and the last $\lceil \frac{n}{2} \rceil$ samples are from Gamma distribution with parameters α_2, β_2 and γ_2 (hypothesis H_1 is true). Since the detector is parameter unaware, it estimates the parameters $\hat{\alpha_0}$, $\hat{\beta_0}$, $\hat{\gamma_0}$, $\hat{\alpha_1}$, $\hat{\beta_1}$, $\hat{\gamma_1}$, $\hat{\alpha_2}$, $\hat{\beta_2}$ and $\hat{\gamma_2}$ from the n RTT samples. Equation 3.2 is then evaluated using the parameter estimates and the n RTT samples to determine the value of the likelihood ratio L. The likelihood ratio is evaluated for samples in each of the two sets of n RTT samples 10,000 times. This produces 10,000 samples of $L|H_0$ and 10,000 samples of $L|H_1$. For any given value of λ, the fraction of the samples of $L|H_0$ that have a value less than λ is the simulated probability of false alarm for PUD and fraction of samples of $L|H_1$ that have a value less than λ is the simulated probability of detection for PUD. Receiver operating characteristics are generated by varying λ from $-\infty$ to ∞ and noting probabilities of false alarm and detection for each value of λ. Receiver operating characteristics for PUD and PAD are illustrated in the figures below.

ROC curves for three different values of Δt are shown in Figure 5.1. As expected, performance of both PUD and PAD improves as Δt increases. ROC curves for three different values of the window size n are shown in Figure 5.2. The performance of both PAD and PUD improves with an increase in the window size.

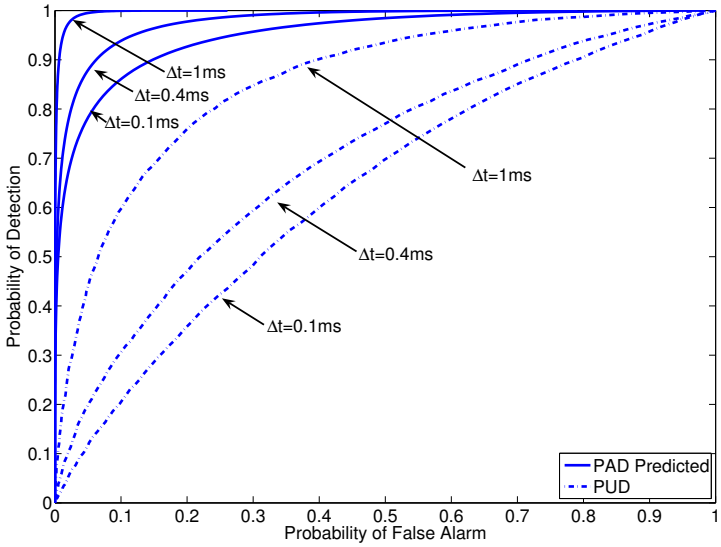

Figure 5.1. PAD and PUD ROCs for three different values of Δt (where $\Delta t = \gamma_2 - \gamma_1$) and fixed values of other parameters ($\alpha_0 = 2$, $\beta_0 = 4$, $\alpha_1 = 2$, $\beta_1 = 4$, $\alpha_2 = 2$, $\beta_2 = 5$, $\gamma_0 = \gamma_1$, $n = 100$).

It is also clear from Figures 5.1 and 5.2 that PUD performs poorly in comparison to the ideal detector for these parameters. The parameters used to generate the plots in Figures 5.1 and 5.2 are $\alpha = 2$ and $\beta = 4$. These parameters model RTTs of a path with one or more very heavily loaded routers in the path. The PUD has better performance when there is less congestion in the end to end path. This is demonstrated below with parameter estimates obtained using PlanetLab measurements.

RTT measurements were conducted using the PlanetLab infrastructure for 21 days in October-November 2006. The Gamma distribution parameters were estimated for each day using all the RTT samples collected on that day. If there was a route change on any day, only the subset of RTTs collected when there was no route change were used to estimate the parameters for that day. Estimates of α and β for five days are shown in Tables 5.1 and 5.2. There were

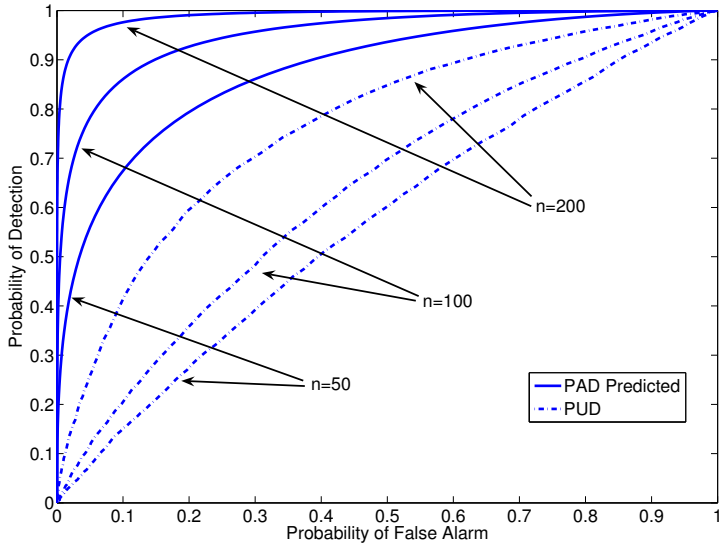

Figure 5.2. PAD and PUD ROCs for three different values of n (where $\Delta t = \gamma_2 - \gamma_1$) and fixed values of other parameters ($\alpha_0 = 2$, $\beta_0 = 4$, $\alpha_1 = 2$, $\beta_1 = 4$, $\alpha_2 = 2$, $\beta_2 = 5$, $\gamma_0 = \gamma_1$, $\Delta t = 0.1ms$).

a large number of route changes on October 24 on one of the paths (data set 4) and a statistically significant number of RTT samples with no route change could not isolated. The four data sets labeled 1, 2, 3 and 4 represent the paths between planck227.test.ibbt.be (Ghent, Belgium) - planetlab1.larc.usp.br (Sao Paulo, Brazil), kupl2.ittc.ku.edu (Lawrence, Kansas) - planetlab01.cnds.unibe.ch (Bern, Switzerland), planetlab1.eecs.iu-bremen.de (Bremen, Germany) - planetlab1.ls.fi.upm.es (Madrid, Spain) and planetlab1.cslab.ece.ntua.gr (Athens, Greece) - planetlab1.iii.u-tokyo.ac.jp (Tokyo, Japan).

Data set	Oct 22	Oct 23	Oct 24	Oct 25	Oct 26
1	0.099	0.1326	0.1191	0.1115	0.1126
2	0.0919	0.0908	0.0907	0.0909	0.0915
3	0.5577	0.72	0.6856	0.4179	0.4062
4	0.1182	0.1193	-	1.7320	1.6243

Table 5.1. Estimates of the parameter α from PlanetLab measurements

Data set	Oct 22	Oct 23	Oct 24	Oct 25	Oct 26
1	1.0704	3.6073	3.4260	2.6908	2.6706
2	2.0672	1.4810	1.5020	1.4665	1.3061
3	0.5306	0.4547	0.4181	0.6183	0.7557
4	2.9245	2.9919	-	0.5748	0.6072

Table 5.2. Estimates of the parameter β from PlanetLab measurements

For the parameters shown in Tables 5.1 and 5.2, a window size of 100 samples and $\Delta t = 1ms$, performance of PUD is comparable to the performance of the ideal detector. The performance of both PAD and PUD for these parameters is close to ideal because it is possible to achieve a probability of detection close to 1 and probability of false alarm close to 0 with both detectors. Simulations were conducted to find out the value of the threshold λ for which probability of detection is 0.99999. This value of threshold λ was then used to find the probability of false alarm for both PAD and PUD. The probabilities of false alarm found using different combinations of parameters for PAD and PUD are shown in Tables 5.3 and 5.4.

Data set	Oct 22	Oct 23	Oct 24	Oct 25	Oct 26
1	6.9e-39	5.6e-23	1.5e-24	2.6e-27	2.9e-27
2	4.9e-35	5.7e-41	5.5e-41	6.4e-41	2.7e-41
3	3.4e-29	1.2e-28	9.2e-32	5.8e-30	2.4e-26
4	6.1e-26	1.2e-25	-	1.3e-9	1.6e-9

Table 5.3. Probability of false alarm when probability of detection is 0.99999 for PAD obtained via analysis

It is clear from Tables 5.3 and 5.4 that probability of false alarm is very low when probability of detection is 0.99999 for both PUD and the ideal detector. Probability of false alarm for PUD is zero for most of the combinations of parameters. This is because only 10,000 samples of L were generated using the simulation. Probability of false alarm for PAD has very low values that are not

Data set	Oct 22	Oct 23	Oct 24	Oct 25	Oct 26
1	0	0	0	0	0
2	0	0	0	0	0
3	0	0	0	0	0
4	0	0	-	0.0092	0.0029

Table 5.4. Probability of false alarm when probability of detection is 0.99999 for PUD obtained using simulations

zero because these probability values were generated using the analysis.

5.3 Acceptable performance regions

Extensive simulations were conducted to find the range of parameter values for which PUD has acceptable performance. Acceptable performance is defined to be achieved by a detector when $P_D \geq 0.999$, $P_F \leq 0.001$. Parameters α and β were varied from 0.1 to 4 and from 0.1 to 3 respectively in steps of 0.1, parameter n was varied from 100 to 300 in steps of 100 samples and parameter ΔT was varied from 1ms to 4ms in steps of 1ms. For each combination of the values of α, β, n and ΔT, 10,000 samples of $L|H_0$ and 10,000 samples of $L|H_1$ were generated. The RTT samples needed to find $L|H_0$ and $L|H_1$ were samples drawn from a Gamma distribution. Threshold λ was then varied from $-\infty$ to ∞ to determine if PUD has acceptable performance for any value of threshold for the given parameters. Here the detection algorithm is defined to have acceptable performance when probability of detection is greater than 0.999 and probability of false alarm is less than 0.001. Simulation results with n fixed at 100 samples are shown in Figure 5.3. Parameter space for which PUD has acceptable performance is to the bottom and left of each curve. For example, when $\alpha = 3$ and $\beta = 2$, route changes with a minimum RTT change of 4ms can be detected with $P_D \geq 0.999$ and $P_F \leq 0.001$ using PUD, however if minimum RTT changes by 3, 2 or 1ms, PUD cannot detect

these changes with acceptable performance. Note that the curves shown in Figure 5.3 were fitted from the data using a polynomial of degree 4. Simulation results that depict the parameter space over which PUD has acceptable performance when $n = 200$ and $n = 300$ are shown in Figures 5.4 and 5.5. As expected, parameter space over which PUD has acceptable performance increases with an increase in n.

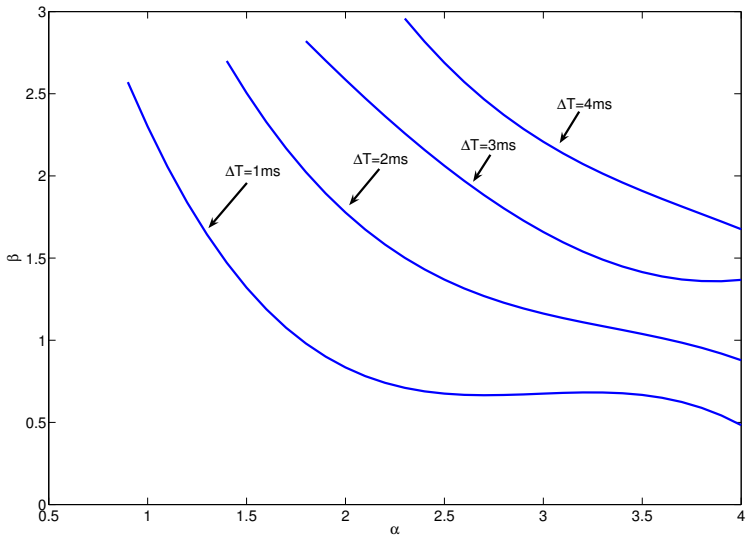

Figure 5.3. Parameter space for which PUD has acceptable performance ($P_D \geq 0.999$, $P_F \leq 0.001$) is to the bottom and left of each curve. Window size n is fixed at 100 samples and $\alpha_0 = \alpha_1 = \alpha_2 = \alpha$, $\beta_0 = \beta_1 = \beta$, $\beta_2 = \beta + 0.5$.

Similar simulations were conducted to find the range of parameter values for which the heuristic route change detection algorithm has acceptable performance. Parameters α and β were varied from 0.5 to 5 and 0.5 to 3 in steps of 0.1 respectively and the window size n was varied from 100 samples to 300 samples in steps of 100 samples. The parameter ΔT was fixed at 1ms and the simulations were not repeated for different values of ΔT because it is expected that the parameter

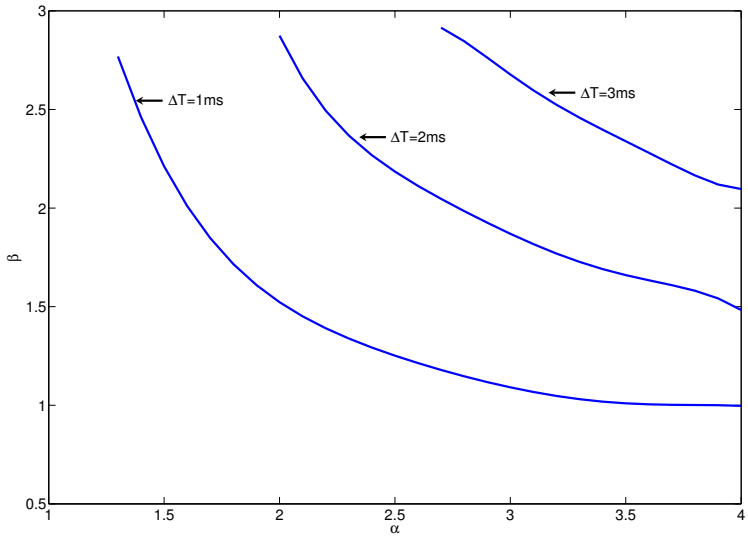

Figure 5.4. Parameter space for which PUD has acceptable performance ($P_D \geq 0.999$, $P_F \leq 0.001$) is to the bottom and left of each curve. Window size n is fixed at 200 samples and $\alpha_0 = \alpha_1 = \alpha_2 = \alpha$, $\beta_0 = \beta_1 = \beta$, $\beta_2 = \beta + 0.5$.

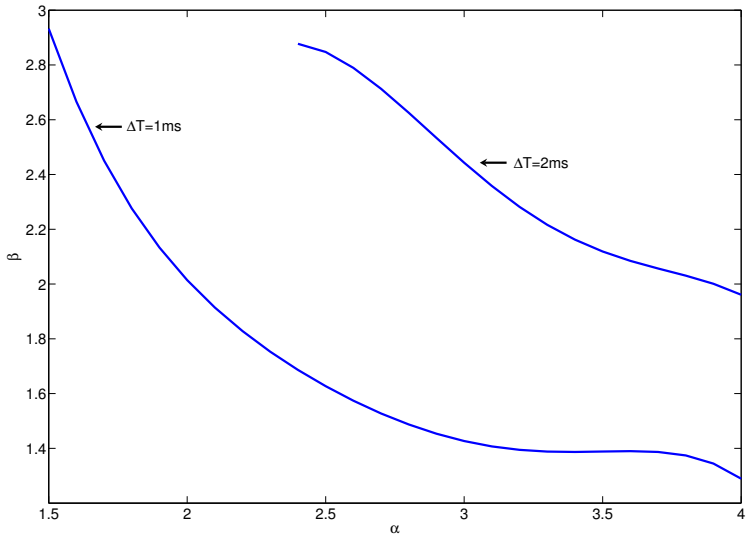

Figure 5.5. Parameter space for which PUD has acceptable performance ($P_D \geq 0.999$, $P_F \leq 0.001$) is to the bottom and left of each curve. Window size n is fixed at 300 samples and $\alpha_0 = \alpha_1 = \alpha_2 = \alpha$, $\beta_0 = \beta_1 = \beta$, $\beta_2 = \beta + 0.5$.

space is not a function of the parameter ΔT (the heuristic algorithm just looks at the past few windows of samples to decide whether or not it can detect route changes and if the congestion is high, it does not even attempt to detect the route change). For each combination of the parameter values, two traces are generated, one that has 10,000 route changes and another that has no route changes. The heuristic algorithm is then applied to these traces to find out the probabilities of detection and false alarm. If the probability of detection is greater than 0.999 and probability of false alarm less than 0.001, then the heuristic algorithm has acceptable performance for that set of parameter values. Figure 5.6 shows the range of parameter values for which the heuristic algorithm has acceptable performance for three different window size values.

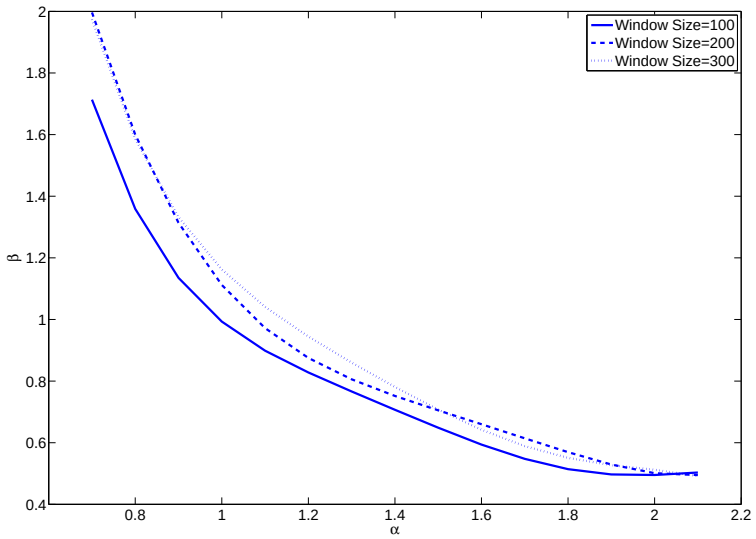

Figure 5.6. Parameter space for which the heuristic algorithm has acceptable performance ($P_D \geq 0.999$, $P_F \leq 0.001$) is to the bottom and left of each curve. Parameter ΔT is fixed at 1ms.

Parameter spaces of all three algorithms for window size of 100 samples and ΔT=1ms are shown in the same graph in Figure 5.7. As expected, PAD has the

largest region of acceptable performance followed by PUD and heuristics based algorithms. Similar parameter spaces of all three algorithms for window size of 200 and 300 samples and ΔT=1ms are shown in Figures 5.8 and 5.8. Note that performance of PAD and PUD improves with an increase in the window size but the performance of the heuristics-based algorithm does not improve. It can be concluded that for large window sizes, the performance loss in using heuristics-based algorithm is greater.

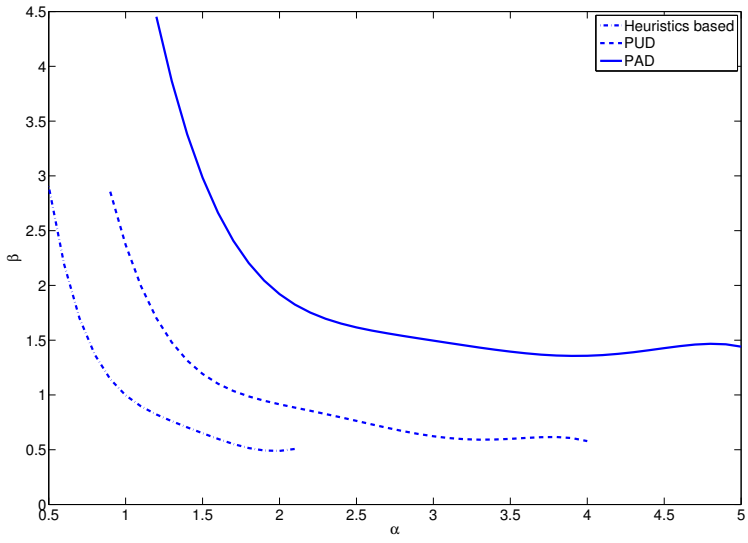

Figure 5.7. Parameter space for which the heuristic, PAD and PUD algorithms have acceptable performance ($P_D \geq 0.999$, $P_F \leq 0.001$) is to the bottom and left of each curve. Parameter ΔT is fixed at 1ms and window size is 100 samples for all three algorithms. Also, the parameters $\alpha_0 = \alpha_1 = \alpha_2 = \alpha$, $\beta_0 = \beta_1 = \beta$, $\beta_2 = \beta + 0.5$ for both PUD and PAD.

5.4 Measured data

The RTT samples used to plot ROC curves discussed in the previous section were drawn from pseudo random numbers that follow a Gamma distribution. In

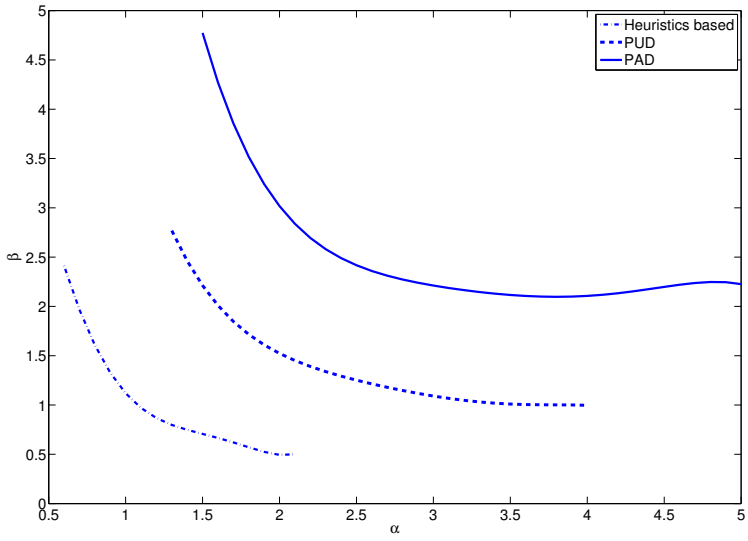

Figure 5.8. Parameter space for which the heuristic, PAD and PUD algorithms have acceptable performance ($P_D \geq 0.999$, $P_F \leq 0.001$) is to the bottom and left of each curve. Parameter ΔT is fixed at 1ms and window size is 200 samples for all three algorithms. Also, the parameters $\alpha_0 = \alpha_1 = \alpha_2 = \alpha$, $\beta_0 = \beta_1 = \beta$, $\beta_2 = \beta + 0.5$ for both PUD and PAD.

this section, these performance curves are plotted using RTT samples that were collected using the PlanetLab infrastructure. To plot the ROC curves for measured RTT data, the data was first segmented into statistically homogeneous regions with no route changes. The minimum RTT of these samples was then subtracted from all the RTT samples to change the minimum to zero. These RTT samples were then divided into windows of size n samples each. The likelihood ratio was then calculated for each of these n sample windows. This produces samples for L when hypothesis H_0 is true. The minimum RTT of the last $\lceil \frac{n}{2} \rceil$ samples was then changed by adding Δt for each of the n sample windows. Likelihood ratio was then calculated again for each of these n RTT sample windows. This produces samples for L when hypothesis H_1 is true. For any given value of threshold λ, the

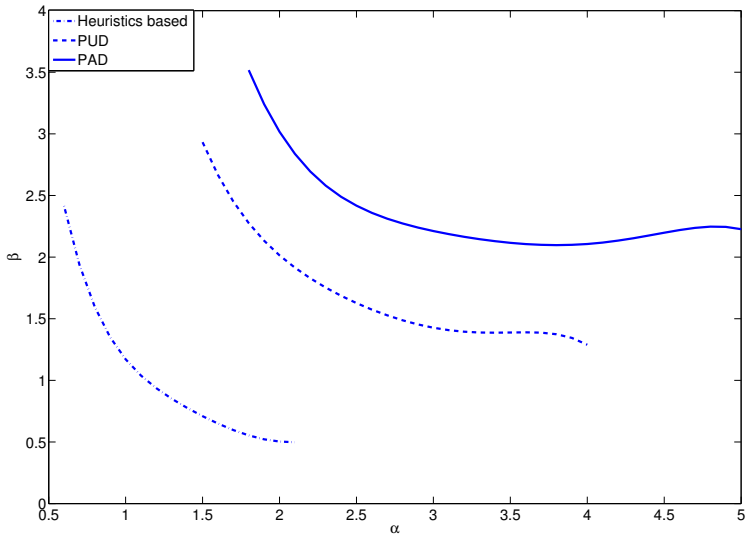

Figure 5.9. Parameter space for which the heuristic, PAD and PUD algorithms have acceptable performance ($P_D \geq 0.999$, $P_F \leq 0.001$) is to the bottom and left of each curve. Parameter ΔT is fixed at 1ms and window size is 300 samples for all three algorithms. Also, the parameters $\alpha_0 = \alpha_1 = \alpha_2 = \alpha$, $\beta_0 = \beta_1 = \beta$, $\beta_2 = \beta + 0.5$ for both PUD and PAD.

fraction of the samples of $L|H_0$ that have a value less than λ is the probability of false alarm for PUD and fraction of samples of $L|H_1$ that have a value less than λ is the probability of detection for PUD. Receiver operating characteristics are generated by varying λ from $-\infty$ to ∞ and noting probabilities of false alarm and detection for each value of λ. The ROC curves in Figures 5.10 and 5.11 were plotted using RTT samples collected on October 23, 2006. As expected, performance of PUD improves with an increase in the window size and minimum RTT change ΔT. The ROC curve shown in Figure 5.12 was plotted using RTT samples collected on October 25, 2006. A window size of 100 samples is sufficient to detect route changes with a high value of probability of detection and small probability of false alarm on this day.

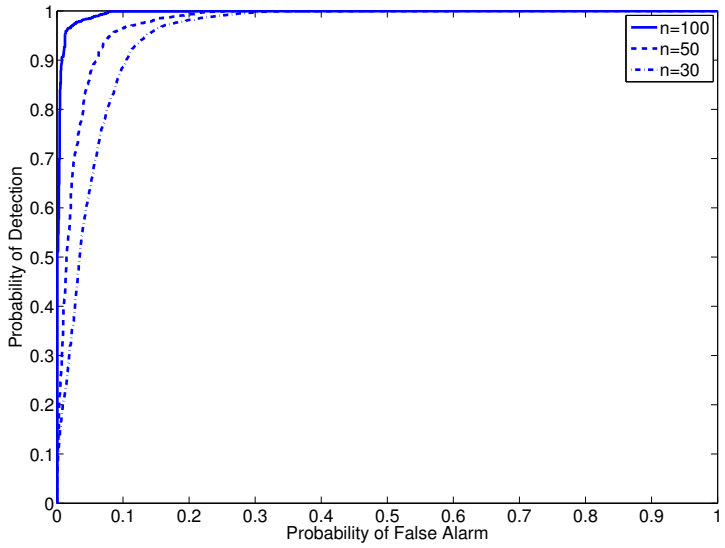

Figure 5.10. PUD ROCs for three different values of n and Δt fixed at 1ms. RTT samples are from data set 4 collected on October 23, 2006

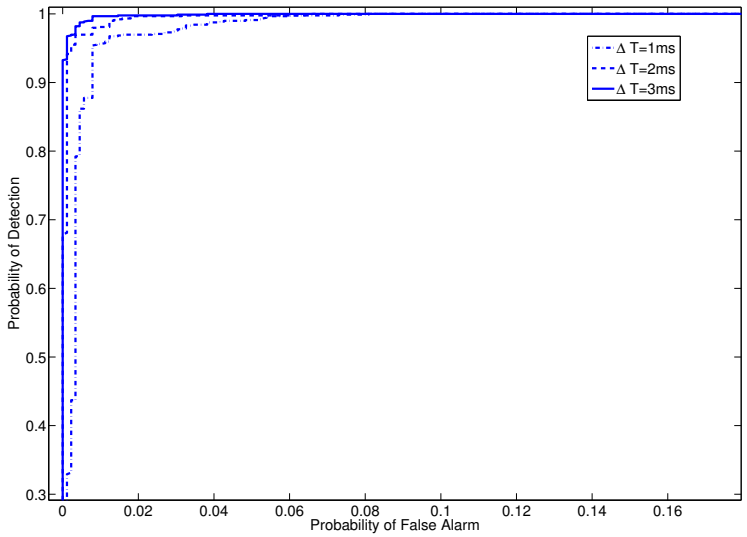

Figure 5.11. PUD ROCs for three different values of Δt and with n fixed at 100 samples. RTT samples are from data set 4 collected on October 23, 2006

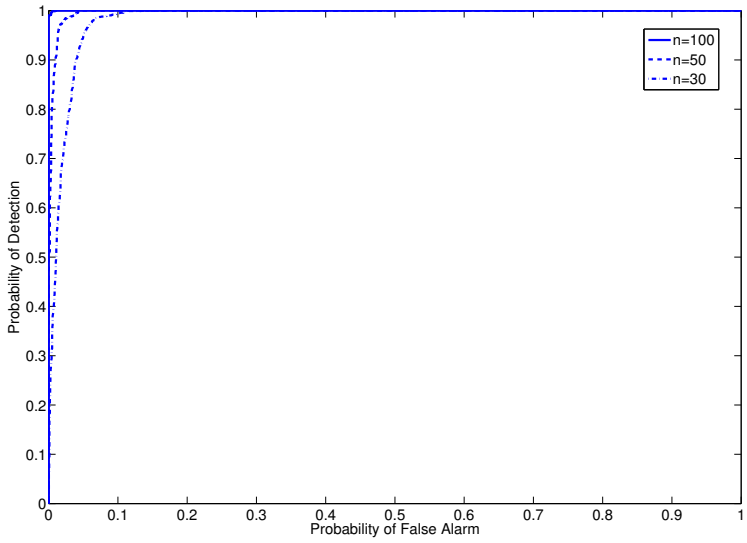

Figure 5.12. PUD ROCs for three different values of n and with ΔT fixed at 1 ms. RTT samples are from data set 4 collected on October 25, 2006

5.5 Summary

Simulation results for the PUD were presented in the form of ROC curves in this chapter. It was shown using these ROC curves that the PUD performs poorly as compared to the PAD (or the ideal detector) for some parameter values. RTT measurements collected using the PlanetLab infrastructure were used to find estimates of the α and β for these paths. The goal in doing this was to get an idea of the range of α and β values that are representative of most of the Internet paths. For the parameter values that were estimated using the measurement data, it was found that both PAD and PUD have very good performance. This is because all of these Internet paths were lightly loaded and there was no congestion. Extensive simulations were conducted to find the parameter space over which PUD has acceptable performance (where acceptable performance is defined as $P_D \geq 0.999$ and $P_F \leq 0.001$). It was found that the region of acceptable performance increases

with an increase in ΔT or the window size as expected. Acceptable performance region for the heuristic detector was also obtained in this chapter. It was shown that the PAD has the largest region of acceptable performance followed by PUD and then by the heuristics-based detector. This is an important result because it shows that PUD is the practical detector of choice because it has a larger region of acceptable performance than the heuristics-based algorithm. PUD can detect route change events with better accuracy than the heuristics-based detector when the router queues are heavily loaded. Moreover it was shown that the difference in performance of heuristics-based algorithm and the PUD increases with an increase in the window size. Finally, PUD was applied to Internet measurement traces in which multiple route changes were induced to evaluate its performance.

The acceptable performance region curves shown in Figures 5.7, 5.8 and 5.9 are very useful for determining the detection algorithm to use and the minimum required probing rate given some performance constraints. For example, consider the case where route changes that occur 1 minute apart in time are to be detected and assume that from historical data it is known that the path gets congesting raising the α and β values to 3 and 1.4 respectively. From the three figures it is clear that only PUD can detect route changes with acceptable performance and only when window size is 300 samples. Since route changes that occur 1 minute apart in time are to be detected, the maximum inter-sample time is 200ms. Also, it is clear from these figures that the heuristic algorithm does not have acceptable performance even when the probing rate is 5 samples per second. If it is known from historical data that there is no congestion in this path, a lower sampling rate of 100 samples per second can be used. This procedure of determining the minimum sampling rate can be automated and implemented in the detector. A

detector can use the last few samples to estimate the α and β parameter values and then use the information in Figures 5.7, 5.8 and 5.9 to determine the minimum required window size and the minimum sampling rate. The detector can then adjust its sampling rate accordingly in real-time so as to achieve acceptable performance.

This chapter concludes the series of chapters on route change detectors. In the next chapter, it will be shown that the PF scheduler used in wireless networks can cause RTM impairments. A new scheduler that mitigates the starvation vulnerability of the proportional fair scheduler is also developed and evaluated in the next chapter.

Chapter 6

Scheduler-Induced Imparments in Infrastructure-Based Wireless Networks

6.1 Introduction

Methods for detecting RTM application impairments were introduced in Chapter 2. Impairments may occur during congestion or route change events. Methods for detecting congestion and route change events were also developed in Chapters 2, 3, 4 and 5. Measured RTTs are used together with packet loss information to detect congestion and route changes. These detection methods are based on certain assumptions about the random variable that models the RTTs (e.g., RTTs are Gamma distributed). These assumptions about the RTT may not hold when there are one or more wireless links in the end-to-end path. Wireless links are typically characterized by link rate variations (due to mobility, fading, etc.), high error rates and very high available bandwidth variations. For these reasons, the wireless links

typically exhibit very high delay variations. A study of infrastructure-based wireless networks was initiated to better understand the delay characteristics of these networks. During this study, it was found that the proportional fair scheduler that is commonly used in these networks induces RTM application impairments. As a part of this work, these impairments were identified using field experiments. More importantly, new mechanisms were developed to illustrate these performance issues. The contribution of this work is the finding that impairments are induced by the proportional fair scheduler and also the development and analysis of a new scheduler to improve the performance.

Many infrastructure-based wireless networks (e.g., Evolution-Data Optimized (EVDO) [XY06] and High-Speed Downlink Packet Access (HSDPA)) use the proportional-fair scheduling algorithm. This algorithm is designed to achieve good network throughput by scheduling users that are experiencing their better-than-average channel conditions without compromising long-term fairness. It will be shown in this chapter using field data that this fairness-ensuring mechanism can be easily corrupted, accidentally or deliberately, to starve users and severely degrade performance reducing TCP throughput and thus inducing RTM impairments. The performance degradation is quantified using results from experiments that were conducted in both in-lab and with a production CDMA 1xEVDO network. It is shown that delay jitter can be increased by up to 1 second and TCP throughput can be reduced by as much as $25 - 30\%$ by a single malicious user. A modification to the proportional fair scheduling algorithm that mitigates this starvation problem is also proposed and analysed in this chapter. Using ns-2 simulations, it is shown this modification to the proportional fair scheduling algorithm mitigates starvation without compromising the fairness ensuring and throughput optimizing

mechanisms of the base algorithm.

6.2 The PF algorithm and starvation

As with any managed wireless network, access to the wireless channel in 3G networks is controlled by Base Stations (BSs) to which mobile devices or Access Terminals (ATs) are associated. The focus here is on Proportional Fair (PF) - the scheduling algorithm [VTL02] used to schedule transmissions on the downlink in most 3G networks. In these networks, downlink transmission is slotted. For example, in CDMA-based EV-DO networks, slot size is 1.67ms. BSs have per-AT queues and employ PF to determine the AT to transmit to in a specific time slot.

The inputs to PF are the current channel conditions reported on a per-slot basis by each AT. Specifically, each AT uses its current Signal-to-Noise Ratio (SNR) to determine the required coding rate and modulation type and hence, the *achievable rate* of downlink transmission. In the EV-DO system, there are 10 unique achievable data rates (in Kilobits per second) - 0, 38.4, 76.8, 153.6, 307.2, 614.4, 921.6, 1228.8, 1843.2 and 2457.6. Assume that there are n ATs in the system. Denote the achievable data rate reported by AT i in time slot t to be R_t^i ($i = 1 \ldots n$). For each AT i, the scheduler also maintains A_t^i, an exponentially-weighted average rate that user i has achieved, i.e.,

$$A_t^i = \begin{cases} A_{t-1}^i(1-\alpha) + \alpha R_t^i & \text{if slot allocated} \\ A_{t-1}^i(1-\alpha) & \text{otherwise} \end{cases}$$

Slot t is allocated to the AT with the highest ratio $\frac{R_t^i}{A_{t-1}^i}$. Parameter α has a value that is usually around 0.001 [JPP00]. Thus, an AT will be scheduled less often

when it experiences fading and more often when it does not.

The basic observation behind this work is that an AT can (deliberately or accidentally) influence the value of its $\frac{R_t}{A_{t-1}}$ ratio thereby affecting the slot allocation process. An AT can do this simply by receiving data in an *on-off* manner. To see why, consider an AT that receives no data for several slots. Its A_t would slowly reduce and approach zero. After several inactive slots, when a new packet destined for that AT arrives at the base station, that AT has a low value of A_t and is likely to get allocated the slot because its ratio is very high. This AT keeps getting allocated slots until its A_t increases enough. During this period, all other ATs are starved. Starvation due to on-off behavior occurs because PF reduces A_t during the off periods. This implies that PF "compensates" for slots that are not allocated even when an AT has no data to receive!

6.3 Experiment configuration

The initial experiments were conducted using a production EV-DO network in USA. The ATs are IBM T42 Thinkpad laptops running Windows XP equipped with commercially-available PCMCIA EV-DO cards. The laptops have 2GHz processors and 1GB of main memory. All ATs connect to the same base station and sector. Data to the ATs is sourced from Linux PCs with 2.4GHz processors and 1GB of memory. All of these PCs are on the same subnet and 10 or 11 hops away from the ATs.

Two ATs - AT1 and AT2 were used for the first experiment. AT1 receives a long-lived periodic UDP packet stream consisting of 1500-byte packets with an average rate of 600Kbps. AT2 is assigned the role of a malicious AT and hence, receives traffic in an on-off pattern from its sender. Specifically, it receives

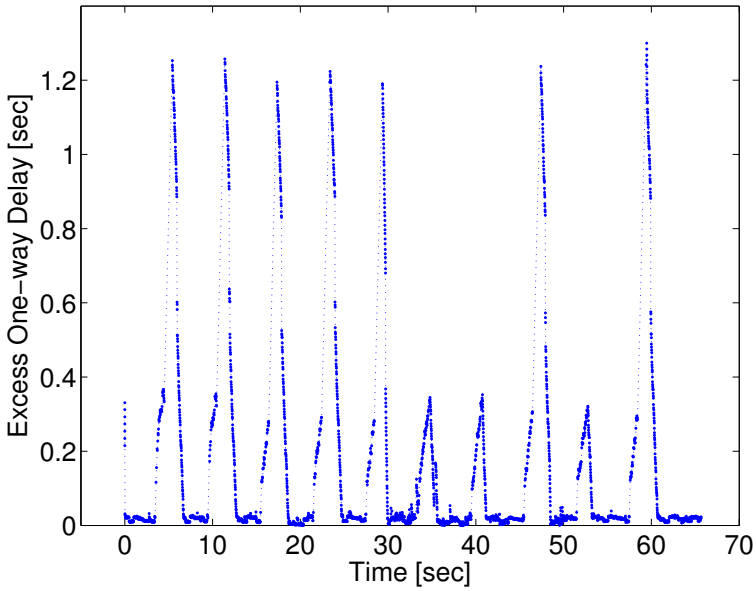

Figure 6.1. "Jitter" caused by a malicious AT in a commercial EV-DO network.

a burst of 250 packets of 1500 bytes every 6 seconds. The "jitter" experienced by AT1 is shown in Figure 6.1. Since the ATs are not time-synchronized with the senders, jitter is calculated as the excess one-way delays over the minimum delay. Well-defined increases in jitter are observed whenever a burst is sent to AT2. These results clearly show that AT1 experiences extraordinary increase in "jitter". Similar results are observed with other parameter settings (results not shown here). With all of the parameter settings, however, the jitter increases vary from 300ms to 1 second. The variability is likely due to traffic to other ATs and queueing effects at other hops. Hence, to understand and quantify the attack scenarios better, a more controlled laboratory was used because it eliminates unknowns such as cross-traffic.

The laboratory configuration includes the Base Station, the Radio Network Controller (RNC) and the Packet Data Serving Node (PDSN) (see [JPP00]). The links between the Base Station, RNC and PDSN are 1Gbps Ethernet links. The

Base Station serves 3 sectors of which only one is used for this study. The ATs and senders are the same as before. *Tcpdump* [tcp] traces are collected at the senders and ATs. Due to the peculiarities of PPP implementation on Windows XP, the timestamps of received packets are accurate only to 16ms. However, these inaccuracies are small enough to not affect the results. For TCP-based experiments, *tcptrace* and *tcpdump* are used to analyze the sender-side traces. There are three main differences with a commercial network. First, laboratory base stations use lower power levels than commercial networks due to shorter distances and in the interest of our long-term health. Since the goal is not to characterize fading and PF's vulnerability does not depend on channel characteristics, this does not affect the validity of the results. Second, the number of ATs connected to the base station can be controlled in the laboratory. Third, the number of hops from the senders to the ATs is only 3. This eliminates the additional hops on normal Internet paths and queueing effects on those hops. The impact of this is discussed in Section 6.4.2. Moreover, this is realistic in networks that use split-TCP or TCP-proxy [WZZ+06].

The laboratory configuration poses a few challenges. First, even though the experiments were conducted in the laboratory, the wireless conditions varied significantly. Hence, up to 30 runs of each experiment (a particular parameter setting) were conducted to calculate a good estimate of the required performance metric with a small enough confidence interval. The runs of the different parameter settings used to plot a figure were also interleaved so that they all experienced the same wireless conditions on average. A second challenge is that ATs become disassociated with the base station after around 12 seconds of inactivity. Also, the initial few packets sent to an inactive AT encountered large delays due to channel

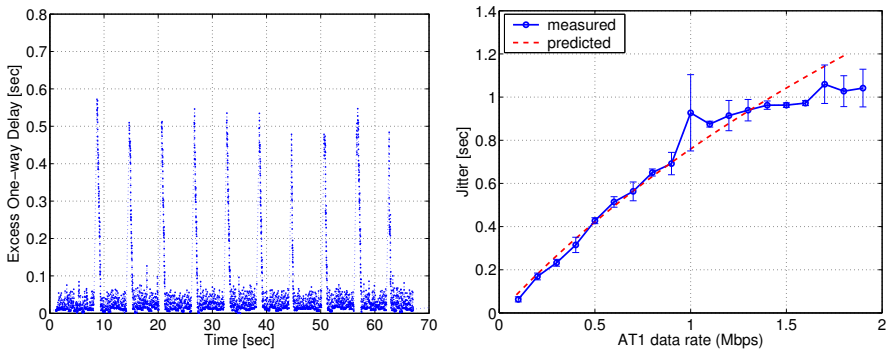

Figure 6.2. (a) Results of "jitter" experiment performed in the lab configuration. The excess of one-way (unsynchronized) delays are shown. (b) The maximum amount of "jitter" - measured and predicted - that can be caused as a function of the data rate of the long-lived flow to AT1. As noted before, fair queueing would cause negligible "jitter" if channel capacity is not exceeded.

setup and other control overhead. To prevent the ATs from becoming inactive, a low rate background data stream of negligible overhead was used.

6.4 Experiment Results

This section discusses the laboratory experiment results to quantify the PF induced starvation. Impact on non-reactive UDP-based applications is discussed first and then, on TCP-based applications. This section concludes with a discussion on how common traffic patterns can also trigger PF-induced starvation and briefly discuss a preliminary replacement for PF.

6.4.1 UDP-based applications

The results of a laboratory experiment are shown in Figure 6.2 (similar to that of Figure 6.1). A long-lived UDP flow of average rate 600Kbps is sent to AT1 and bursts of 150 packets to AT2 every 6 seconds. The results mirror the behavior observed in the commercial network, namely, large "jitter" whenever a burst is

sent. Notice the reduction in the variability of results due to the absence of other ATs and queueing at other hops.

Recall that the PF algorithm compares the ratios of all ATs to allocate slots. Intuitively, the "jitter" of AT1 depends on the value of A_t of AT1 just before a burst to AT2 starts. The expression for "jitter" J experienced by AT1 when both ATs experience unchanging wireless conditions and hence, have constant achievable data rates $R1_t = R1$ and $R2_t = R2$ in every time slot t can be derived as follows. Assume that $A1_T = \beta 1_T R1$ and $A2_T = \beta 2_T R2$ are the moving averages for AT1 and AT2 in time slot T, the last slot before a burst to AT2 starts. Under these conditions, the PF scheduler allocates all time slots t that follow time slot T to AT2 until

$$\frac{R1}{A1_{t-1}} > \frac{R2}{A2_{t-1}} \tag{6.1}$$

For every time slot after time slot T that is allocated to AT2, $A1_{t-1}$ reduces and $A2_{t-1}$ increases as follows

$$A1_t = A1_T(1-\alpha)^{t-T} = \beta 1_T R1(1-\alpha)^{t-T} \tag{6.2}$$

$$\begin{aligned} A2_t &= A2_{t-1}(1-\alpha) + \alpha R2 \\ &= \beta 2_T R2(1-\alpha)^{t-T} + \alpha R2[1 + (1-\alpha) + ... + (1-\alpha)^{t-T-1}] \\ &= \beta 2_T R2(1-\alpha)^{t-T} + R2[1-(1-\alpha)^{t-T}] \\ &= R2[1-(1-\alpha)^{t-T}(1-\beta 2_T)] \end{aligned} \tag{6.3}$$

Substituting the above expressions into Equation 6.1 above, it follows that: -

$$\begin{aligned}
\frac{R1}{\beta 1_T R1(1-\alpha)^{t-T}} &> \frac{R2}{R2[1-(1-\alpha)^{t-T}(1-\beta 2_T)]} \\
\frac{1}{\beta 1_T(1-\alpha)^{t-T}} &> \frac{1}{[1-(1-\alpha)^{t-T}(1-\beta 2_T)]} \\
\beta 1_T(1-\alpha)^{t-T} &< [1-(1-\alpha)^{t-T}(1-\beta 2_T)] \\
(1-\alpha)^{t-T}(1+\beta 1_T-\beta 2_T) &< 1 \\
t-T &< \frac{log(\frac{1}{1+\beta 1_T-\beta 2_T})}{log(1-\alpha)}
\end{aligned}$$

Hence, the "jitter" J can be expressed as follows

$$J = \left\lceil \frac{log(\frac{1}{1+\beta 1_T-\beta 2_T})}{log(1-\alpha)} \right\rceil \tag{6.4}$$

The predicted values of "jitter" assuming $R1 = 1.8$Mbps and $\beta 2_T = 0$ are shown in Figure 6.2 (b). The predicted values were compared with the ones obtained experimentally in which the rate of AT1's flow was varied from 100Kbps to 2Mbps. For each experiment, the maximum "jitter" experienced by AT1 is shown in Figure 6.2. Comparing the results of these experiments with $\beta 2_T = 0$ makes sense because the bursts are separated long enough that AT2's A_t is close to zero. It is clear that the experimental results closely follow the analytically predicted values. Also, the jitter experienced by AT1 increases almost linearly with the *entire* data rate to AT1. Thus, an AT1 with a single video over IP application of 100Kb/s may experience only 100ms increase in "jitter" whereas additional concurrent web transfers by this video user would cause larger "jitter". As another example, an AT receiving a medium-rate video streams of 600Kb/s could experience a jitter increase of more than 0.5 seconds. This can cause severe degradation in video quality.

6.4.2 Effect on TCP Flows

It will now be shown that TCP-based applications are also susceptible to PF-induced starvation. For the first experiment, the UDP flow to AT1 was replaced with a long-lived TCP transfer of 20MB. As before, an on-off UDP stream was sent to AT2 in which every burst consists of 150 1500-byte packets once every 3 seconds

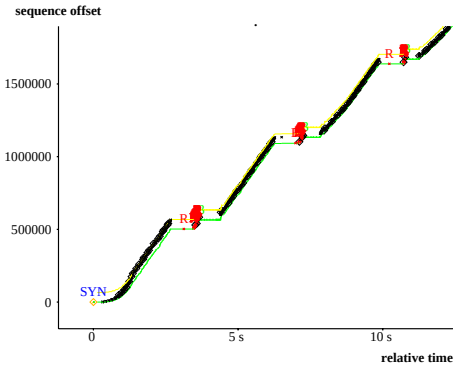

Figure 6.3. Results of *tcptrace* analysis of AT1. Timeouts are caused whenever AT2 received a burst.

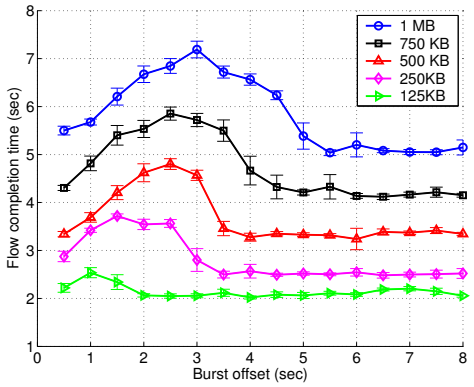

Figure 6.4. Increase in flow completion time for short TCP flows. 95% confidence intervals are plotted.

- an average rate of 600Kb/s. Sender-side *tcpdump* [tcp] traces were analysed using *tcptrace* [Ost]. The time sequence graph with TCP sequence number of the bytes transmitted on the y-axis and time of the flow to AT1 in the x-axis is shown in Figure 6.3(a). The SYN packet is marked at time 0. The black dots represent transmitted packets (x-value is time of transmission and y-value is the sequence number). Periodic retransmissions are seen every 3 seconds corresponding to each burst of the flow to AT2. This demonstrates how a malicious user can easily cause TCP timeouts to other users.

TCP timeouts in the above experiment could be caused due to one of two reasons. The first reason is that AT1 is starved long enough that its buffer overflows and some packets are dropped. The second reason is that the buffer is large

enough but AT1's packets are delayed long enough that TCP experiences a *spurious timeout*. It turns out that per-AT buffers in EV-DO base stations are usually 80 to 100KB in size, which is larger than the default TCP receiver window size of 64KB in Linux and Windows (other versions use 32KB and 16KB [Har]). This was verified this using sender side *tcpdump* traces. It might be argued that the laboratory configuration causes more spurious timeouts because we have fewer hops than typical Internet paths. In fact, our configuration reflects the common practice of wireless providers in using split-TCP or TCP proxies [WZZ+06]. Moreover, as wireless speeds go up, delays are only going to decrease.

Short Flows: The impact on TCP performance due to spurious timeouts caused by a malicious user will now be studied. Let us first consider short TCP flows for which flow completion times are the suitable performance metric. For these experiments, UDP flow to AT1 is replaced with TCP transfers ranging from 125KB to 1MB. Since short flows spend a significant fraction of time in slow start, A_t is likely to be small early on. Hence, the starvation duration is likely to depend on the offset of the burst from the start time of the TCP flow. To understand this better, experiments were conducted for various values of the burst offsets. For each offset and flow size, the experiment was repeated 30 times and the plot of the average flow completion times is shown in Fig. 6.4. The following four observations were made. First, for a large enough offset, the burst has no impact because the TCP flow is already complete. Second, the probability of a timeout increases as the offset increases. This confirms our intuition that, during slow start, A_t of AT1 is smaller and hence, starvation duration is smaller. Maximum performance impact is realized when the offset is $2 - 3$ seconds. This is observed when we plot the average number of retransmissions too (figure not shown here). Third,

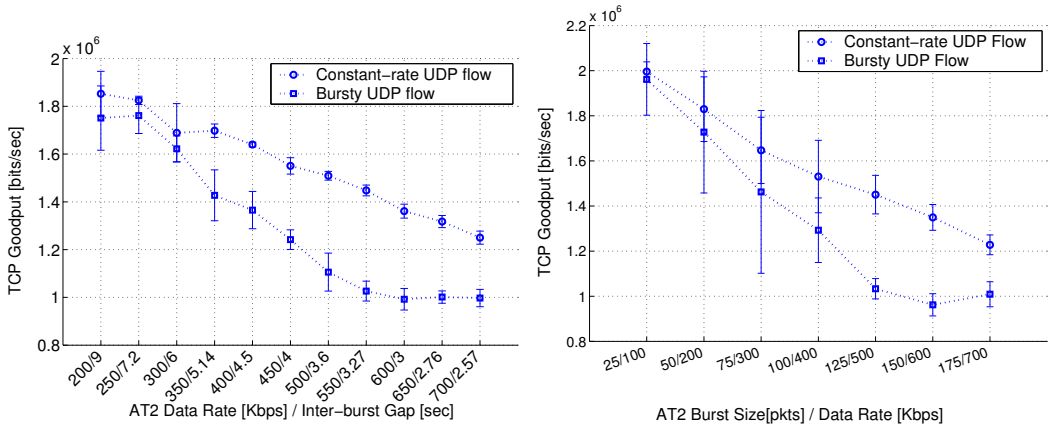

Figure 6.5. Plots illustrating the reduction in TCP goodput as a function of the burst size (a) and burst frequency (b) of an on-off UDP flow.

the inverted-U shape shows that the probability of a timeout decreases when the burst starts towards the end of the flow. Fourth, for downloads of 250KB and above, there is a $25-30\%$ increase in flow completion time. Note, however, that A_t depends on the *total* data rate to AT1. Hence, if AT1 receives other data flows simultaneously, its A_t would be larger and more timeouts may result.

Long Flows: Goodput is a suitable performance measure for long-lived flows. A long-lived flow is started to AT1. The malicious AT, AT2, receives on-off traffic in the form of periodic bursts. To understand how AT2 can achieve the maximum impact with minimal overhead, experiments were conducted with various burst sizes and frequencies. Since the average rate to AT2 changes based on the burst size and frequency, one experiment cannot be compared to the other. Instead, each experiment is compared to an experiment in which AT2 receives a constant packet rate UDP stream of the same average rate. The TCP goodput achieved with such well-behaved traffic captures the effect of the additional load. Any further reduction in goodput that is observed with on-off UDP flows essentially captures the performance degradation due to unnecessary timeouts. The

average TCP goodput achieved in our experiments with on-off and well-behaved UDP flows to AT2 are plotted in Figure 6.5. In the (a) plot, the inter-burst gap for a burst size of 150 1500-byte packets was varied. As expected, the slope of goodput with well-behaved UDP flows is almost linear with slope close to -1. The performance impact of malicious behavior is clearly shown with the maximum reduction in goodput when the inter-burst gap is around $3 - 3.5$ seconds. In this case, the goodput reduces by about 400Kbps - almost 30%. Larger gaps cause fewer timeouts and smaller gaps cause bursts to be sent before AT2's A_t has decayed to a small enough value. In the (b) plot, the burst size was varied for a 3-second inter-burst gap. It was found that bursts of $125 - 150$ packets cause the largest reduction in goodput of about $25 - 30\%$.

6.5 Parallel PF Algorithm

PF is vulnerable to "on-off" traffic primarily because it reduces $A[t]$ (by multiplying it with $1 - \alpha$) even when an AT is not backlogged. A naive solution is to freeze the value of $A[t]$ for such ATs. But, a frozen $A[t]$ value does not adapt to changes in the number of backlogged ATs or channel conditions. Hence, an AT with a recently unfrozen $A[t]$ can have a ratio that is much lower or higher than other ATs thereby causing starvation. A backlog-unaware algorithm, which always considers ATs to be backlogged, is also not desirable since it would allocate slots to ATs with no data to receive and hence, would not be work conserving.

We propose the following *Parallel PF (PPF)* algorithm that uses a backlog-unaware scheduler instance only to remove the undue advantage an "on-off" user receives at the beginning of "on" periods. A normal instance of PF drives slot allocation. The parallel instance of PF assumes all ATs are backlogged and ex-

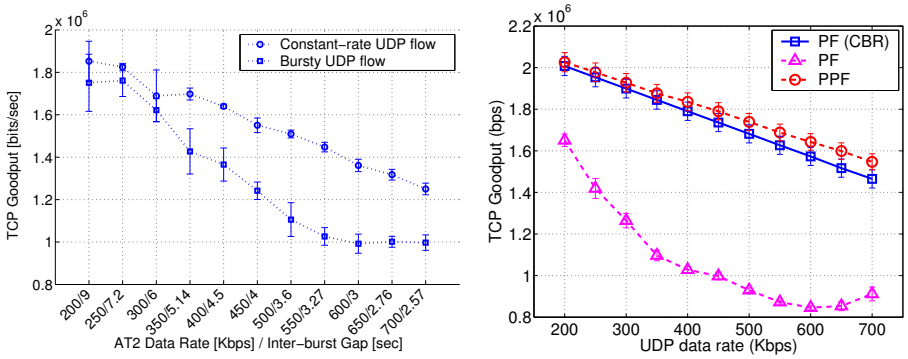

Figure 6.6. **(a)** Comparison of the (experimental) TCP goodput to an AT when another AT receives (1) A periodic (UDP) packet stream. (2) An "on-off" UDP flow with various inter-burst times. TCP Goodput can decrease by up to 30% due to "on-off" flows. **(b)** Similar simulation experiments with PF and PPF. The inter-burst times decreased from 9s to 2.57s. Goodput decrease due to PF is similar to that seen experimentally but higher due to differences in TCP timeout algorithms in *ns-2* and practical implementations. Goodput reduction is eliminated with PPF.

ecutes simultaneously. The notation $A^p[t]$ to refer to the $A[t]$ values maintained by the parallel instance. When a previously idle AT becomes backlogged, all $A[t]$ values are reset to the corresponding $A^p[t]$ values. Thus, when a previously idle AT becomes backlogged, differences in achieved throughput of backlogged and idle ATs are forgotten. Also, notice that as long as an idle AT does not become backlogged, PPF is equivalent to PF.

To test if PPF is vulnerable to "on-off" traffic patterns, the laboratory-based configuration (see [BMZF07] and Figure 6.6(a)) was recreated using *ns-2* simulations with two ATs - AT1 and AT2. AT1 received a long-lived TCP flow and AT2 received a (malicious) "on-off" UDP flow consisting of 225KB bursts sent at various inter-burst time periods. The simulations used a wireless link, governed by PF or PPF, that connected to a wired 100Mbps link with mean round trip times of 250ms. Achievable data rates were assigned based on measurements in a commercial EV-DO network. To collect these 30-minute long traces, the Qual-

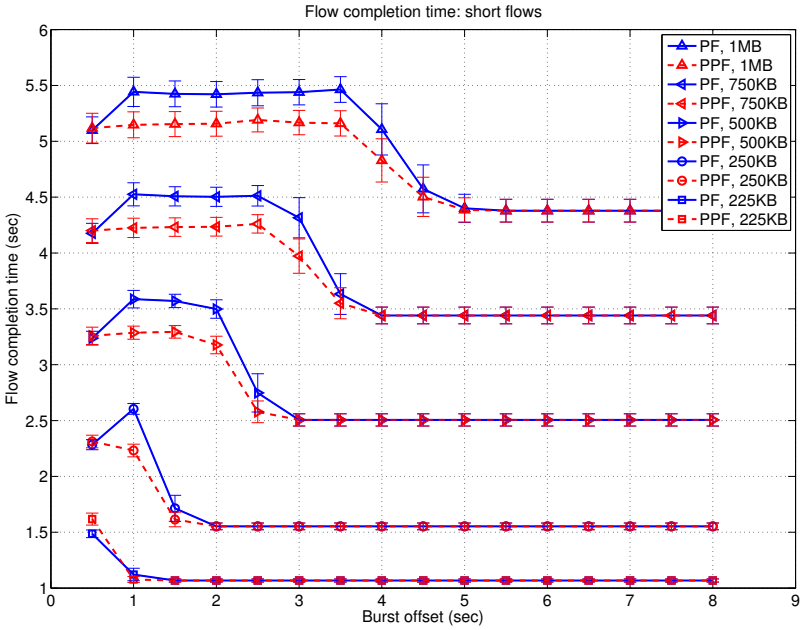

Figure 6.7. TCP flow completion times with PF and PPF schedulers. Measurement driven ns-2 simulations were used to plot these results.

comm CDMA Air Interface Tester [CDM06] software was used on a stationary AT and a mobile AT moving at an average speed of 40mph. The TCP goodput obtained with PF and PPF is plotted in Figure 6.6 (b). The results clearly show that, with PPF, the TCP goodput is not affected by the "on-off" flow. This is the reason why the TCP goodput with PPF is slightly higher than the goodput with PF and a CBR flow consisting of periodically-sent UDP packets. To understand how much improvement in flow-completion times of short flows can be obtained by replacing PF scheduler with PPF scheduler the laboratory experiment deiscussed earlier in Section 6.4 was recreated using ns-2. Improvement in short flow completion times can be seen in Figure 6.7. As expected, using PPF reduces the flow completion times of short flows.

The proposed PPF algorithm uses the achievable rate feedback from the ATs

to maintain parallel values of the average rate and hence can work only when data rate values are reported by the ATs. The connection timer at the AT expires after about 12 seconds of inactivity and the AT stops reporting its achievable rate values to the base station. When new data arrives for the AT, a new connection is established between the core network and the AT and the average is reset to 0 again. This AT gets all the time slots for some time, starving all other ATs despite there being a PPF scheduler to reduce the starvation. To overcome this problem, we propose an algorithm that allows the average to grow quickly and converge to a value such that sharing between ATs can begin. This is achieved by not having a fixed value of the parameter α but instead having the value of α shrink from $\alpha = 1$ down to $\alpha = \frac{1}{1000}$. For the first time slot when new data to the AT arrives and a new connection is established, value of α equals 1 and the average is 0. In the second time slot, $\alpha = \frac{1}{2}$, in the third, $\alpha = \frac{1}{3}$ and so on. After 1000 slots, the value of α is $\frac{1}{1000}$ and it does not shrink after this. This method of updating the value of α allows the average to change faster than it would have had the value of α been fixed at $\frac{1}{1000}$.

6.6 Summary

Proportional fair scheduler is commonly used for downlink scheduling by most 3G wireless equipment makers and is widely deployed. The contribution of this work is the finding that PF can be easily corrupted, accidentally or deliberately causing real-time multimedia impairments. Scheduler induced impairments were rigorously quantified in this work using experiments conducted in both laboratory and production network settings. It was observed that the delay jitter can be increased by as much as 1 second and TCP throughput can be reduced by as much

as 25-30 % by a single malicious user. An important contribution of this work is a new scehduling algorithm (the parallel proportional fair scheduler) that mitigates the scheduler-induced impairments. It is shown using ns-2 simulations that the new scheduler significantly reduces the impairments and improves the throughput and delay performance. The parallel scheduler however cannot work when the AT's session transitions to an inactive state as in this state, the instantaneous channel conditions are not reported by the AT using the DRC channel. The shrinking alpha algorithm proposed in this work can be used then to change the average rates faster allowing impairments to be reduced significantly.

Chapter 7

Conclusions and Future Work

7.1 Conclusions

Improving network function by matching response to network conditions (or the estimate of network conditions) is not a new idea and has been used in the Internet for decades. For example, TCP uses packet loss feedback and end system available buffer size feedback to adjust the sending rate. New methods for improving network functions are using the same basic idea of matching the response to network conditions. For example, TCP optimizers for wireless networks (e.g., optimizers from Bytemobile [Byt] and Venturi Wireless [Wir]) split the end-to-end TCP connection into wired and wireless parts. In the wireless part, these optimizers use core-to-end active measurements to estimate the available bandwidth and wireless channel conditions and match the sending rate accordingly with the main goal of improving TCP throughput. Cross layer measurement based optimizers (like the one by Mobidia [Mob]) use cross-layer measurement input of the radio conditions to improve network functions at layer 3 and above. To apply the correct response, it is important to first accurately detect the correct network

condition using measurements. As the Internet evolves integrating new physical layer technologies and algorithms the number of possible causes that result in similar observable symptoms at the end node are increasing. For example, after the invention and widespread deployment of BGP in the Internet, BGP convergence delay has now been added to the list of network problems that may cause observable symptom of packet losses at the end node. Since the growing complexity of the Internet is resulting in an increasing number of events to causing similar observable symptoms at the end system, it is becoming important to develop advanced techniques to detect and identify these events. Also, due to the increasing security and proprietary concerns, service providers are blocking more and more information (e.g. ICMP blocking, SIP/IMS topology hiding [SBC]) that allowed end systems to know more about their networks. The decrease in the amount of information available at the end system to allow detection and identification of network events strengthens the case for the development of advanced end-to-end event detection and identification techniques.

Some of the main contributions of this work are the development of new methods for detection and identification of events like RTM impairments, congestion and route changes using only the delay and loss information. Burst loss, disconnected, high random loss and high delay RTM impairment events were defined and methods to detect these events from delay and loss time series were developed. Using 26 days of PlanetLab data collected over 9 different end node pairs it was found that mean time between RTM impairments varied from 3.5 hours to 268 hours depending on the path and the mean duration of impairments varied from 4 minutes to 92 minutes for different node pairs. Metrics like time between and duration of impairments provide the end users information about the network that is

very understandable. It is demonstrated using PlanetLab measurements that the methods developed in this dissertation can be used to detect RTM impairments. Also, the RTM impairments observed on these paths were correlated with the congestion and route change events to illustrate what type of impairment events are caused by these network events. Heuristic-based methods for detecting congestion and route changes from delay and loss information were also developed and evaluated using the same PlanetLab measurement data. Congestion was detected on two of the nine paths and on these paths it occurred for 6-8 hours during the day on weekdays. Route changes were observed on all the nine paths over which measurements were conducted. Mean duration of loss impairments that occurred just before route changes (113.5 sec) was found to be five times longer than the mean duration of loss impairment that occurred during congestion (22.64 sec). The details of all the results from this measurement study are discussed in section 2.4.

From the PlanetLab measurement study, it was found that the heuristics-based route change detection algorithm was able to detect 71% of all visible layer 2 route changes. Route changes that occurred too close together in time or the ones for which the minimum RTT changed by less than 0.5 ms could not be detected. A model-based optimal detector (PAD) was developed and analysed to find out how close the performance of heuristics-based algorithm is to the best possible performance. ROC curves were used to compare the simulated and the predicted performance and to show that the analysis developed in this dissertation accurately predicts the performance. Although the PAD is ideal, it cannot be implemented in practice because of the assumption that the parameters are known in advance. A practical model-based algorithm (PUD) was also developed

here to find out if the model-based approach can be used to design a detector that performs better than the heuristics-based detector. Extensive simulations were conducted to find the region of the parameter space over which the three algorithms have acceptable performance (where acceptable performance is defined as $P_D \geq 0.999$ and $P_F \leq 0.001$). The region of acceptable performance is largest for the PAD as expected, followed by PUD and then by the heuristics-based detector. This shows that the model-based detector has accpetable performance over a larger set of parameter values than the heuristics-based detector and may be the preferred practical detector for this reason. The PUD was also applied to measured RTT data from PlanetLab to evaluate the algorithm on network measurements.

Another very important contribution of this work is the discovery that the widely deployed PF scheduler can be easily corrupted, accidentally or deliberately, to starve flows and cause RTM impairments in wireless networks. In this dissertation, field experiments were used to rigorously quantify the impact of starvation observable at the transport layer. A combination of both laboratory and production network measurements were used in this study to demonstrate the PF starvation vulnerability. It is shown using measurements that the delay jitter can be increased to 1 second and the TCP throughput can be decreased by as much as 25-30% by a single malicious user. The analysis for predicting starvation duration when the channel conditions are fixed was also developed and validated. Inter-burst gap and burst duration were varied to find the parameter values at which an attacker can cause maximum damage and it was found that this malicious AT can reduce TCP throughput by 25-30%. A parallel PF algorithm was proposed to mitigate the starvation vulnerability of the PF algorithm. It was shown using

ns2 simulations that when the parallel PF algorithm is used instead of the PF algorithm, the malicious user is not able to starve any flows. Also, the parallel PF is a variant of the PF algorithm and for this reason it has the same throughput optimality and fairness properties as PF. Since parallel PF algorithm requires that inactive ATs should keep on reporting their achievable rates and since ATs stop reporting achievable rates after a few seconds of inactivity, flows can still be starved when ATs come on after long periods of inactivity. An adaptive alpha updating mechanism was designed to deal with this problem and it was shown that the flow starvation problem can be mitigated by using this new algorithm.

7.2 Future Work

Probability of detection and false alarms for the PAD can be predicted very accurately using the analysis developed in this dissertation. However, the PAD is the ideal detector and the requirement that the parameter values should be known in advance limits its applicability. The analysis developed for PAD was used to predict the performance bounds for all detectors. The performance curves for PUD were obtained using extensive simulations because the analysis for PUD was not developed. Since PUD is based on the assumption that the parameters of Gamma distribution are not known but are estimated, the analysis for predicting the performance of PUD is more complicated than the one for PAD. Note that for PUD, the right hand side of Equation 3.3 has parameter estimates instead of the parameter values (like in PAD). Since the parameter estimated of the three parameter Gamma distribution are random variables whose mapping function is non-trivial, this analysis is more complicated. However some simplifying assumptions may lead to analytical expressions for predicting the performance of the

PUD. This analysis for predicting performance of PUD is not just of academic interest but also has practical significance because it can be used to find the optimal decision threshold for any given set of parameter values. It has already been shown in this work that PUD is the practical detector of choice because of its performance advantage over the heuristic detector and with the performance prediction analysis PUD can predict optimal thresholds in real time since it does not take much computations to predict the optimal threshold using the analysis.

Although PAD cannot be used in practice in most cases because the parameter values are not known in advance, it may be possible to use PAD in some cases like for detecting route flapping between two paths. If there is persistent route flapping between two paths, the detector can learn the parameter values of both paths over time. After some time, when the detector has collected enough samples from both paths and has gained enough confidence in the parameter estimates of both paths, PAD can be applied to detect route changes because the detector is already aware of the parameter values of both paths. The design issues like how many samples to collect before applying PAD and how to detect that the route flapping has stopped so as to stop applying PAD and start using PUD can be explored in future work.

References

[ABBM03] H. Kaplan A. Bremler-Barr, E. Cohen and Y. Mansour. Predicting and bypassing end-to-end Internet service degradations. *IEEE Journal on Selected Areas in Communications*, 21(6):961–978, June 2003.

[AMD04] S. Bhattacharyya C. Chuah A. Markopoulou, G. Iannaccone and C. Diot. Characterization of failures in an ip backbone. In *Proceedings of IEEE INFOCOM 2004*, pages 2307–2317, Hong Kong, March 2004.

[AZJ03] Z. Wang A. Zeitoun and S. Jamin. Rttometer: Measuring path minimum rtt with confidence. In *Proceedings of 3rd IEEE Workshop on IP Operations and Management (IPOM 2003)*, pages 127–134, Kansas City, USA, October 2003.

[BCL+04] Tom Beigbeder, Rory Coughlan, Corey Lusher, John Plunkett, Emmanuel Agu, and Mark Claypool. The effects of loss and latency on user performance in unreal tournament 2003. In *Proceedings of ACM SIGCOMM 2004 Workshops on NetGames '04*, pages 144–151, 2004.

[BJFD05] Soshant Bali, Yasong Jin, Victor S. Frost, and Tyrone Duncan. Characterizing user-perceived impairment events using end-to-end measurements. *Accepted for publication in International Journal of Communication Systems*, 2005.

[BK46] M. S. Bartlett and D. G. Kendall. The statistical analysis of variance heterogeneity and logarithmic transformation. *Journal of the Royal Statistical Society*, 8:128–138, 1946.

[BMZF07] S. Bali, S. Machiraju, H. Zang, and V. Frost. A Measurement Study of Scheduler-based Attacks in 3G Wireless Networks. In *Proc. of Passive and Active Measurement (PAM) Conference*, 2007.

[BSUB98] M. Borella, D. Swider, S. Uludag, and G. Brewster. Internet packet loss: measurement and implications for end-to-end QoS. In *ICPPW '98: Proceedings of the 1998 International Conference on Parallel Processing Workshops*, pages 3–15, 1998.

[Byt] Bytemobile. `http://www.bytemobile.com/`.

[CBD02] G. Iannaccone C. Boutremans and C. Diot. Impact of link failures on voip performance. In *Proceedings of the 12th International Workshop on Network and Operating Systems Support for Digital Audio and Video*, pages 63–71, Miami, Florida, USA, May 2002.

[CDM06] CDMA Air Interface Tester. `http://www.cdmatech.com/download_library/pdf/CAIT.pdf`, 2006.

[CHNY02] Mark Coates, Al Hero, Robert Nowak, and Bin Yu. Internet tomography. *IEEE Signal Processing Magazine*, 19:47–65, 2002.

[CJT04] Y. Levy F. Saheban C.R. Johnson, Y. Kogan and P. Tarapore. VoIP reliability: A service provider's perspective. *IEEE Communications Magazine*, 42(7):48–54, July 2004.

[CMR03] L. Ciavattone, A. Morton, and G. Ramachandran. Standardized active measurements on a tier 1 ip backbone. *IEEE Communications Magazine*, 41:90–97, 2003.

[CT99] M. Claypool and J. Tanner. The effects of jitter on the perceptual quality of video. In *Proceedings of ACM Multimedia Conference*, pages 115–118, Orlando, Florida, USA, November 1999.

[Don01] Sean Donelan. Internet outage trends. http://www.nanog.org/mtg-0102/donelan.html, Feb. 2001. NANOG meeting.

[DP00] Nick G. Duffield and Francesco Lo Presti. Multicast inference of packet delay variance at interior network links. In *Proceedings of IEEE INFOCOM 2000*, Tel-Aviv, Israel, March 2000.

[DP04] N.G. Duffield and F.L. Presti. Network tomography from measured end-to-end delay covariance. *IEEE/ACM Transactions on Networking*, 12:978–992, 2004.

[DPZ03] D. Massey S. F. Wu D. Pei, L.Wang and L. Zhang. A study of packet delivery during performance during routing convergence. In *Proceedings of IEEE/IFIP International Conference on Dependable Systems and Networks (DSN)*, 2003.

[FHPW00] Sally Floyd, Mark Handley, Jitendra Padhye, and Jorg Widmer. Equation-based congestion control for unicast applications. In *SIGCOMM 2000*, pages 43–56, Stockholm, Sweden, August 2000.

[Fro03] Victor S. Frost. Quantifying the Temporal Characteristics of Network Congestion Events for Multimedia Services. *IEEE Transactions on Multimedia*, 5(4):458–465, Aug. 2003.

[G.103] ITU-T Recommendation G.114, May 2003.

[GID02] R. Mortier S. Bhattacharyya G. Iannaccone, C. Chuah and C. Diot. Analysis of link failures in an ip backbone. In *Proc. Of 2nd ACM SIGCOMM Internet Measurement Workshop*, pages 237–242, Marceille, France, November 2002.

[Gil03] G. Hudson Gilmer. The real-time IP network: moving IP networks beyond best effort to deliver real-time applications, 2003. AVICI Systems white paper.

[Har] Carl Harris. Windows 2000 TCP Performance Tuning Tips `http://rdweb.cns.vt.edu/public/notes/win2k-tcpip.htm`.

[HC95] R. V. Hogg and A. T. Craig. *Introduction to Mathematical Statistics*. Prentice-Hall, fifth edition, 1995.

[ICBD04] Gianluca Iannaccone, Chen-Nee Chuah, Supratik Bhattacharyya, and Christophe Diot. Feasibility of IP restoration in a tier-1 backbone. *IEEE Networks Magazine, Special Issue on Protection, Restoration and Disaster Recovery*, 2004.

[ICM+02] G. Iannaccone, C. Chuah, R. Mortier, S. Bhattacharyya, and C. Diot. Analysis of link failures in an IP backbone. In *Proc. of ACM SIGCOMM Internet Measurement Workshop*, Nov 2002.

[Isw] Iswest sdsl service level agreement. http://www.iswest.com/serviceagree-ment.html.

[JBG04] J.H.James, Chen Bing, and L Garrison. Implementing VoIP: A Voice Transmission Performance Progress Report. *IEEE Communications Magazine*, 42(7):36–41, July 2004.

[JCBG95] H. Crepin J.-C. Bolot and A.V. Garcia. Analysis of audio packet loss in the internet. In *Proceedings of the 5th International Workshop on Network and Operating System Support for Digital Audio and Video*, pages 154–165, Durham, NH, USA, April 1995.

[JJG04] C. Bing J.H. James and L. Garrison. Implementing VoIP: A voice transmission performance progress report. *IEEE Communications Magazine*, 42(7):36–41, July 2004.

[JPP00] A. Jalali, R. Padovani, and R. Pankaj. Data Throughput of CDMA-HDR: A High Efficiency-high Data Rate Personal Communication Wireless System. *Proc. of IEEE Vehicular Technology Conference*, 3:1854–1858, May 2000.

[JS00] W. Jiang and H. Schulzrinne. QoS measurement of Internet real-time multimedia services. In *Proceedings of NOSSDAV, Chapel Hill, NC*, June 2000.

[JS02] W. Jiang and H. Schulzrinne. Comparison and optimization of packet loss repair methods on voip perceived quality under bursty loss. In *NOSSDAV '02: Proceedings of the 12th International Workshop on Network and Operating Systems Support for Digital Audio and Video*, pages 73–81, Miami Beach, FL, USA, May 2002.

[Kle75] L. Kleinrock. *Queueing Systems Volume 1: Theory.* Wiley, 1975.

[KPD03] R. Cruz K. Papagiannaki and C. Diot. Network performance monitoring at small time scales. In *IMC '03: Proceedings of the 3rd ACM SIGCOMM Conference on Internet Measurement*, pages 295–300, Miami Beach, Florida, October 2003.

[KPH04] D. Veitch K. Papagiannaki and N. Hohn. Origins of microcongestion in an access router. In *Proc. Passive and Active Measurment Workshop*, Antibes Juan-Ies-Pins, France, April 2004.

[KR02] R. Koodli and R. Ravikanth. One-way loss pattern sample metrics. In *RFC 3357, Internet Engineering Task Force*, 2002.

[LABJ00] Craig Labovitz, Abha Ahuja, Abhijit Bose, and Farnam Jahanian. Delayed Internet routing convergence. In *Proceedings of ACM SIGCOMM*, pages 175–187, 2000.

[LAJ98] C. Labovitz, A. Ahuja, and F. Jahanian. Experimental study of Internet stability and wide-area backbone failures. Technical Report CSE-TR-382-98, University of Michigan, 1998.

[Law82] J. F. Lawless. *Statistical Models and Methods for Lifetime Data.* Wiley, 1982.

[MCN02] R. Castro M. Coates and R. Nowak. Maximum likelihood network topology identification from edge-based unicast measurements. *ACM Sigmetrics Performance Evaluation Review*, 30(1):11–20, June 2002.

[ME98] W. Q. Meeker and L.A. Escobar. *Statistical Methods for Reliability Data*. Wiley, 1998.

[MEP93] N. Hastings M. Evans and B. Peacock. *Statistical distributions*. Wiley, 2nd edition, 1993.

[MKT98] Sue B. Moon, Jim Kurose, and Don Towsley. Packet Audio Playout Delay Adjustment: Performance Bounds and Algorithms. *Multimedia Systems*, 6(1):17–28, 1998.

[MMS05] I. Saniee M. Mandjes and A. Stolyar. Load Characterization and Anomaly Detection for Voice Over IP Traffic. *IEEE Transactions on Neural Networks*, 16(5):1019–1026, September 2005.

[Mob] Mobidia. `http://www.mobidia.com/`.

[MT00] V. Markovski and L. Trajkovic. Analysis of loss episodes for video transfer over UDP. In *Proceedings of the SCS Symposium on Performance Evaluation of Computer and Telecommunication Systems (SPECTS'2K)*, pages 278–285, 2000.

[MTK03] Athina P. Markopoulou, Fouad A. Tobagi, and Mansour J. Karam. Assessing the Quality of Voice Communications over Internet Backbones. *IEEE/ACM Transactions on Networking*, 11(5):747–760, 2003.

[Muk92] Amarnath Mukherjee. On the dynamics and significance of low frequency components of internet load. Technical Report MS-CIS-92-83, University of Pennsylvania, December 1992.

[MYT99] J.F. Kurose M. Yajnik, S.B. Moon and D.F. Towsley. Measurement and modeling of the temporal dependence in packet loss. In *Proceedings of IEEE INFOCOM 1999*, pages 345–352, New York, NY, USA, March 1999.

[NC04] James Nichols and Mark Claypool. The effects of latency on online Madden NFL football. In *NOSSDAV '04: Proceedings of the 14th International Workshop on Network and Operating Systems Support for Digital Audio and Video*, pages 146–151, 2004.

[NGDD02] J. Horowitz Nicholas G. Duffield, Francesco Lo Presti and D.Towsley. Multicast topology inference from measured end-to-end loss. *IEEE Transactions on Information Theory*, 48(1):26–35, Jan 2002.

[NJB94] S. Kotz N.L. Johnson and N. Balakrishnan. *Continuous univariate distributions : Vol. 1.* John Wiley, New York, 2nd edition, 1994.

[Ost] Shawn Ostermann. tcptrace, `http://jarok.cs.ohiou.edu/software/tcptrace`.

[pla04] Timing problem on planetlab (bad NTP). http://lists.planetlab.org/pipermail/users/2004-March/000050.html, March 2004.

[PW02] Lothar Pantel and Lars C. Wolf. On the impact of delay on real-time multiplayer games. In *NOSSDAV '02: Proceedings of the 12th*

International Workshop on Network and Operating Systems Support for Digital Audio and Video, pages 23–29, 2002.

[RHdB05] G. Karagiannis J. Loughney R. Hancock, I. Freytsis and S. Van den Bosch. Next steps in signaling: Framework. In *RFC 4080, Internet Engineering Task Force*, June 2005.

[SB88] K. Sam Shanmugan and Arthur M. Breipohl. *Random Signals: Detection, Estimation and Data Analysis*. John Wiley & Sons Inc., 1988.

[SBC] Acme Packet SBC. `http://www.acmepacket.com/`.

[SSLB05] Charles Shen, H. Schulzrinne, Sung-Hyuck Lee, and Jong Ho Bang. Routing dynamics measurement and detection for next step internet signaling protocol. In *Proc. of 2005 Workshop on End-to-End Monitoring Techniques and Services*, Nice, France, May 2005.

[tcp] tcpdump. `http://www.tcpdump.org`.

[TKM98] I. Sidhu G.M. Schuster J. Grabiec T.J. Kostas, M.S. Borella and J. Mahler. Real-time voice over packet-switched networks. *IEEE Network*, 12(1):18–27, Jan/Feb 1998.

[UHD02] R. Mortier U. Hengartner, S. Moon and C. Diot. Detection and analysis of routing loops in packet traces. In *Proceedings of the 2nd ACM SIGCOMM Workshop on Internet Measurement*, pages 107–112, Marseille, France, November 2002.

[VTL02] P. Viswanath, D. Tse, , and R. Laroia. Opportunistic Beamforming using Dumb Antennas. *IEEE Transactions on Information Theory*, 48:1277–1294, June 2002.

[WHZ00] Dapeng Wu, Yiwei Thomas Hou, and Ya-Qin Zhang. Transporting Real-Time Video over the Internet: Challenges and Approaches. *Proceedings of the IEEE*, 88(12):1855 – 1877, 2000.

[Wir] Venturi Wireless. `http://www.venturiwireless.com/`.

[WJS03] K. Koguchi W. Jiang and H. Schulzrinne. Qos evaluation of voip end-points. In *Proceedings of the IEEE International Conference on Communications*, pages 1917–1921, Anchorage, AL, USA, May 2003.

[WWTK03] W. Wei, B. Wang, D. Towsley, and J. Kurose. Model-based identification of dominant congested links. In *Proceedings of the 3rd ACM SIGCOMM conference on Internet Measurement*, Miami Beach, Florida, October 2003.

[WZZ+06] W. Wei, C. Zhang, H. Zang, J. Kurose, and D. Towsley. Inference and Evaluation of Split-Connection Approaches in Cellular Data Networks. In *pam*, 2006.

[XY06] Wang Xiaoyi and Qu Yajiang. Enhanced proportional fair scheduling for cdma2000 1x ev-do reverse link. In *Wireless and Optical Communications Networks, 2006 IFIP International Conference on*, April 2006.

[YT03] Shing Yin and Ken Twist. The coming era of absolute availability. http://www.chiaro.com/pdf/rhk.pdf, May 2003. RHK white paper.

[ZDPS01] Y. Zhang, N. Du, V. Paxson, and S. Shenker. On the constancy of Internet path properties. In *Proceedings of ACM SIGCOMM Internet Measurement Workshop*, San Francisco, California, USA, November 2001.